AN INVESTIGATION INTO AN ELECTROMAGNETIC FLOWMETER FOR USE WITH LOW CONDUCTIVITY LIQUIDS

Thesis submitted for the degree of
Doctor of Philosophy
To the University of Wales, Cardiff

By

David Lincoln

School of Engineering

September 2006

ProQuest LLC
789 East Eisenhower Parkway
P.O. Box 1346
Ann Arbor, MI 48106-1346

Declaration

This work has not previously been accepted in substance for any degree and is not concurrently submitted in candidature for any degree.

Signed.....(Candidate) Date.....9/3/7.....

Statement 1

This thesis is being submitted in partial fulfilment of the requirements for the degree of PhD.

Signed.....(Candidate) Date.....9/3/7.....

Statement 2

This thesis is the result of my own independent work/investigations, except where otherwise stated. Other sources are acknowledged by explicit references.

Signed.....(Candidate) Date.....9/3/7.....

Statement 3

I hereby give consent for my thesis, if accepted, to be available for photocopying and for inter-library loan, and for the title and summary to be made available to outside organisations.

Signed.....(Candidate) Date.....9/3/7.....

Statement 4

I hereby give consent for my thesis, if accepted, to be available for photocopying and for inter-library loans **after expiry of a bar on access** approved by the Graduate Development Committee.

Signed.....(Candidate) Date.....9/3/7.....

Acknowledgements

I would like to thank Roger Turner and Ray Keech for their advice, guidance, support and encouragement throughout this project. I would also like to thank Michael Armitage (my buddy) and Peter Asquith for their assistance and friendship over the years.

I would also like to thank my tutors Daphne and Tim O'Doherty who have been a continual source of support throughout the course of this research.

I must also thank my wife Marie for her patience and support over the past few years, without whom I would never have been able to complete this project.

Abstract

Scientists have been researching the performance of electromagnetic flow meters with insulating liquids for almost 50 years. Although working prototypes have been developed, these devices have only operated under laboratory conditions and have not yet reached the performance standard required of a commercially manufactured flow meter.

This study has investigated the performance of three different designs of flow meter with low conductivity liquids. Two of the flow meters were novel in design having long electrodes and magnetic fields. It was found that the long electrode flow meters performed better with low conductivity liquids than the conventional flow meter.

Also as part of this project a model of a flow meter was developed that could predict the likely behaviour of different electrode and coil geometries. Using the model analysis the optimal flow meter design for use with insulating oil was investigated. The favoured design had a rectangular flow conduit with elongated large area electrodes covering the entire surfaces of two of the opposing faces.

Based on the modelling work a flow meter was developed and its performance evaluated using digital signal processing software. When the flow system was tested on oil the results showed no discernable flow signal within the large noise voltage. A subsequent theoretical analysis of the set-up revealed that the developed flow meter suffered from stray capacitance, which was shunting the signal. The development of a replacement flow meter is described that was able to measure the flow of an insulating liquid.

Nomenclature

Symbols	Description	Units
A	Cross sectional area	m^2
a	Plate thickness or half height of electrode	m
b	Bandwidth	Hz
B	Magnetic flux density	T
$\underline{B}$	Magnetic flux density vector	T
B_x	Magnetic flux density in the x-direction	T
c	Speed of sound	m / s
d	Diameter or Distance between electrodes (unless otherwise stated)	m
D	Molecular diffusivity (of the liquid)	m^2 / s
E_y	Electric field in the y-direction	V / m
e	Eddy current skin depth	m
G	Virtual current potential, current = ∇G	
H	Magnetic field strength	A / m
I	Current	A
$\boldsymbol{i}$	Unit vector	
$\boldsymbol{j}$	Unit vector	
$\boldsymbol{k}$	Unit vector	
k	Boltzmann constant, 1.381×10^{-23}	J / K
K	Dielectric constant	
l	Electrode length	m

Symbols	Description	Units
l_c	Conductor length	m
L	Half length of magnetic field	m
m	Mass	Kg
n	Sample number	
P_n	Johnson noise power	W
P_e	Eddy current power loss	W
Q	Charge	C
q_w	Charge at the near wall region	C / m^3
Q_v	Volumetric flow rate	m^3 / s
r	Pipe radius	m
R	Resistance	Ω
R_t	Total resistance	Ω
R_e	Resistance at ends of magnetic field	Ω
R_s	Source resistance or impedance	Ω
R_0	Circular electrode resistance	Ω
R_l	Line electrode resistance	Ω
Re	Reynolds number	
s	Standard deviation	
S	Electrode Separation distance	m
T	Temperature	K
t	Time	s
t_{95}	95% confidence level of the student's statistic	
u	Liquid velocity	m / s

Symbols	Description	Units
$\hat{u}$	peak velocity	m / s
$\bar{u}$	Average velocity	m / s
U_{lam}	Laminar flow velocity	m / s
U_{turb}	turbulent flow velocity	m / s
u_z	Liquid velocity in the z-direction	m / s
$\underline{u}$	Velocity vector	m / s
$U_{\bar{u}}$	Expanded uncertainty of the mean velocity	m / s
V	Potential difference	V
$\underline{W}$	Weight Function vector	
w	Width of flow duct	m
X	Signal Magnitude	
x_1	Sine component	
x_2	Cosine component	
x_ϕ	Phase rotated component	
y	Distance from pipe wall	m
Z	Attenuation Factor	
β	Electrode half angle	°
Δ	Change or difference	
δ	Laminar sub-layer thickness	m
ε_0	Electric field constant or Permittivity of free space	F / m
ε_r	Relative permittivity	F / m
θ	Angle	°

Symbols	Description	Units
λ_D	Debye length	m
μ	Dynamic viscosity	kg / (m.s)
μ_r	Relative permeability	H / m
μ_0	Permeability of free space	H / m
ξ	Zeta potential	V
ρ_D	Density	kg / m^3
ρ_R	Resistivity	Ω.m
σ	Electrical conductivity	mhos / m
τ	Volume	m^3
ϕ	Phase angle	°, radians
ω	Angular frequency $= 2.\pi.f$	Hz

Contents

Chapter 1

Introduction

1.1. An Introduction to Fluid Flow Measurement

Fluid flow measurement is a common everyday occurrence. There are countless examples of domestic, industrial or medical uses. Domestically it is the basis of the metering of water or gas supplied to homes. In the chemical, food, beverage and pharmaceutical industries flow meters are widely used to control processes or to measure ingredient quantities, from processed food and drinks to paints (ABB, 2002). Triple heart by-pass operations are performed daily; once the heart has been by-passed the machine that pumps the blood around the body uses a flow meter to ensure the correct flow rate is used during the operation (Lansdowne, 2006).

1.2. Methods of flow measurement

The diversity of fluids to be measured has resulted in the development of a vast range of flow measurement devices. These devices utilise a number of physical principles relating to the particular fluid being measured. A brief description of some of the different flow measurement techniques used to measure the flow of liquids and gases will now be given.

1.2.1. Differential Pressure

The most common principle used in flow measurement is differential pressure (DP), which accounts for some 30% of the market (Franklin 2001). A differential pressure flow meter uses some form of restriction in the flow to

create a pressure drop; this pressure drop is then measured and related to the flow rate. The orifice plate is the most common example of a differential pressure flow meter. Orifice plates are used to measure the flow of liquids and gases including steam (Furness, 1989). A conventional square edged orifice plate is illustrated in figure 1.1.

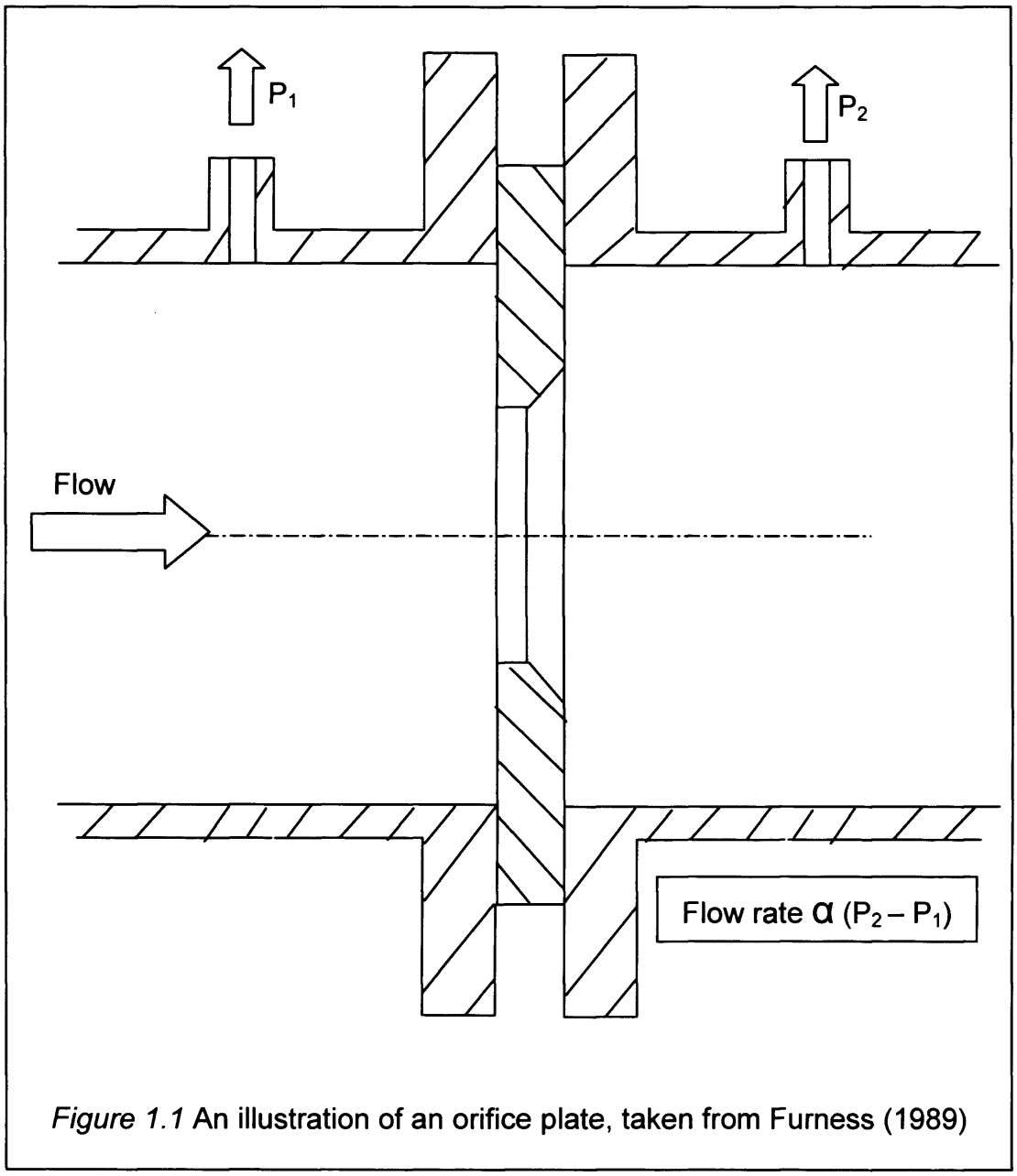

Figure 1.1 An illustration of an orifice plate, taken from Furness (1989)

The orifice plate performance is affected by hydraulic conditions such as swirl; it also has a relatively high pressure drop (Furness, 1989).

The venturi flow tube is a differential pressure flow meter that is less sensitive to upstream conditions than an orifice plate. A classical venturi flow tube is illustrated in figure 1.2. The venturi tube is much more expensive to manufacture than an orifice plate due to its size, however for applications where pressure drop is a problem the venturi tube has a pressure recovery section which reduces the pressure drop.

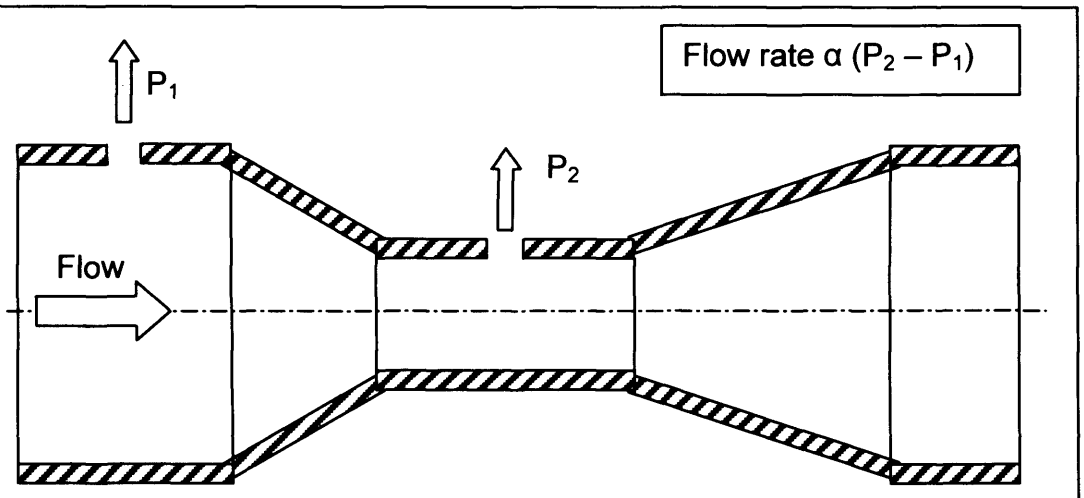

Figure 1.2. A Venturi tube, taken from Furness (1989)

Other examples of DP devices include; flow nozzles and Dall tubes, which are also low loss devices (Furness, 1989)

1.2.2. Displacement Flow meters

Positive displacement (PD) flow meters have been in use since the 1800's (Barnes and Foran 2001). They operate by stopping the upstream fluid, collecting a known volume from it and then depositing the volume of fluid back into the pipe. By counting the quantity of known volumes collected the total

volume through the pipe can be calculated or, through timing, the flow rate can be determined. PD flow meters are actually a form of hydraulic motor, which rotates under the action of the fluid. Figure 1.3 shows a sequence of pictures that describe the fluid flow through a Bi-rotor Positive Displacement Flow meter (Barnes and Foran 2001).

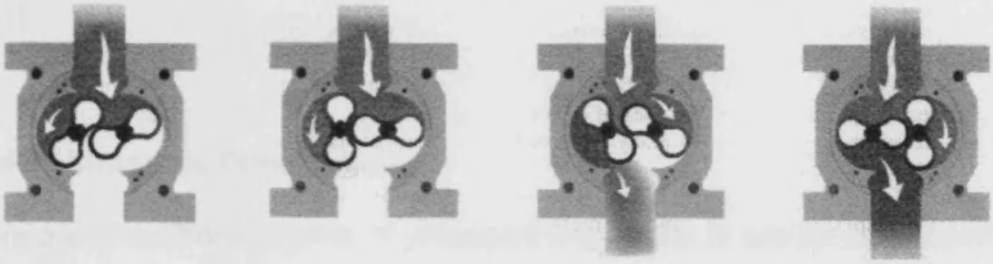

Figure 1.3. A sequence of pictures describing the flow of fluid through a Bi-rotor Displacement flow meter (Barnes & Foran, 2001).

Displacement flow meters produce one of the best performances of all flow measurement devices; they are commonly used as a reference flow meter for the calibration of other flow meters (Furness, 1989). They are generally unaffected by installation conditions but in certain applications filtering of the process liquid is required to ensure the flow meter does not become clogged or damaged. They are expensive to manufacture compared with an orifice plate and also have moving parts that are subject to wear and damage.

1.2.3. Coriolis Mass Flow meters

The coriolis mass flow meter is a very ingenious design of flow meter. In simple terms a liquid is flowed through a bend in a pipe, the coriolis force the liquid exerts onto the tube is then measured. This force can be related to its

mass using Newton's 2nd Law of motion. Measuring mass flow is becoming a more popular form of measurement. The problem with volumetric flow measurement is that the volume is dependent upon the temperature at which it is measured, whereas the mass is independent of temperature (Furness, 1989). Coriolis flow meters are expensive to manufacture and are only generally available in pipe sizes up to 250 mm diameter (Smith and Ruesch, 2001)

1.2.4. Ultrasonic flow meters

There are two different forms of ultrasonic flow meter in use for closed conduit flow measurement (Brown and Lynnworth, 2001).

1.2.4.1. Doppler flow meters

The first form is the Doppler flow meter, which operates on the principle that a sound wave will be reflected off an object. After reflection from a moving object the frequency of the beam is altered. The change in frequency of the reflected beam is related to the velocity of the moving object (Furness, 1989). Doppler flow meters are reliant on moving objects within the flowing liquid; these objects can be solids or gases or even turbulent liquid eddies. Furness (1989) describes Doppler flow meters as flow monitors rather than flow meters and comments that they are largely responsible for giving ultrasonic flow meters a poor reputation. Within a flowing liquid the individual particles will be travelling at different speeds due to their location within the velocity profile. The ultrasonic receiver will be receiving signals containing a range of frequencies. The flow meters associative electronics cannot easily distinguish

between these signals and consequently large measurement errors can be produced.

1.2.4.2. Transmission flow meters

Similarly to Doppler flow meters transmission flow meters also have a transmitter and a receiver, however these flow meters measure the time difference between the transmitted and received beam (Brown and Lynnworth, 2001). Figure 1.4 shows the basic principle of a transmission flow meter.

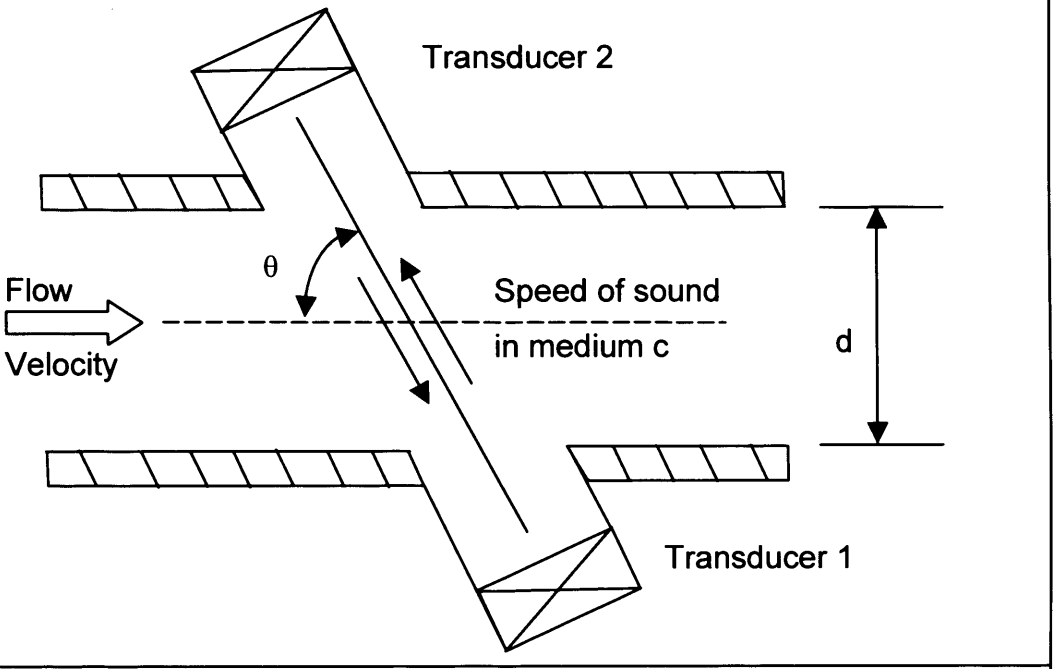

Figure 1.4. Operation of a Transmission flow meter (Furness, 1989)

By referring to figure 1.4 the flow velocity is calculated using equation 1.1 (Furness, 1989).

$$u = \frac{\Delta t.c^2}{2.d.\cos\theta} \qquad (1.1)$$

The exact angle and location within the pipe of the transducers varies depending on the manufacturer and the design of flow meter (Brown and Lynnworth, 2001). The position of the path within the pipe affects the velocity measurement. In the pursuit for more accurate devices multi-path transmission flow meters have been developed that improve the accuracy of measurement with different velocity profiles (Brown and Lynnworth, 2001). Transmission flow meters can be used on gases or liquids but can only be used with clean fluids, as particles will affect the measurement. They are expensive compared with more conventional flow techniques but should become more common in the future as they can be used with almost any pipe size and are a non-invasive measurement device (Furness, 1989).

1.2.5. The Aqueous Electromagnetic flow meter

Michael Faraday discovered electromagnetic induction in 1831; Faraday proved that conductive material moving at right angles to a magnetic field experiences an electromotive force perpendicular to its motion and the magnetic field (Young, Freedman 1996). In the 1920's flow meters using electromagnetic induction were developed, early applications included the measurement of ship speed (Shercliff 1962).

1.2.5.1. Basic Principle of the Electromagnetic Flow meter

The basic construction and design of a commercial electromagnetic flow meter consists of a pair of coils mounted on the top and bottom of an electrically insulated flow tube. A pair of electrodes protrude through the flow tube wall perpendicular to the pipe axes and largely normal to the direction of

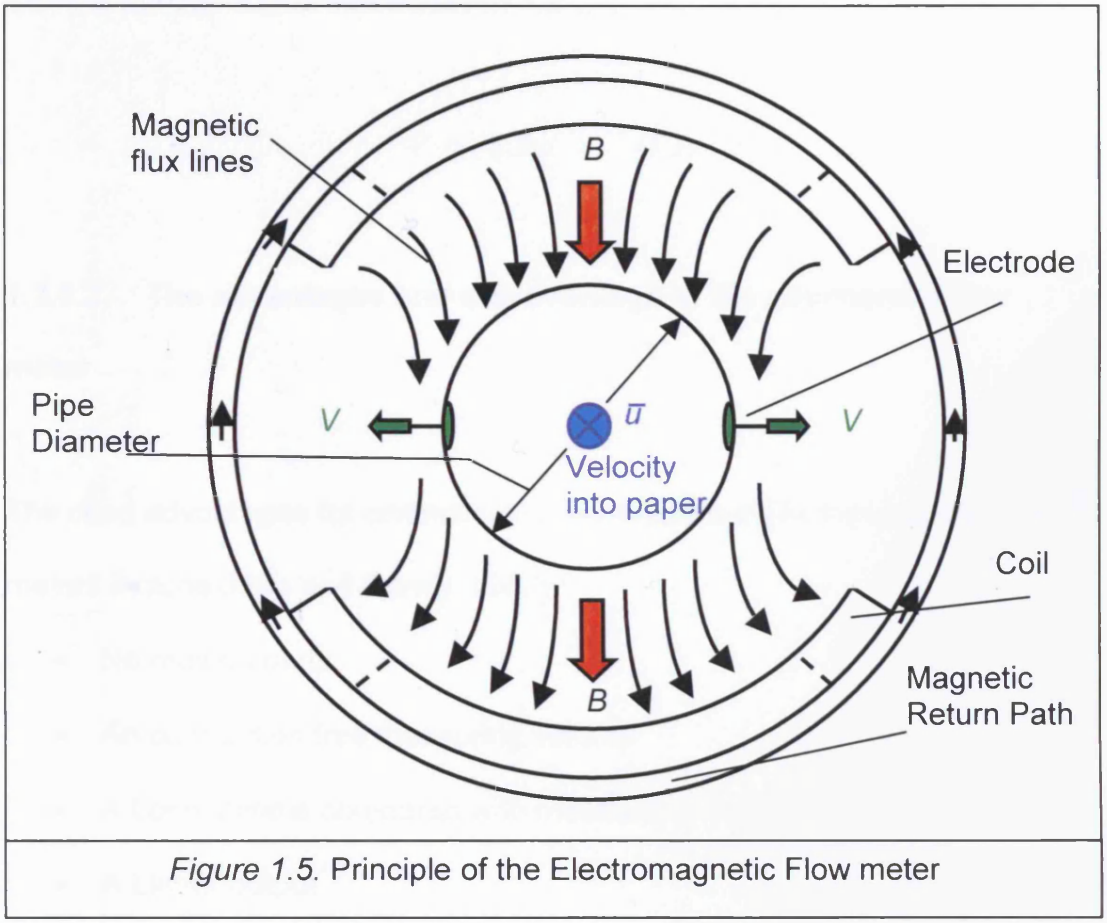

Figure 1.5. Principle of the Electromagnetic Flow meter

the generated magnetic field. As the liquid passes through the pipe, it moves through the magnetic field and the positive and negative ions within the liquid experience a force upon them. The forces on the ions cause them to migrate and result in an electric field being generated across the pipe. The Voltage generated across the pipe is measured between the electrodes, as illustrated in figure 1.5.

In simple terms the potential difference (V) generated at the electrodes is directly proportional to the Magnetic flux density (B) across the pipe, the distance between the electrodes (d) and the average velocity of the liquid running through it ($\overline{u}$), see equation 1.2.

$$V \alpha \overline{u}.B.d \qquad (1.2)$$

1.2.5.2. The advantages and disadvantage of the commercial flow meter

The cited advantages for commercially manufactured Electromagnetic flow meters include (Mills and Doney, 2001):

- No moving parts
- An obstruction free measuring volume
- A Long lifetime compared with mechanical meters
- A Linear output

The limitation is that conventional designs are limited to operating with liquid conductivities of 5 μS/cm, with some special designs operating down to a minimum of 0.01 μS/cm (Mills and Doney, 2001). The reasons for this limitation will be discussed in greater detail in Chapter 2.

1.2.5.3. The Associative Electronics

The flow meter is only half of the total flow measuring system; it requires electronics to drive the field in the coils and detect the flow signal present at the electrodes. The coils are not driven with a D.C. current as D.C. voltages generated in the pipe cause the electrodes to become permanently polarised, leading to spurious measurements (Shercliff 1962). The waveforms used are generally a pulsed square wave or a sinusoidal A.C. wave. Initially manufacturers employed a Sinusoidal waveform, as they could use the local A.C. mains voltage supply. It was also relatively simple to measure the amplitude of the electrode signal. A major problem associated with A.C. systems concerns the stability of the measurement. Since the electrode wiring passes through the magnetic field it can act like the secondary winding in a transformer resulting in a quadrature voltage. Depending on the design, the induced voltages in the measuring circuit can be larger than the flow measurement itself. The quadrature voltages can be nullified during the meters calibration, this is commonly referred to as zero calibration. The magnitude of the quadrature voltage is proportional to the square of the frequency, consequently the higher the frequency the worse the zero errors. The quadrature voltage is not necessarily stable with time due to environmental changes such as temperature. The resulting change in the flow meter output (which is independent of flow) is known as zero drift. The zero drift affects the overall accuracy of the flow measurement and in the manufacturers pursuit for more accurate products the A.C. system has largely been replaced with a pulsed D.C. or square waveform.

An example of an A.C. waveform is shown in figure 1.6. The voltage generated at the electrodes lags behind the drive waveform due to the generation of eddy currents within the flow meter construction. By laminating the iron circuit the eddy currents can be reduced.

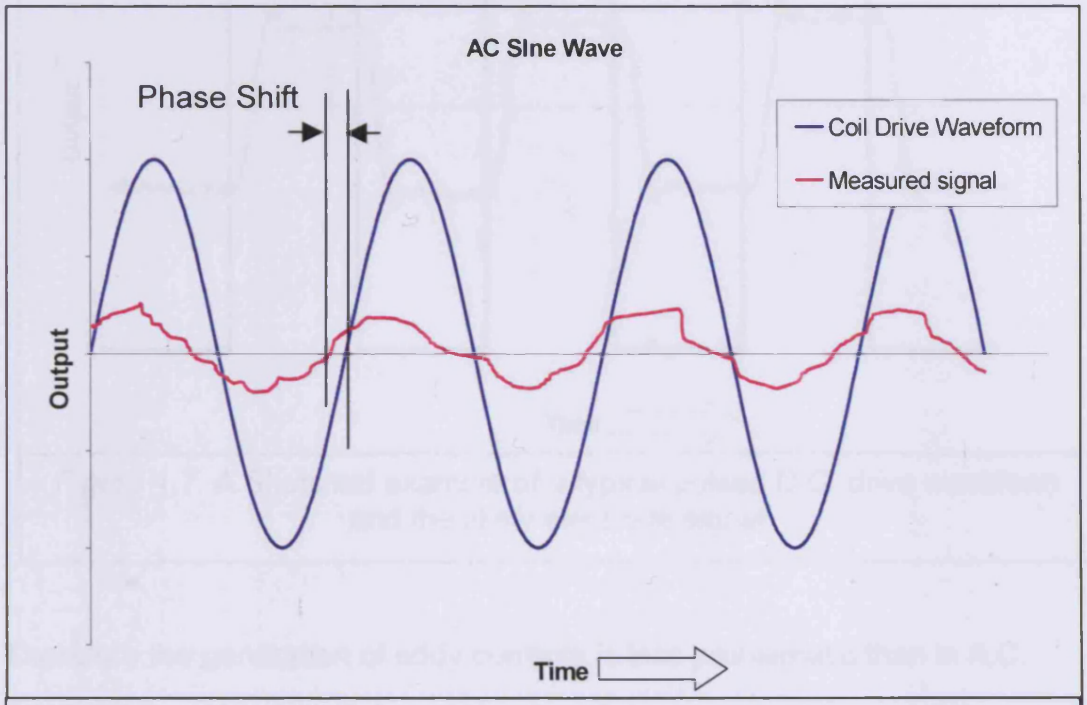

Figure 1.6. A sketched example of an A.C. drive waveform and the likely flow signal

The effective coil drive frequency of a pulsed D.C. system is typically 6Hz (Asquith, 2003a) compared with an A.C. system, which is typically between 50 to 70 Hz (Schwiderski, 2003).

In a pulsed D.C. flow meter system the actual measurement takes place after the magnetic field has stabilised as shown in figure 1.7.

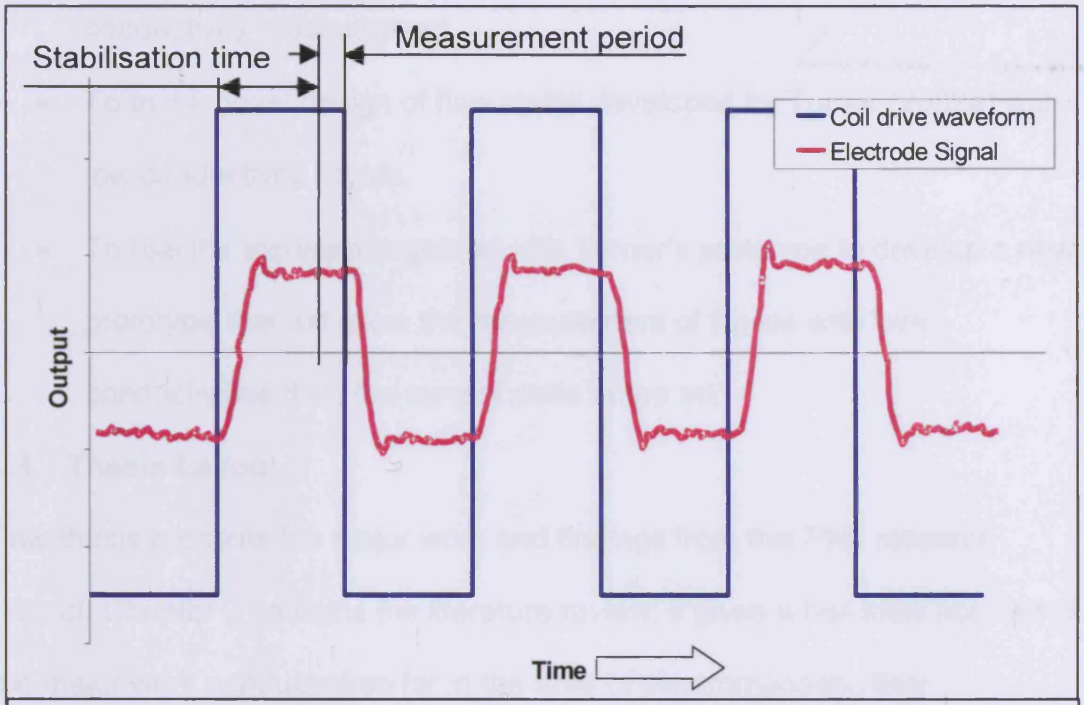

Figure 1.7. A Sketched example of a typical pulsed D.C. drive waveform and the likely electrode signal

Therefore the generation of eddy currents is less problematic than in A.C. measuring systems.

1.3. Discussion

This completes a brief description of some of the different flow metering techniques. An introduction to the electromagnetic flow meter and the methods of operation has been given. The main limitation of the electromagnetic flow meter is considered to be its inability to measure low conductivity liquids.

The main objectives of this project are therefore:

- To gain an understanding of the problems associated with low conductivity measurement.
- To test a novel design of flow meter developed by Turner (2002a) with low conductivity liquids.
- To use the experience gained with Turner's prototype to develop a new prototype that will allow the measurement of liquids with lower conductivities than the current state of the art.

1.4. Thesis Layout

This thesis presents the major work and findings from this PhD research project. Chapter 2 contains the literature review; it gives a historical account of the major work conducted so far in the area of electromagnetic flow measurement with respect to low conductivity liquids. In chapter 3 the construction and testing of Turner's prototype is described. The performance with low conductivity liquids is presented and the perceived limitations for measuring low conductivity liquids discussed. Chapter 4 presents the theoretical and experimental work conducted using the weight function process. Different geometries of flow meter are explored with a view to improving low conductivity flow measurement. In chapter 5 the development of a new flow meter is described and a description of the electronics used to operate the flowmeter is given. Chapter 6 contains the major results from testing the new flow meter system with different conductivity liquids. Finally chapter 7 lists the major conclusions from this research project and makes recommendations for further work.

Chapter 2

Literature Review

2.1. Introduction

Published research into the development of the dielectric flow meter has largely emanated from the work of Cushing of Engineering-Physics Co (EPCO). Cushing (1958) derived the governing equations for predicting the signal amplitude or attenuation when operating with either conducting or insulating fluids. Cushing et al (1962, 1964, 1965) designed, built and tested flow meters for use with cryogenic fluids and also dielectric liquids such as oil. Cushing (1974, 1999, 2002) continued his research into dielectric flow meters and has produced numerous scientific papers, reports and patents; some of which will be discussed in greater detail later.

Research by other scientists has also taken place including Amare (1995), who researched the use of dielectric liquids on Electromagnetic flow meters and reported the successful measurement of a dielectric liquid. Durcan (1998) continued the research work conducted by Amare (1995) and also produced a working prototype that measured dielectric liquids. A team from Cranfield University (in association with Fischer & Porter/ABB Limited) were tasked to characterise the noise generation means associated with dielectric flow measurement. The group released a series of scientific papers detailing their work in predicting the behaviour of a flow meter under a number of conditions (Hemp et al, 2002; Rosales et al, 2002a, 2002b; Hemp and Young, 2003; Rosales and Sanderson, 2003).

The work that inspired this project was conducted by Turner (2002, 2003 & 2005). A recent patent by Turner (2005) describes a flow meter design that could improve the measurement quality when used with lower conductivity liquids.

2.2. Electromagnetic Induction in Insulators

Faraday's original experiment involved rotating a metal disc perpendicular to a magnetic field, the device, known as a Faraday disc dynamo, measured a potential difference between the disc axle and the circumference of the disc (Young and Freedman, 1996). Within a moving conductor there are ions or charges that can move freely under the influence of a magnetic field. An insulating material or a dielectric material (as it is sometimes called) is a material that has no free ions and does not readily conduct electricity. In 1904, Wilson produced a Faraday disc dynamo with a dielectric disc, and like Faraday he also measured a potential difference (Wilson, 1905). When a changing magnetic field is applied to a dielectric material its charges begin to move but are bounded to their respective molecule (Cushing, 1999). Each molecule within the dielectric material exhibits a net charge and the material becomes polarised (Young and Freedman, 1996). An illustration of the polarisation of a moving insulator under the influence of a magnetic field is shown in figure 2.1

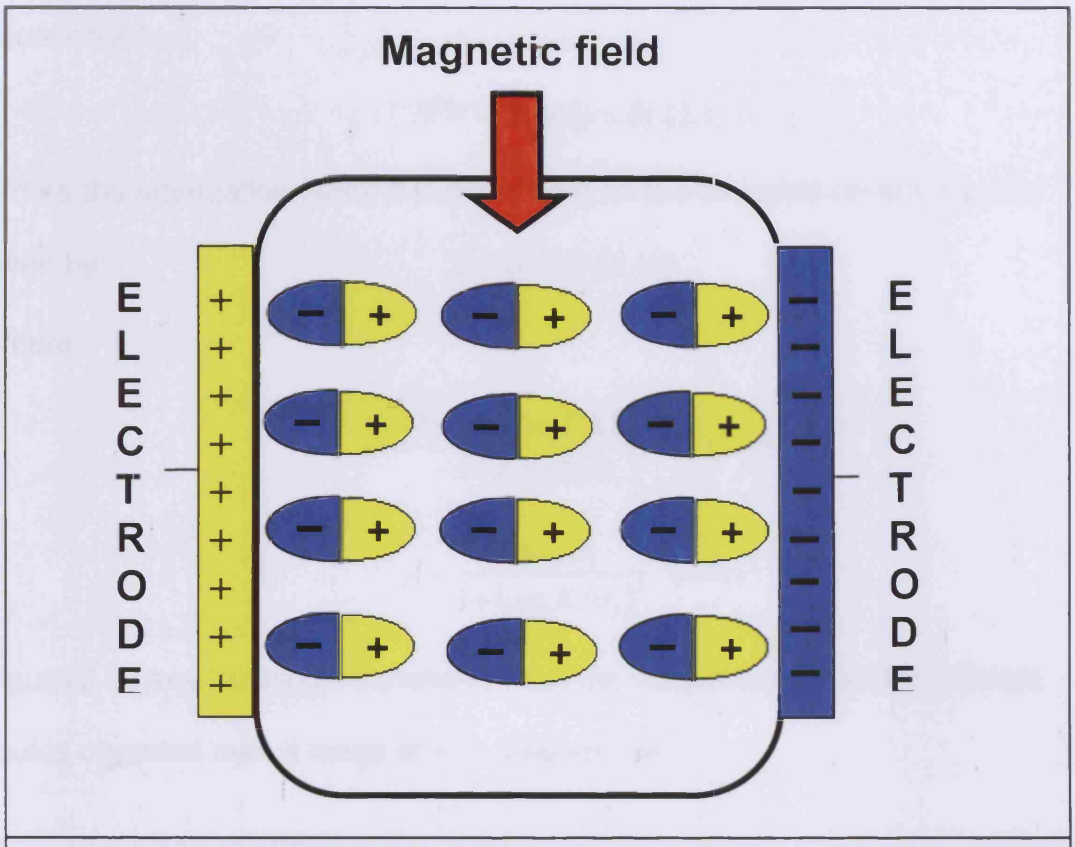

Figure 2.1. Polarisation of a moving dielectric under the influence of a magnetic field

The insulating properties of a material are defined by the dielectric constant. The dielectric constant represents the capacitance ratio of two identical capacitors, one with an insulating material between the plates and one with a vacuum between the plates (Young and Freedman, 1996).

2.3. A Summary of Cushing's work

Cushing (1958) derived an equation relating the output potential of any flow meter design, operated with any fluid, to the flow velocity as shown in equation 2.1:

$$\nabla^2 V = Z.div(u \times B) \quad (2.1)$$

Where the attenuation factor Z is dependent on the dielectric constant and is given by:

$$Z = \alpha + i\beta \quad (2.1a)$$

Where:

$$\alpha = \frac{1+(\omega\varepsilon_0/\sigma_1)^2 K(K-1)}{1+(\omega\varepsilon_0 K/\sigma_1)^2} \quad (2.1b)$$

$$\beta = \frac{\omega\varepsilon_0/\sigma_1}{1+(\omega\varepsilon_0 K/\sigma_1)^2} \quad (2.1c)$$

Figure 2.2 uses Cushing's equation to plot the attenuation factor for different liquids operated over a range of A.C. frequencies.

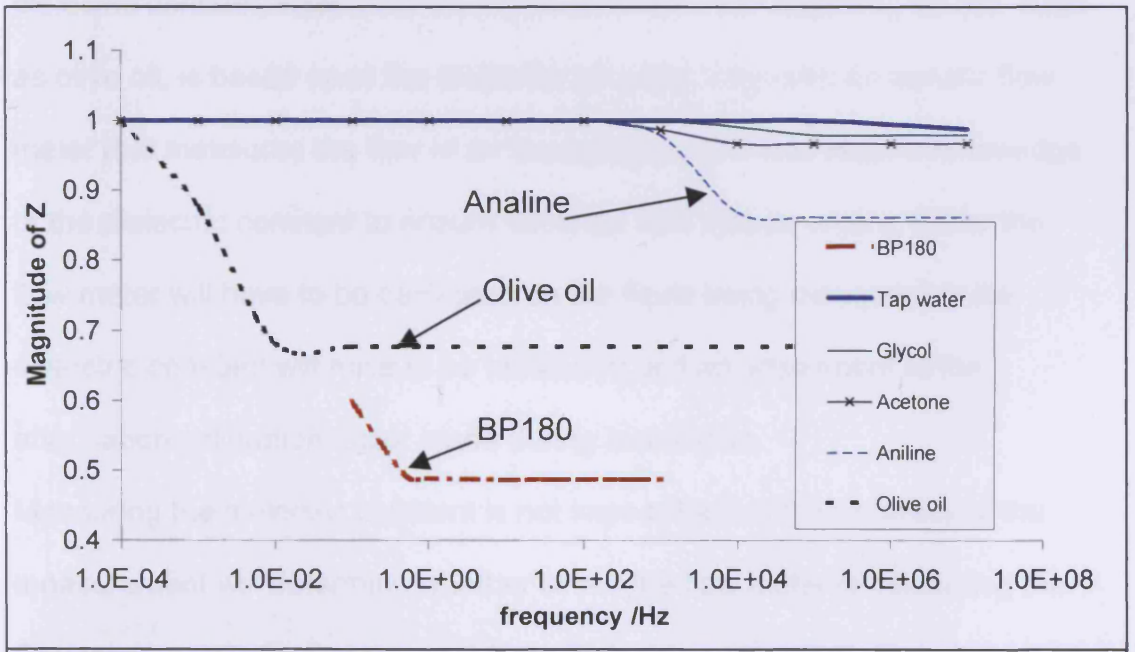

Figure 2.2. Graph of Attenuation factor for different liquids

Figure 2.2 shows that the flow rate of tap water, Glycol and Acetone can be measured using a flow meter which is operating at frequencies nearing 1 kHz without any signal degradation. These liquids are conductive liquids and contain free ions, which move freely under the influence of the magnetic field. At frequencies greater than 1 kHz conduction currents are not formed, instead the potential is generated based upon the polarisation of the molecules. As these conductive liquids are not very good insulators, their dielectric constants are relatively high, for example water (of any conductivity), K = 81 (Kaye and Laby, 1989), compared with a good insulator BP180 Dielectric oil, K = 2.0 (Amare, 1995). Therefore the higher the dielectric constant the closer the signal attenuation remains to unity. With the insulating liquid BP180 Dielectric oil, where there are no free ions, the potential generated at frequencies above 1 Hz is based upon the polarisation of the molecules. The attenuation of BP180 at 100 Hz is lower than olive oil (K = 3.1 (Cushing, 1958)) because its dielectric constant is less. As the signal attenuation of insulating liquids, such as olive oil, is based upon the dielectric constant, any electromagnetic flow meter that measures the flow of an insulating liquid would require knowledge of the dielectric constant to ensure accurate flow measurement. Either the flow meter will have to be calibrated on the liquid being measured or the dielectric constant will have to be measured and an adjustment to the attenuation calibration factor made during installation.

Measuring the dielectric constant is not impossible but the accuracy of the measurement will determine whether or not the flow meter is measuring the flow rate accurately. For example if the dielectric constant of olive oil were to

change from 3.1 to 3.0 the attenuation factor changes by 1.6 %. For the electromagnetic flow meter to compete in this market it will need to be at least as accurate as alternative established measuring devices. Orifice plates are accurate within a tolerance of ± 0.6 % of measured flow rate (Hussain, 2001). Therefore the Electromagnetic flow meter has to be able to cope with small changes in dielectric constant.

Cushing et al (1962) reported the successful flow measurement of a dielectric liquid. The flow meter had a 25 mm diameter bore composite flow tube consisting of an inner Teflon liner with two separate fibreglass outer layers. The two Sensing electrodes were attached to the outer surface of the Teflon tube. They were 50 mm long and subtended a half angle (β) of 70°. A 5 mm thick fibreglass tube was wound over the top of the electrodes. The driven screens were positioned on the outer surface of the fibreglass layer; and were 127 mm long subtending a half angle (β) of 75°. A second 4 mm thick tube of fibreglass was wound over the top of the driven screens and an outer ground screen of length 152 mm was wrapped around the tube and covered 359° of the circumference.

To reduce eddy currents the electrodes and driven screens were formed from a number of vertical strands of wire connected to a horizontal bus bar as illustrated in figure 2.3.

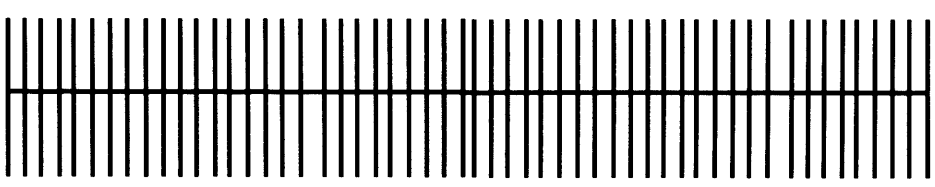

Figure 2.3. Cushing et al (1962) Electrode design

The flow meter was operated with an A.C. coil drive frequency of 10 kHz. The magnetic circuit consisted of two saddle coils approximately 100 mm long with 57 turns of wire. A cylindrical powdered iron magnetic return circuit was positioned around the outside of the coils.

The report concentrates on the design of the system and although they comment on successfully measuring a flow signal the report does not provide a plot of the flow signal detailing the quality of the measurement. They do comment on the stability problems associated with operating at such a high frequency saying that the quadrature voltage was unstable with time.

In 1964 Cushing et al (1964) reported their findings in developing an A.C. flow meter for use with liquid hydrogen. Liquid hydrogen has a dielectric constant of approximately 1.25, this compared with the oil measured previously having a dielectric constant of 2.2 (Cushing et al 1962). The novel approach taken to tackle the stability problems found previously involved using one of the diametrically opposed electrodes to measure the flow signal whilst the other was driven with a signal equal in magnitude but opposite in polarity to the quadrature voltage. The flow tube was 25 mm in diameter. The electrodes were photo etched onto both sides of a copper clad double-sided Mylar sheet. The electrode was 102 mm long with a half angle (β) of 70° and the driven screen was 152 mm long with a half angle (β) of 80°. A screening layer covered a length of 267 mm over the entire circumference of the tube.

Cushing et al (1964) reported that they were successful in their objectives and a graph within the report shows a flow signal, which is linear with changing flow rate. The zero stability was found to be problematic due to changes in

dielectric constant of the fibreglass with temperature. They claimed that once thermal equilibrium was reached the zero stability improved and the sensor became repeatable.

The true stability of the flow meter cannot have been as good as Cushing had hoped as later on Cushing (1971) presented a paper detailing the design of another flow meter which had a conductive liner. He argued that producing a flow meter with no "transformer voltage" affect was impossible. The proposed frequency of operation for this latest prototype was 1 kHz. The chosen frequency was as high as possible without the unstable quadrature voltage becoming problematic and as high as possible to be outside the major noise amplitude present in turbulent insulating liquid flows.

2.4. Summary of Amare's Work

Amare's PhD thesis (1995) described his experimental work in measuring the flow of an insulating liquid (BP180). The sensor design consisted of a flow tube manufactured from a 50 mm outside diameter Perspex pipe of length 375 mm. The capacitive electrodes were assembled on the outside surface of the pipe. They were manufactured using a flexible printed circuit board and were similar in design to those of Cushing et al (1962) shown in figure 2.3. Amare (1995) also had a frame surrounding the electrode, which could be driven to reduce capacitive losses, as shown in figure 2.4.

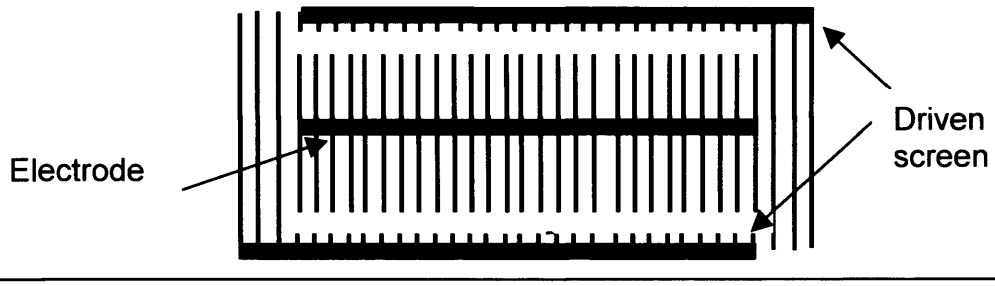

Figure 2.4. Amare (1995) electrode design

The electrode was 72 mm long with a half angle (β) of 60° and the screen was 100 mm long with a half angle (β) of 85°. The frequency of operation was 1.5 kHz. The magnetic circuit consisted of two air-cored coils with no magnetic return path. Amare reported the successful measurement of a dielectric oil (BP180), but found that zero stability was problematic.

2.5. Summary of Durcan's Work

Durcan's (1998) PhD thesis did not become available to study until the latter stages of this research and had no bearing on the work carried out, however as he was successful in measuring the flow of a dielectric liquid his research is worth briefly discussing.

Durcan's (1998) PhD thesis describes how he re-tested Amare's prototype and critically analysed the performance of the prototype when tested on dielectric oil. Durcan investigated the stability of the measurement and used Amare's prototype as the foundation for producing a more stable flow meter. Durcan's prototype was designed to operate at a frequency of 1.37 kHz compared with Amare's 1.5 kHz. According to Durcan this reduced the

quadrature voltage by 8.6 %. The capacitive electrodes were identical to those used by Amare. When tested the flow meter still suffered from stability problems due to the unstable quadrature voltages generated through operating at high frequencies.

2.6. Characterisation of the noise generated within a dielectric liquid.

A paper by Hemp et al (2002) investigated the experimentally measured noise generated when dielectric oil was flowed through a current sensing capacitive electrode flow meter. They investigated the performance of an electrode of length 36 mm, subtending a half angle (β) of 22°. They found that the noise spectra shape was distinctive, as shown in figure 2.5.

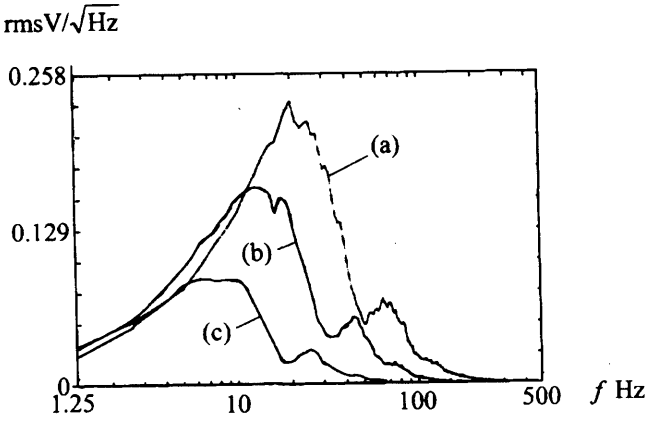

Figure 2.5. Experimentally measured noise spectra. (a) u = 1.65 m/s; (b) u = 1.15 m/s; (c) u = 0.78 m/s. Taken from Hemp et al 2002.

Figure 2.5 shows that the noise spectra has a dominant peak followed by a secondary smaller peak before the noise decays in what looks to be an exponential fashion. Hemp et al (2002) claimed that the frequency at the

minima between the two peaks occurs at approximately the mean flow velocity / electrode length.

The effect on the measured noise spectrum with varying electrode dimensions was investigated; the following electrode dimensions were tested:

1) Electrode length l = 36 mm and half angle $\beta = 22°$
2) Electrode length l = 140 mm and half angle $\beta = 22°$
3) Electrode length l = 140 mm and half angle β close to 90°

Hemp et al (2002) found that by increasing the electrode length the bandwidth of the noise at low frequencies narrows and the amplitude increases but at higher frequencies the amplitude is not affected by the electrode geometry. Based upon their experimentation they concluded that the geometry of the electrode does not have a significant effect upon the noise magnitudes. To increase the signal level they recommended using a current sensing large area electrode with a magnetic field extending over the entire length of the electrode. They believed that this might allow a flow meter to be designed that could operate at a frequency as low as 200 Hz.

Rosales and Sanderson (2003) produced a very good explanation of the different noise mechanisms that are present in conductive flows, these are:

- Turbulent eddies within the flow generating irregular voltages.
- Particles within the flow impacting the electrode.
- Disruptions in the charge layer close to the surface of the pipe wall.

As an aqueous liquid flows through a pipe a particular ionic species is adsorbed onto the pipe wall. Ions of an opposing charge are then attracted towards the wall causing a double layer or diffuse charge layer. This charge layer causes streaming currents or electrification within the liquid. If the flow is turbulent then the boundary layer at the wall is disturbed and so is the diffuse charge layer. Disturbances in the charge layer vary the magnitude of the streaming currents travelling along the wall of the pipe. As a consequence of disturbances in the charged layer the potential sensed by the electrodes is noisier than expected due to the influence of the modulated streaming currents. Abedian and Sonin (1982) derived an expression for the convection current in turbulent pipe flow. They describe previously defined ideas such as the Debye length (λ_D), which is the distance the charged layer (caused by electrification of the wall) extends into a laminar flow. The Debye length (λ_D) is given in equation 2.2 and is inversely proportional to the liquid conductivity (σ).

$$\lambda_D = \left(\frac{\varepsilon_r D}{\sigma} \right)^{1/2} \qquad (2.2)$$

Abedian and Sonin applied the idea of the debye length (λ_D) to turbulent flows. For aqueous liquids the charged layer is only present near the wall and does not protrude as far as the laminar sub-layer thickness (δ). For low conductivity liquids the charged layer extends beyond the laminar sub-layer

thickness (δ). In figure 2.6 an illustration of the difference between the charge distribution in a conducting and insulating medium is given.

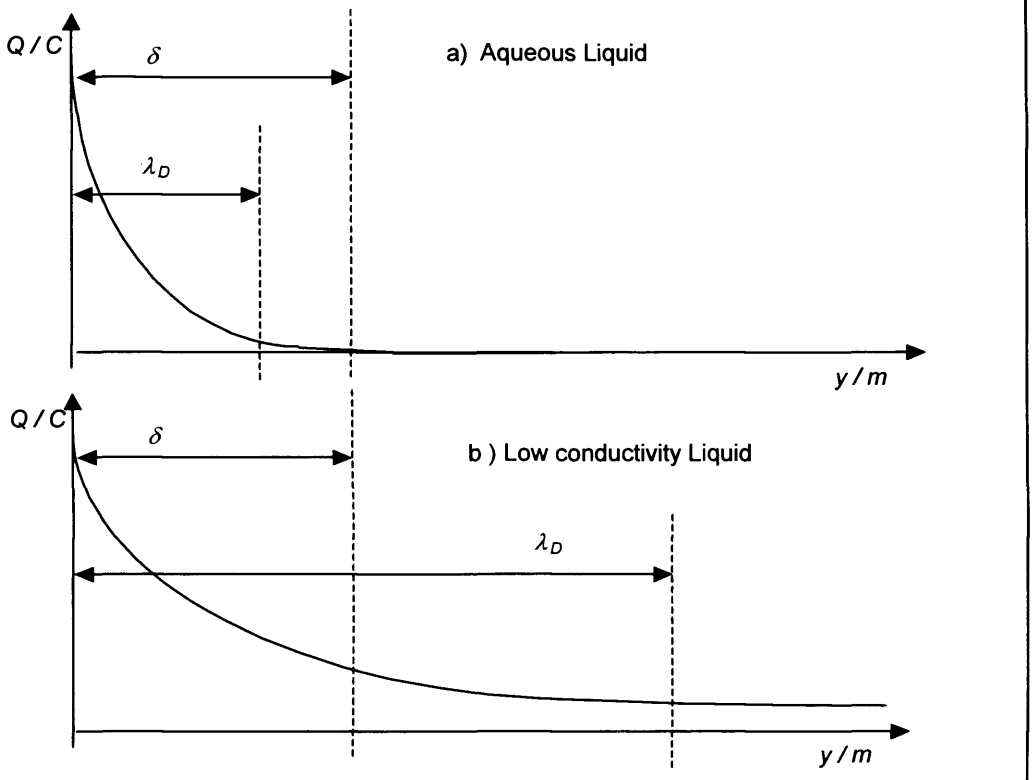

Figure 2.6. Charge distribution in the region near the pipe wall for turbulent flow conditions compared with the laminar sub-layer thickness for a) an Aqueous liquid and b) a Low conductivity liquid, taken from Abedian and Sonin (1982)

In low conductivity liquids turbulent flows will inevitably induce modulation of the charge layer but steady laminar flow would not. The modulation of this charged layer was experimentally verified by Hemp et al (2002) by adjusting

the flow between laminar and turbulent flow and observing a high increase in noise amplitude as the flow became turbulent.

An additional noise mechanism present with insulating liquids is caused by small charged particles (typically 10 μm in diameter) inducing charge onto the electrode (Rosales and Sanderson 2003). Cushing et al (1962) had previously observed a similar noise spectrum to figure 2.5. They theorised that the noise was related to frictional forces within the flow caused by foreign particles acquiring charge through not following the streamlines of the liquid. Filtering the oil made a significant improvement in noise level as the filtering removed some of the particles present in the oil (Hemp et al 2002). Rosales et al (2002b) modelled the effect of charged particles within the flow and concluded that the charged particles induced signals onto the electrode plates and further more that the charged particles produced noise levels, which dominated over the turbulent fluctuations.

2.7. A summary of Turner's Theoretical Work

A patent by Turner (2006) describes a flow meter design having a long magnetic field and a long electrode. Conventional flow meters have a coil length approximately 0.9 times the pipe diameter with point contact electrodes. Turner claims that this new design of sensor will have a lower source impedance compared to conventional sensors when used with low conductivity liquids. A lower source impedance will result in an improvement in the signal to noise ratio. Turner (2002a) describes the analysis by Shercliff (1962) in predicting the potential distribution at any position within an

insulated duct subjected to a uniform magnetic field. Referring to the diagram in figure 2.7 expressions for the potential distribution inside and outside the field region were calculated.

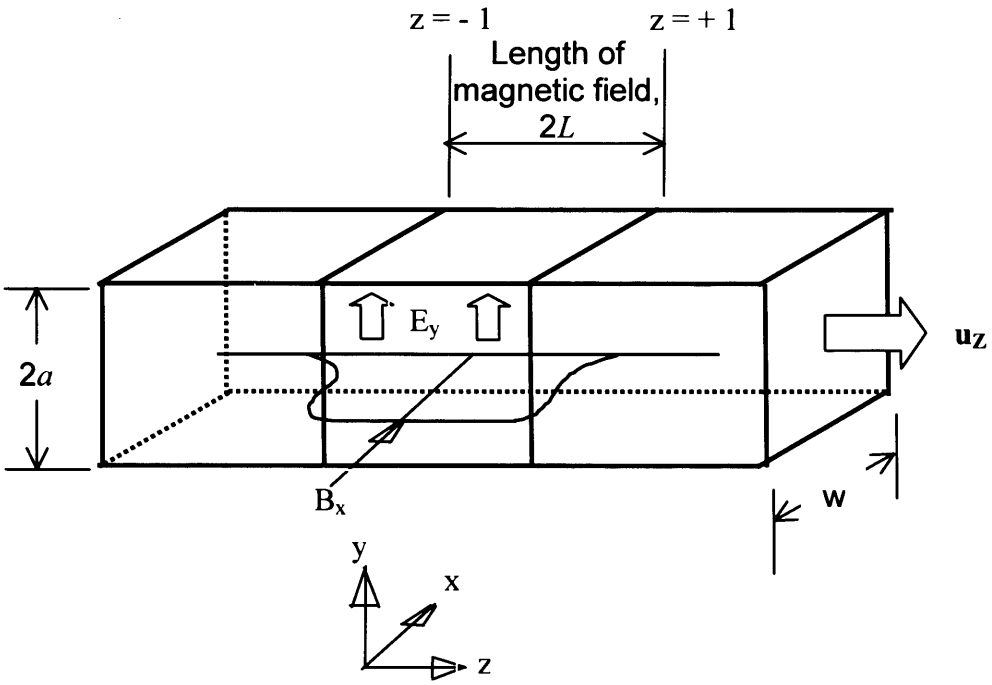

Figure 2.7. Layout within a rectangular duct Electromagnetic flowmeter

Within the field region (-1 < z < 1):

$$V = u_Z B_X a\left\{\frac{y}{a} + \frac{8}{\pi^2}\sum_{n=1,3,5,\ldots}\frac{(-1)^{(n+1)/2}}{n^2}\cdot\cosh\frac{n\pi z}{2a}\cdot\exp\frac{-n\pi L}{2a}\cdot\sin\frac{n\pi y}{2a}\right\} \quad \text{-(2.3)}$$

Outside the field region (z > 1 and z <-1):

$$V = -u_Z B_X a \frac{8}{\pi^2} \sum_{n=1,3,5,\ldots} \frac{(-1)^{(n+1)/2}}{n^2} \cdot \sinh \frac{n\pi L}{2a} \cdot \exp \frac{-n\pi z}{2a} \cdot \sin \frac{n\pi y}{2a} \quad \text{- (2.4)}$$

Through differentiating equations 2.3 and 2.4 and applying Ohm's law the currents that will circulate at the ends of the magnetic field region (figure 2.8) and the total resistance within the MHD generator can be calculated.

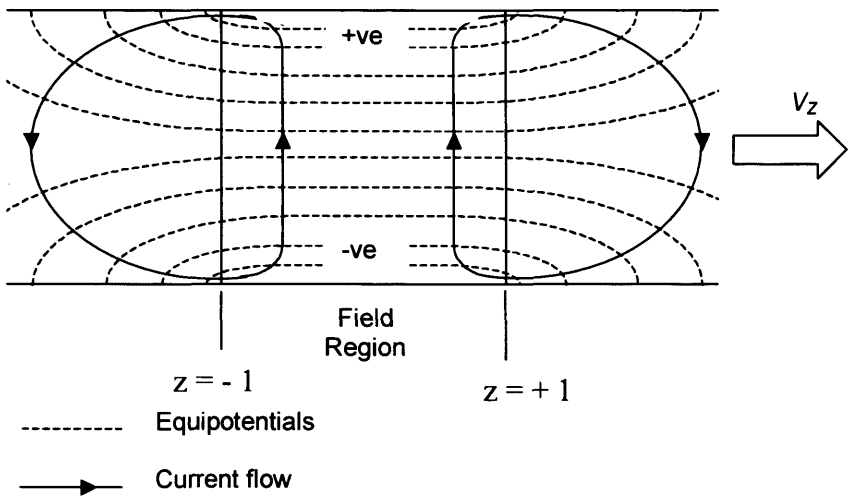

Figure 2.8. A 2-dimensional representation of the potentials generated across the bore of a rectangular duct and the subsequent current flows at either end of the flow meter.

The total resistance, $R_t = \frac{1}{\sigma w} \cdot \frac{1}{\sum_{n=1,3,5,\ldots} \frac{(-1)^{(n+1)/2}}{n^2} \left(1 - \exp \frac{-nhL}{a}\right)}$ - (2.5)

Turner (2002a) uses equation 2.5 to predict the affect of changing the length of the magnetic field region. He found that with a field region greater in length than the electrode separation (L/a > 1) the total resistance is approximately constant.

The resistance associated with the circulating currents at the end of the magnetic field are given by equation 2.6.

$$R_e = \frac{2.69}{\sigma w} \quad \text{- (2.6)}$$

R_e is independent of the length of the magnetic field.

By subtracting the total resistance from the end resistance the source impedance of the generator is given by equation 2.7.

$$R_t - R_e = R_s \approx \frac{1}{\sigma} \cdot \frac{a}{wL} \quad \text{- (2.7)}$$

From this equation it is clear that the cross-sectional dimensions of the duct and the length of the magnetic field influence the source impedance of the generator. Therefore by decreasing the height of the duct or increasing either the magnetic field length or the duct width improvements in the source impedance can be realised. Turner concentrated his research on the effect of changing the length of the magnetic field.

Turner (2002a) argued that the electrode impedance dominated the measurement and that improvements in source impedance through extending the magnetic field will have little effect, without changing the electrode geometry as well.

The electrode resistance for a circular electrode was stated by Turner (2002a) as:

$$R_0 = \frac{2}{\pi \sigma d} \qquad (2.8)$$

A 5 mm diameter electrode in water of conductivity 5 μS/cm has a resistance of approximately 255 kΩ. For comparison the source impedance for a DN50 flow meter with a magnetic field length of 0.25 m is 8 kΩ (Turner 2002a). To

achieve a suitable improvement in impedance measurement the electrode resistance needs to be reduced. This can be achieved by making the electrode area larger and specifically in Turner's analysis by making the electrode longer in the flow direction. Turner (2002a) derived an equation for a line electrode as equation 2.9.

$$R_l = \frac{1}{\pi\sigma l}\log_e\left(\frac{2S}{d}\right) \qquad (2.9)$$

For an electrode of height 8 mm and length 250 mm in a 50 mm bore tube the electrode resistance is 6.43 kΩ. Thus taking advantage of the lower source impedance produced through an elongate magnetic field.

Turner also claimed that an elongate electrode would have a lower noise spectrum than a short electrode when measuring turbulent flows (Turner, 2002b). Eddies within the flow contain charge and as these charged eddies pass over the electrode they modulate the distributed charge layer near the electrode surface, thus generating a noise voltage. Turner (2002b) postulated that as the electrode length increases the charge modulation still occurs however the eddy will be passing over a smaller proportion of the electrode surface thus the noise voltage is averaged over the length of the electrode.

2.8. Discussion

The work published by Cushing et al (1962), Amare (1995) and Durkin (1998) proved that measuring the flow of a dielectric is possible albeit at a frequency of operation where stability issues become problematic. Hemp et al (2002) described the noise mechanisms associated with a flowing dielectric and proposed that by increasing the length of the magnetic field and the area of

the electrode that a higher signal level can be achieved. Turner (2002a) has conducted some theoretical research, which support the views of Hemp et al (2002) but recommends using a line electrode with a long magnetic field. The research conducted by Turner was restricted to contact electrodes where there was a direct resistive path between the electrode surface and the liquid. The work conducted by Hemp et al (2002), Cushing et al (1962), Amare (1995) and Durkin (1998) used capacitive coupled electrodes where the flow tube was between the measuring electrode and the liquid being measured. Based on this literature review research into the benefits of increasing the length of the field region and the size of the electrode will be conducted with the aim of measuring lower conductivity liquids than is presently capable.

Chapter 3

Construction and testing of Turner's prototype

3.1. Introduction

The work of Turner (2002a), reviewed in Chapter 2, was based upon a theoretical analysis. To understand whether the proposed idea of lengthening the field and electrode in the flow direction improves low conductivity measurement some experimentation was required. A prototype flow meter designed by Turner will be discussed along with the experimental testing performed using water and demineralised water. For comparison the same tests were performed on a conventional flow meter operating under the same test conditions.

3.2. Turner's Prototype

The design consisted of a flow tube manufactured from a 400 mm length of DN50 stainless steel pipe with a PN16 Stainless steel flange welded at each end. The flow tube was designed to be insulated from the process liquid using a 4 mm thick Nitrile rubber lining. Nitrile rubber was chosen, as it is chemically compatible with oils, unlike the more common rubber liner materials such as EPDM or Butyl rubber (PDL Handbook Series 1994). The company used to line the flow tube were unable to get the Nitrile to bond adequately. It was essential that the two materials were bonded, as the rubber was flexible and could move about the pipe. If the rubber was allowed to move there was a risk

that it would tear or could affect the accuracy of the flow meter. The author adapted the original design to allow the use of an alternative lining material. The chosen liner material was a rigid PTFE lining. A tube of PTFE that was larger in outside diameter than the bore of the stainless steel pipe was force fitted into the tube. PTFE linings are not bonded to the metal work; instead they rely on an interference fit between the metal tube and the PTFE to keep the lining in the desired position.Once the tube had been inserted the ends of the PTFE tube were stretched to form a flange sealing face. PTFE has an elastic memory and to ensure the PTFE end faces stayed in position additional lining protection flanges were designed by the author (as shown in figure 3.1).

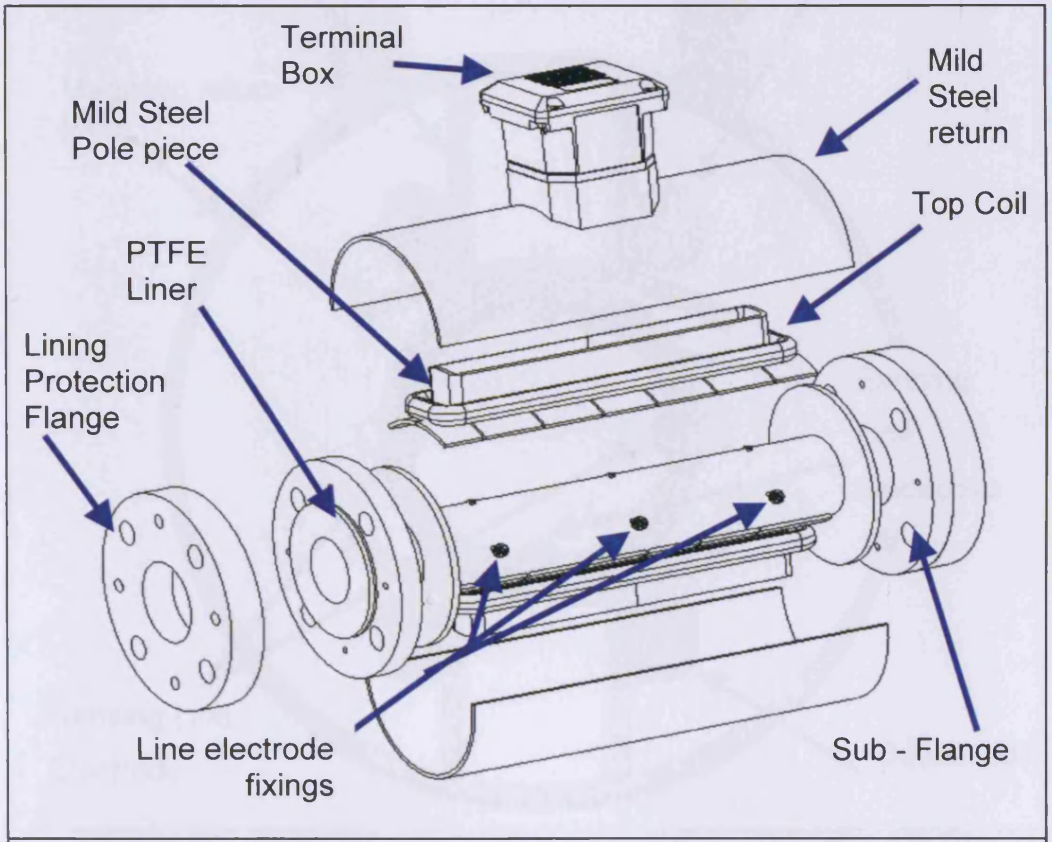

Figure 3.1. An exploded view of Turner's prototype

The electrodes were manufactured by milling a 250 mm long, 8 mm diameter Stainless steel rod into a semicircular cross section. As illustrated in figure 3.2 there were two sensing electrodes located in the horizontal plane and two earthing electrodes in the vertical plane.

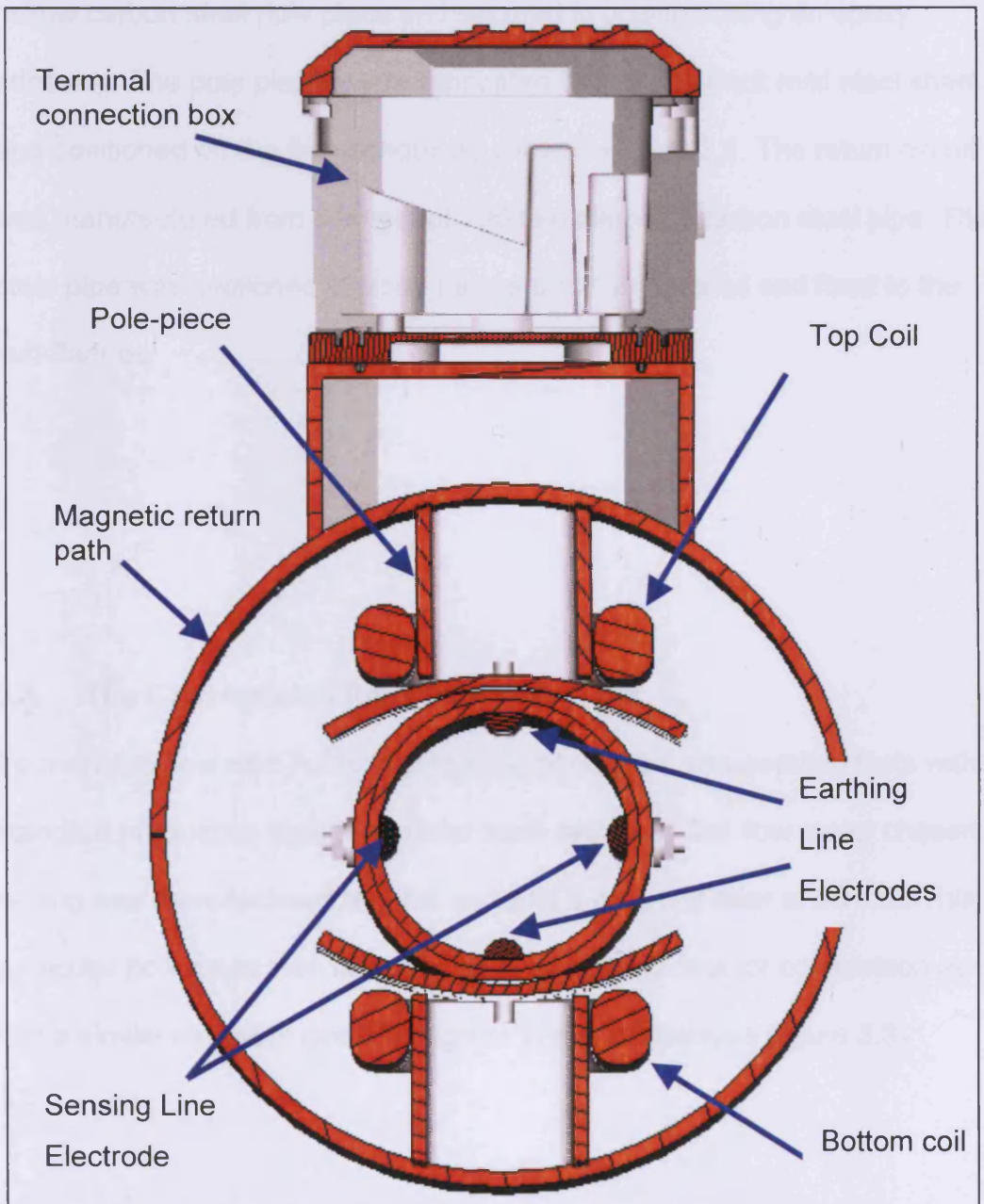

Figure 3.2. A Cross-sectional view through the centre of Turner's prototype

Two elongated flat wound coils connected in series produced the magnetic field; each coil contained 300 turns of wire. The coils were positioned above and below the tube; each coil was located over the top of an elongate but hollow carbon steel pole piece and secured in position using an epoxy adhesive. The pole pieces were fabricated from 3 mm thick mild steel sheet and positioned on the flow conduit as shown in figure 3.1. The return circuit was manufactured from a length of 100 mm diameter carbon steel pipe. The steel pipe was sectioned into two halves and then located and fixed to the sub-flanges.

3.3. The Conventional Reference flow meter

To measure how well Turner's prototype performed, comparative tests with a standard production style flow meter were required. The flow meter chosen for testing was manufactured by ABB and had a bore diameter of 50 mm. This particular flow meter was identified as a good candidate for comparison as it had a similar magnetic circuit design to Turner's prototype (figure 3.3).

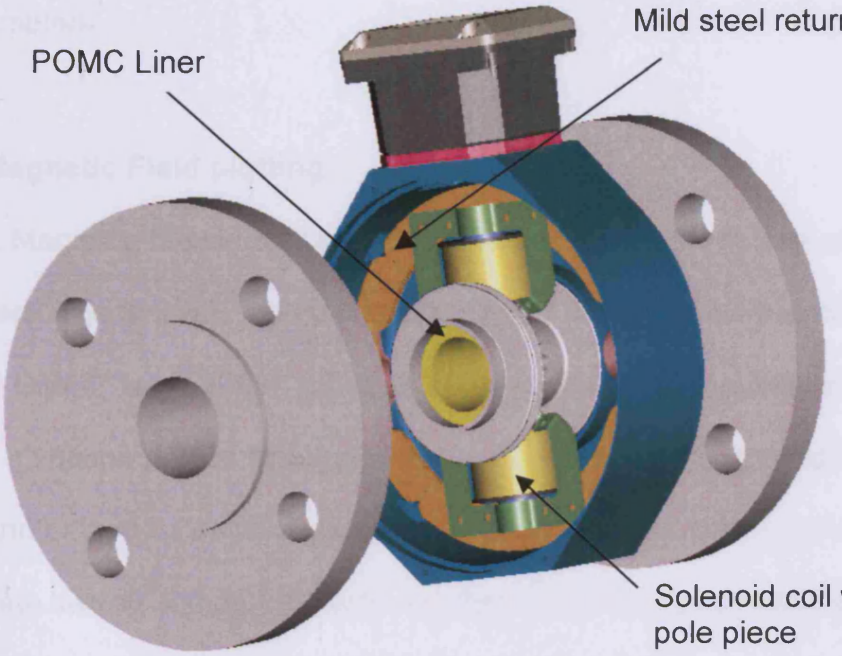

Figure 3.3. A three-dimensional picture of the ABB DN50 Reference flow meter with part of the housing removed

The flow meter consisted of a 90mm long cast stainless steel centre tube, which was lined with a 5 mm thick Acetal polymer tube. Attached to either end of the measuring section was a stainless steel flange. There were two 5 mm diameter sensing electrodes located in the horizontal plane, the circular electrodes protruded through the wall of the plastic tube and were positioned slightly proud of the tube bore. The magnetic circuit comprised of two solenoid coils having 740 turns each. The coils were positioned above and below the measuring tube; they were located over the top of a 4 mm thick carbon steel pole piece, which was connected to a mild steel return circuit.

3.4. Testing Turner's prototype and the reference flow meter

A series of experiments were designed for comparing the performance of the two flow meters.

3.4.1. Magnetic Field plotting

The D.C. Magnetic flux density was measured along the centre line of both flow meters. The flux was measured using a Hall probe, which was connected to a Hirst GM04 Gaussmeter. A hall probe is a piece of semi-conductor which registers a voltage across its edges when a magnetic field is applied through the top and bottom faces (Hirst Magnetic Instruments Ltd. 2006). To conduct an accurate sweep of measurements the flow meter was positioned on V-blocks on top of a traversing table. The flow meter was then moved relative to the hall probe. A picture of the experimental set-up is shown in figure 3.4.

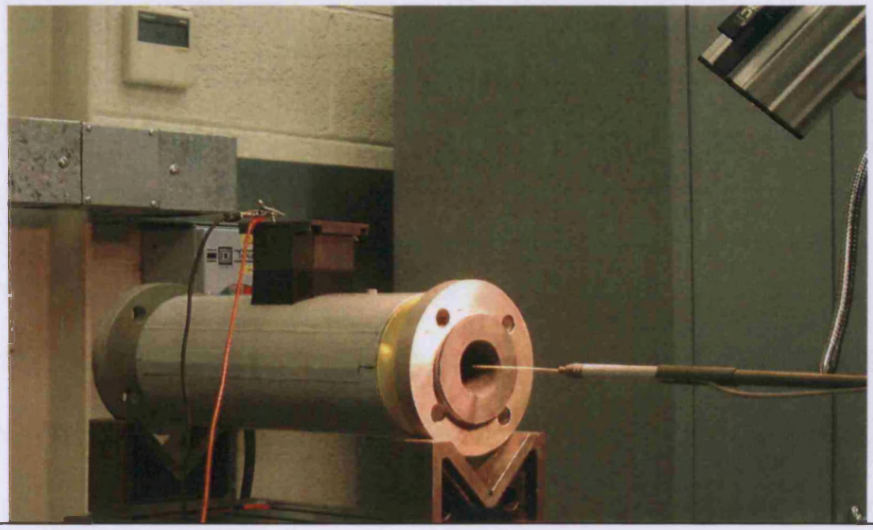

Figure 3.4. Measuring the field pattern along the centreline of Turners prototype

The traverse was adjusted so that the hall probe was in line with the axis of the pipe; the coils were energised with 0.5 Amps current using a Thurlby PL310 D.C. power supply. The flow meter was then moved relative to the probe and measurements were taken at 5 mm increments throughout the flow meter. The test results for Turner's prototype and the reference flow meter are shown in figure 3.5.

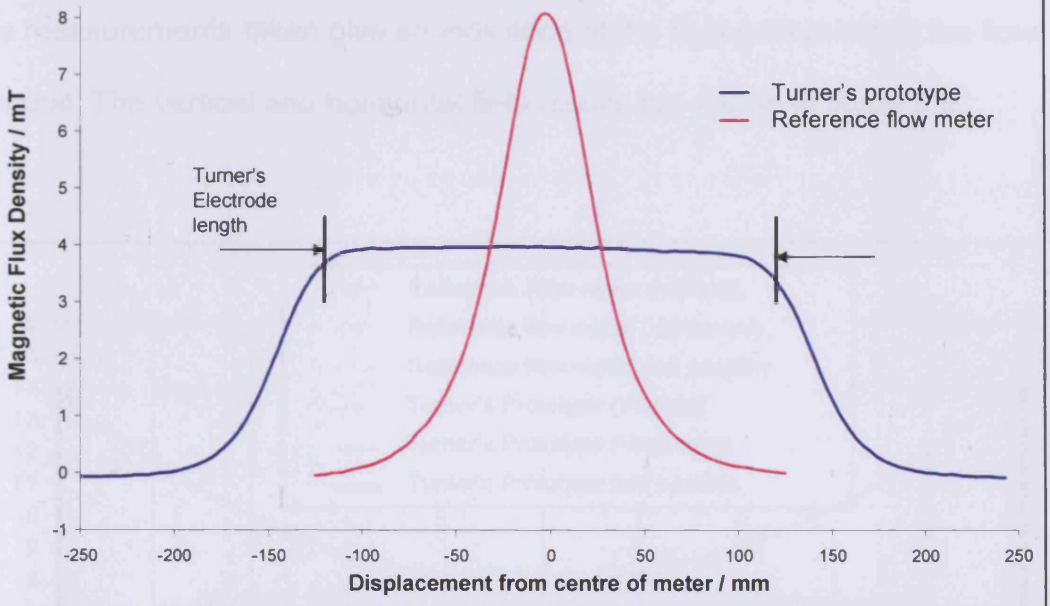

Figure 3.5. Field plot along the pipe axis of both flow meters, The expanded uncertainty = 0.08 mT with 95 % confidence level

The results in figure 3.5 show that Turner's prototype has a much longer field than the reference flow meter; the flux is uniform for approximately 200 mm before it diminishes whereas the reference flow meter has no field of uniformity. The results show that the field is already beginning to drop towards the ends of the electrodes. The magnitude of the uniform field is approximately 4 mT in Turner's prototype compared with a maximum flux of 8.1 mT in the reference flow meter. The number of turns is proportional to the

generated flux level, therefore the field strength of the reference flow meter is greater than Turner's prototype because the coils in the reference flow meter have more turns on them.

Measurements of the vertical and horizontal field at the mid-point of the flow meters were also recorded. Performing vertical and horizontal measurements in the centre of Turner's prototype was difficult as the probe housing made it impossible to measure the field at the wall of the pipe. Despite this problem the measurements taken give an indication of the field pattern within the flow conduit. The vertical and horizontal field results are shown in figure 3.6.

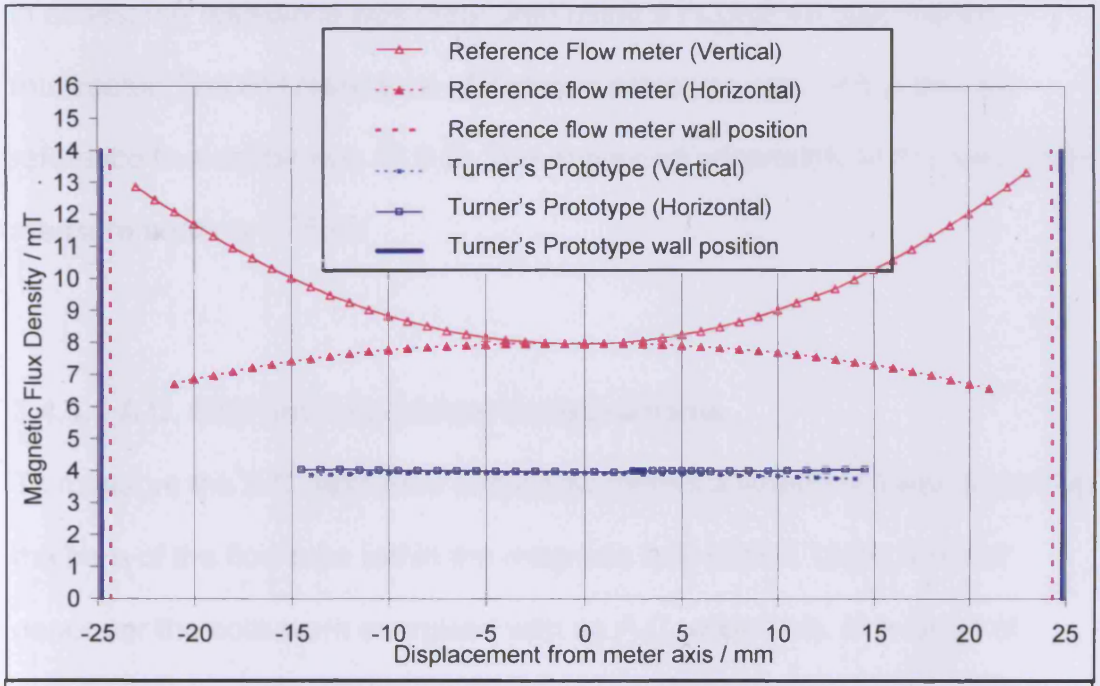

Figure 3.6. Field strength measured horizontally and vertically across the bore at the centre of both flow meters.
The y-axis expanded uncertainty = 0.08 mT with 95 % confidence level
The x-axis expanded uncertainty = 0.5 mm with 95 % confidence level

The results in figure 3.6 show that the field within the bore of Turner's prototype is uniform in the region measured. The field measured at the centre

of the reference flow meter is non-uniform in the horizontal and vertical planes with 17 % and 64 % variation respectively. The difference in flux magnitudes is predominantly due to the greater number of turns in the reference flow meter compared with Turner's prototype.. The shape of the field in the horizontal and vertical axis is related to the shape of the pole pieces and the geometry of the magnetic circuit.

3.4.2. Coil resistance measurements

To measure the coil resistance the coils in both flow meters were connected in series; the resistance was measured using a FLUKE 45 dual display multimeter. The coil resistance of Turner's prototype was 19.5 Ω and the reference flow meter was 13.9 Ω. The expanded uncertainty of the resistance measurements is 0.05 Ω.

3.4.3. A.C. field and impedance measurements

To measure the A.C. response of the flow meters a search coil was placed up the bore of the flow tube within the magnetic field region. Using a signal generator the coils were energised with an A.C. waveform. At a range of frequencies the voltage in the search coil was measured. The voltage and current in the flow meter coils were also recorded. From these measurements the current normalised magnetic flux density was calculated and the results are shown in figure 3.7.

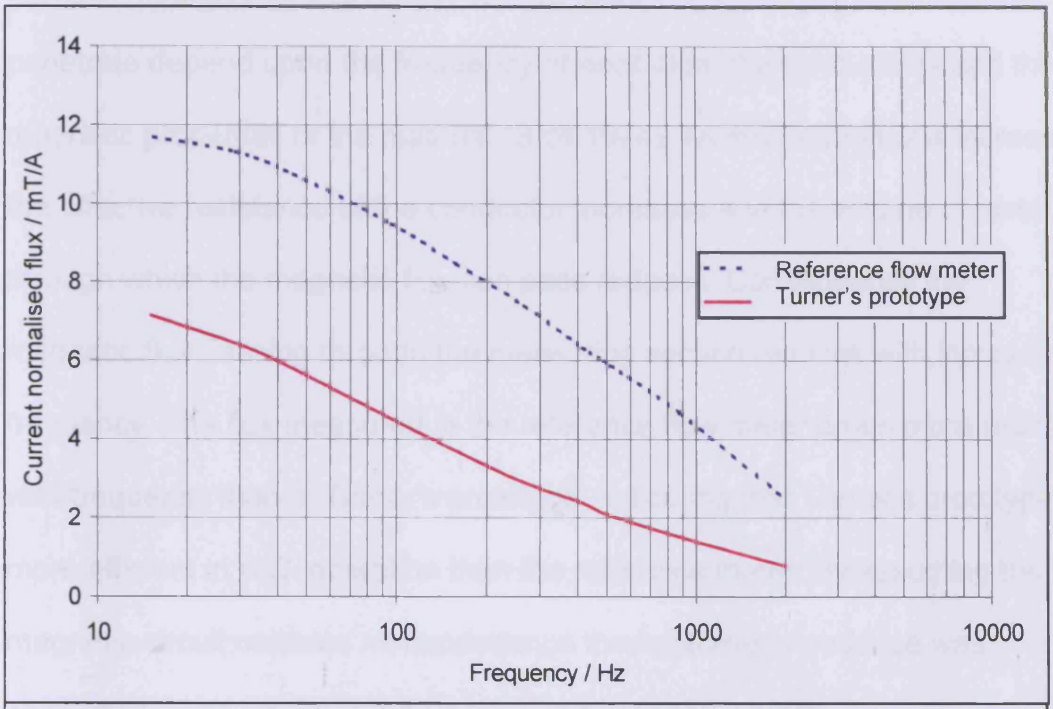

Figure 3.7. A.C. Field Strength for the reference flow meter and Turner's prototype.
The expanded uncertainty = 0.7 % with 95 % confidence level.

Figure 3.7 shows that the reference flow meter generates a larger flux per unit current than Turner's prototype. For operation with A.C. and D.C. current the number of turns in the coils is proportional to the magnetic field strength therefore as the reference flow meter has more turns than Turner's prototype a higher flux per unit current is generated. As the frequency increases the measured flux reduces. Within all A.C. magnetic circuits there are energy losses, these losses are predominantly related to resistance, hysteresis and eddy current losses (Young and Freedman 1996). The magnetic circuits in

both flow meters were not designed to operate efficiently with A.C. waveforms. When the changing magnetic field intersects the iron circuit (and the metallic flow tube), circulating eddy currents are generated within the material. These eddy currents produce a magnetic field that opposes the external magnetic field (Stoll 1974). The depths to which the eddy currents penetrate depend upon the frequency of excitation, the conductivity and the magnetic properties of the material (Stoll 1974). As the frequency is increased the effective resistance of the conductor increases and the volume of metal through which the magnetic flux can pass reduces. Consequently the magnetic flux passing through the measuring section reduces with increasing frequency. The flux measured in the reference flow meter drops more rapidly with frequency than in Turner's prototype, indicating that Turner's prototype is more efficient in A.C. operation than the reference meter. By assuming the magnetic circuit contains no capacitance the inductive impedance was calculated using equation 3.1 (Young and Freedman 1996).

$$V = I\sqrt{R^2 + \omega L} \qquad (3.1)$$

The phase angle was calculated using equation 3.2.

$$\phi = \arctan\left(\frac{\omega L}{R}\right) \qquad (3.2)$$

The inductive impedance and the phase angle of the flow meters are plotted against frequency in figure 3.8.

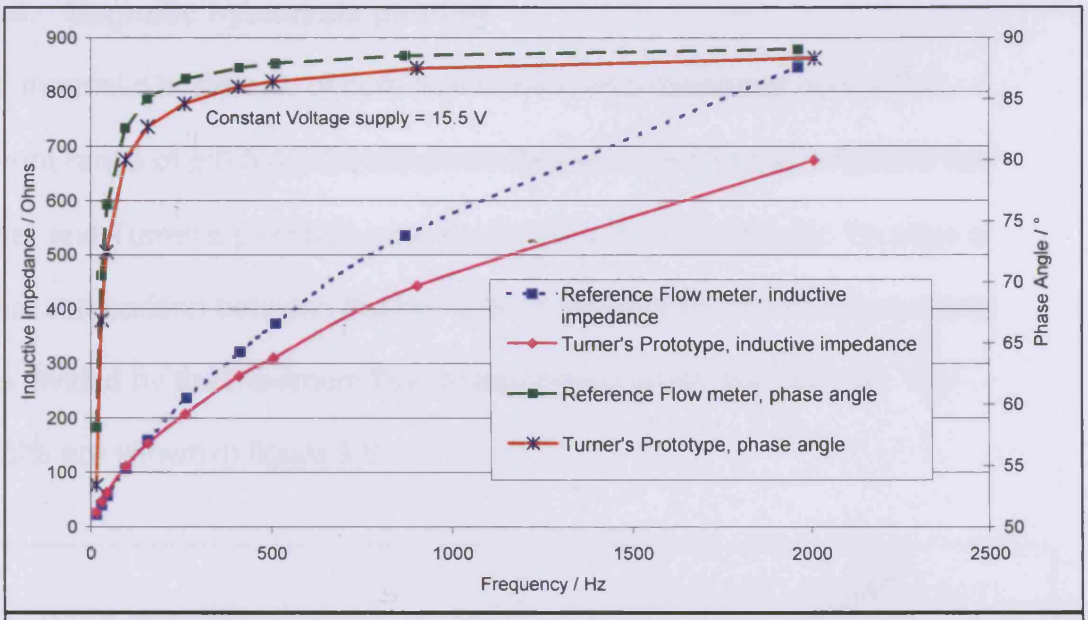

Figure 3.8. The Inductive Impedance and phase angle against Frequency. The expanded uncertainty = 0.7 % with 95 % confidence level.

Figure 3.8 shows that as the frequency increases the phase angle tends towards 90° and the inductive impedance dominates over the resistance. A pure resistor is in phase with the current whereas a pure inductor is 90° out of phase with the current (Young and Freedman 1996). An inductor opposes variations in current and the graph shows that as the frequency increases it becomes more difficult to drive current through the coils. At frequencies above 200 Hz the reference flow meter will have less ampturns than Turner's prototype for a given drive voltage. The results in figure 3.7 show that the current normalised flux in the reference flow meter is greater than Turner's prototype. However the results in figure 3.8 show that with a constant voltage supply Turner's prototype allows more current to flow with frequencies greater than 200 Hz. The current is proportional to the magnetic field strength therefore Turner's prototype will operate more efficiently at higher frequencies.

3.4.4. Magnetic hysteresis plotting

The magnetic hysteresis of both flow meters was measured over a D.C. current range of ± 0.5 A. The maximum flux recorded for the reference flow meter and Turner's prototype was 8 mT and 4 mT respectively. To allow a direct comparison between the two sets of results each flux measurements was divided by the maximum flux measurement within the data set. The results are shown in figure 3.9.

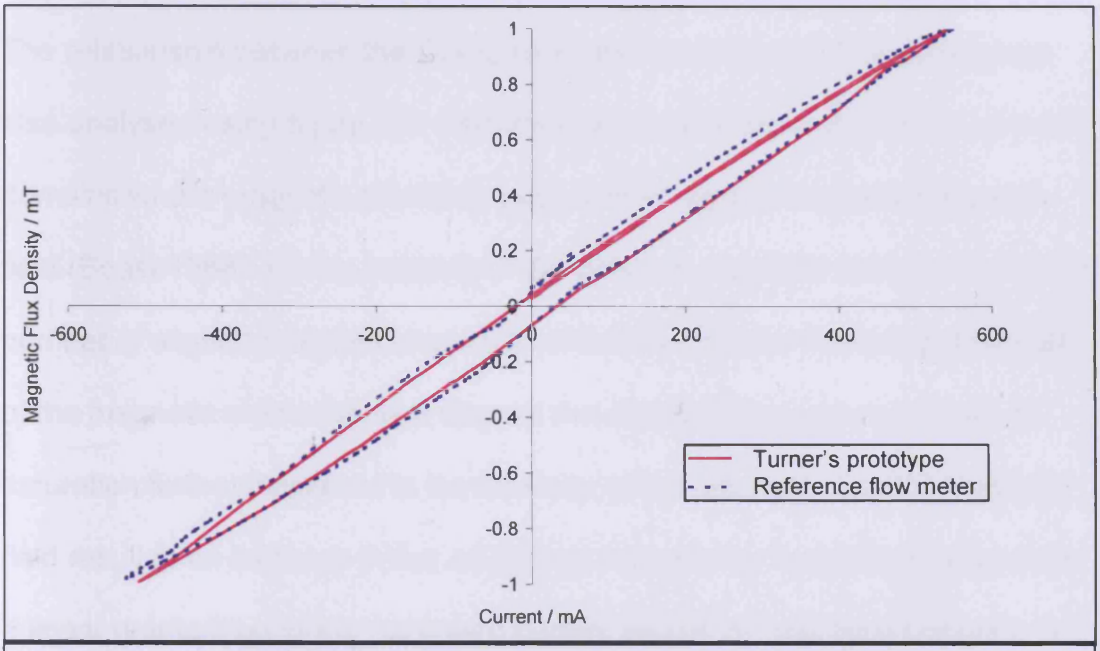

Figure 3.9. Magnetic hysteresis plots for Turner's prototype and the Reference flow meter.
The expanded uncertainty = 1 % with 95 % confidence level

The results show that with no current supplied to the coils some magnetic flux density was measured. When the external field supplied by the coils is removed the iron circuit retains some of the field and remains magnetized (Young and Freedman 1996). The level of magnetization or remanent flux density is calculated by measuring the difference between the flux

measurements where the trace crosses 0 mA. In both circuits some remanence was measured suggesting a degree of magnetisation. The raw data showed that the reference flow meter has a remanent flux of 1 mT whereas Turner's flow meter has 0.5 mT. The area within the loop represents the amount of energy lost during a cycle, therefore the lower the remanence the better. As the reference flow meter generates almost double the flux for the same current, as Turner's prototype there is not much difference in remanence between the flow meters.

The relationship between the Coil current and the magnetic flux density was also analysed using figure 3.9. Ferromagnetic materials such as iron, contain domains where magnetic moments align with an applied external magnetic field (Boast 1964). As the intensity of the external magnetic field increases the number of aligned magnetic moments within the material increases. Once all of the magnetic moments have aligned the material becomes saturated. At saturation further increases in the intensity of the externally applied magnetic field result in an increase in flux as seen in free space. Turner's prototype has a linear gradient up to the maximum current tested; its operating current is 0.5 A therefore the design is fit for purpose. The reference flow meter has a linear gradient up to a current of approximately 0.4 A, above this value saturation is occurring somewhere within the magnetic circuit. The reference flow meter was also designed to operate at 0.5 A and for this reason the reference flow meter is a poorer design than Turner's prototype.

3.4.5. Flow testing

The flow testing was conducted in ABB's flow laboratory at Stonehouse, UK. Testing was conducted on water and demineralised water. Testing on water was conducted using two different flow rigs, a NAMAS approved flow rig and a demineralised water rig. The NAMAS rig was used to analyse the linearity of the two flow meters. It makes use of a large sump located beneath the floor of the factory. The electrical conductivity of this water is 400 μS/cm. This rig is very accurate at measuring low flow rates and was used specifically for characterising the flow meters performance. The demineralised water rig was used to compare the measurement quality in terms of noise levels with different conductivities of water. This rig has a sump, which can be filled with either water or demineralised water. Flow tests were conducted over a more restricted flow range, because of the limitations of the rig. The NAMAS and the demineralised water rig both use gravimetric measurements to calculate the flow rate of the water and they have the same basic design. A diagram illustrating the basic layout of the gravimetric flow calibration rig is given in figure 3.10.

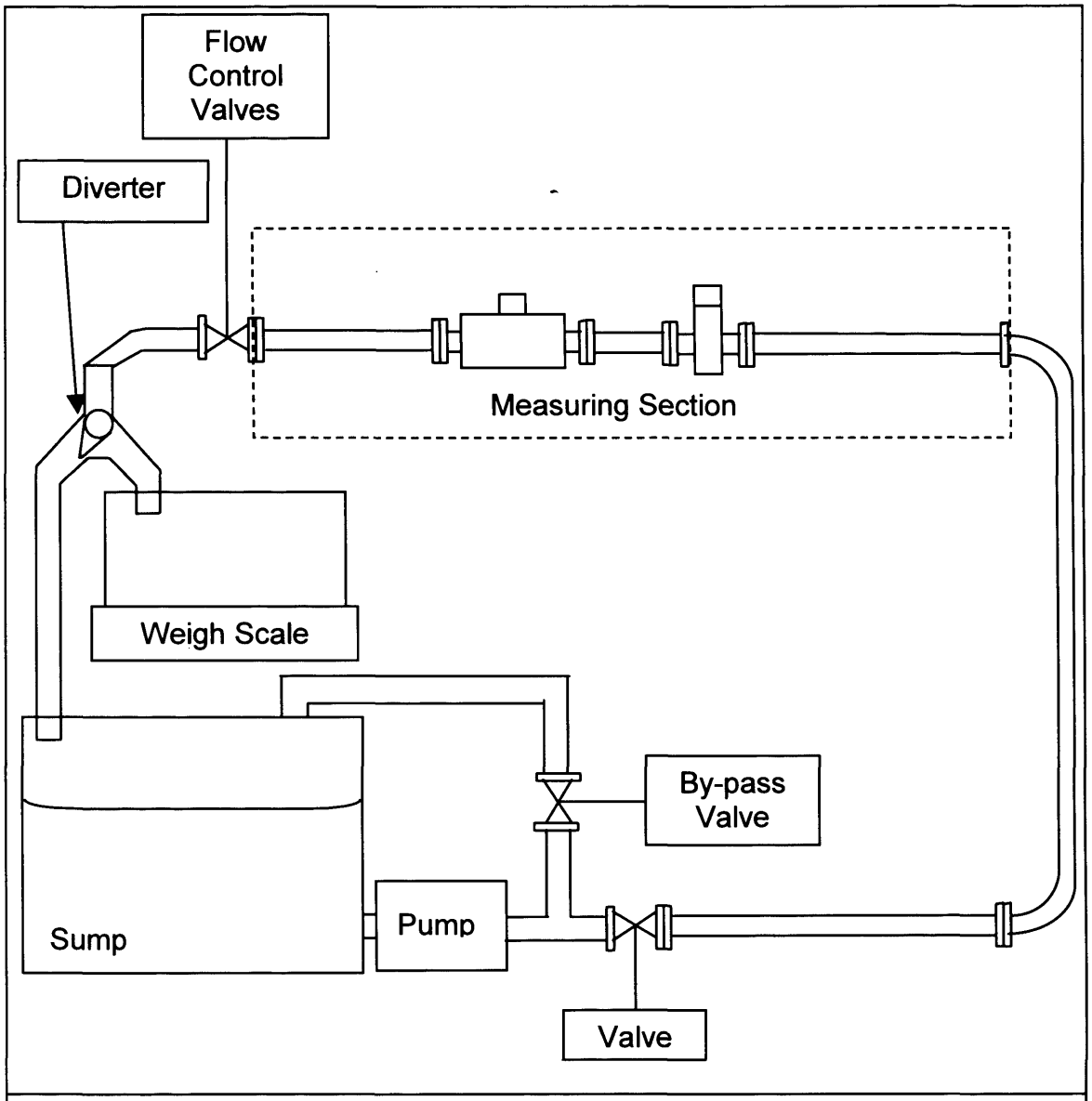

Figure 3.10. A Diagram of a generic gravimetric flow rig

The rig consists of a pump connected to a sump, which drives water around a loop of pipe work. Within the loop of pipe work is a straight section of pipe work known as the measuring section in which the flow meters are installed for testing. Both flow rigs are designed in accordance with ISO 9368-1:1990 to ensure flow disturbances do not adversely affect the measurement of the flow meters under test. The measuring section in the NAMAS rig consists of 32

diameters of upstream pipe work and 12 diameters of downstream pipe work. The demineralised water rig measuring section has 24 diameters upstream and 12 diameters downstream of the flow meter. After the measuring section the pipe work is connected to a valve, which is used in conjunction with the variable speed pump to control the flow rate. A T-piece just after the pump allows water to be by-passed directly back into the sump giving even more control over the line pressure and flow rate. Having passed through the flow control valve the water passes to a diverter valve, which normally returns the water back into the sump.

When a measurement of volumetric flow rate was required the water was diverted into a weigh tank. The time taken to fill the tank, the mass of water collected and the temperature of the process liquid were measured and recorded. By knowing the temperature of the water its density can be calculated and used to convert the mass of water into a volume.

The volumetric flow rate was calculated using equation 3.3.

$$Q_V = \frac{m}{\rho_D t} \qquad (3.3)$$

The flow meters were connected to standard ABB flow meter transmitters called MagMaster's. The MagMaster drives the flow meter coils with a pulsed D.C. waveform and then measures the voltage generated at the electrodes. The MagMaster transmitter converts the electrode voltage into a measurement of velocity. It uses an RS232 output to send the velocity or flow rate measurements once every second to a computer. The flow rate measurements were recorded and stored as text files. The text files were imported into Microsoft Excel where the data could be processed. The flow

rate measurements from the MagMaster were recorded for the time it takes to fill the weigh tank. These measurements were then averaged over the length of the flow run and converted into average flow rate. The flow meter measurements were compared with the actual flow rate and a relative error was calculated.

3.4.5.1. Linearity Testing using the NAMAS flow rig

Each flow meter was installed in the flow rig and its linearity performance tested over a range of water velocities (4 m/s $\geq u \geq$ 0.005 m/s). When the linearity of the flow meter was plotted against velocity an interesting characteristic was seen at low flow rates, as shown in figure 3.11.

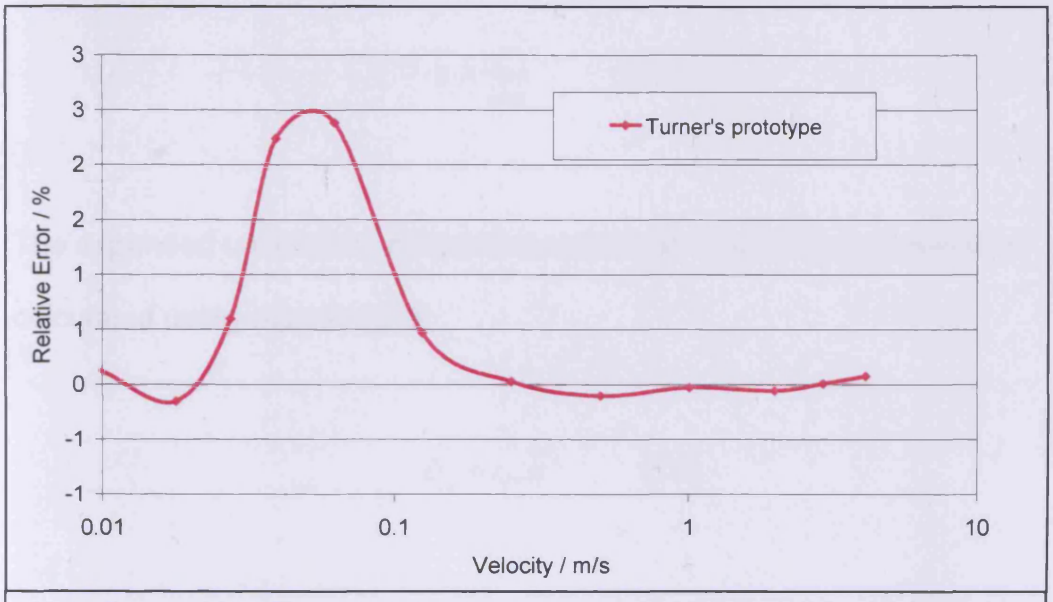

Figure 3.11. Turner's prototype, Measurement error v Velocity

The curve had a distinctive 'hump' characteristic within the region 0.25 m/s and 0.017 m/s. Suspecting that this hump could be caused by changes in

velocity profile, the temperature data recorded during each flow run was used to calculate the Reynolds number for each flow run using equation 3.4.

$$\mathrm{Re} = \frac{\rho_D . u . d}{\mu} \quad (3.4)$$

To check whether measurement error may be a cause for concern a measurement uncertainty analysis was conducted. The run data collected from the flow meter under test was normally distributed and so a student T Distribution was used to calculate the uncertainty of the measurement. The standard uncertainty of the mean was calculated using equation 3.5 (BS ISO 5168:2005).

$$\bar{u} = \frac{s}{\sqrt{n}} \quad (3.5)$$

The expanded uncertainty of the mean at the 95 % confidence level was calculated using equation 3.6.

$$U_{\bar{u}} = t_{95} . \bar{u} \quad (3.6)$$

The uncertainty increases as the flow rate reduces because the voltage generated between the electrodes becomes very small. To compensate for the increase in noise levels the number of measurements recorded was increased and duplicate flow runs were conducted.

Figure 3.12 shows a graph of the linearity of Turner's prototype with Reynolds number.

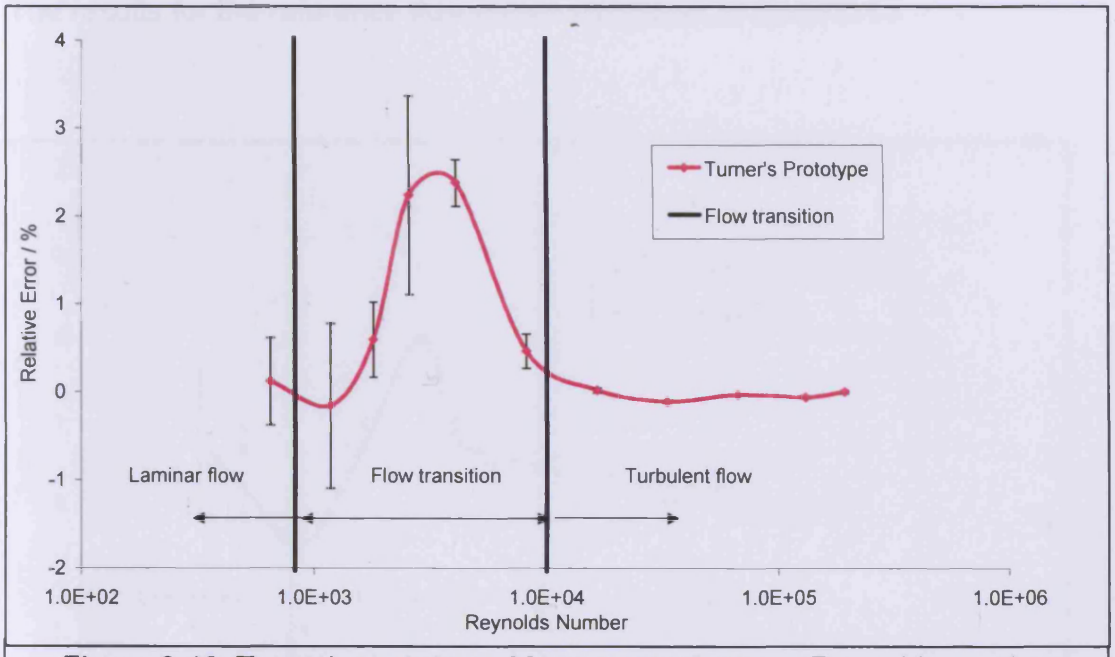

Figure 3.12. Turner's prototype, Measurement error v Reynolds number

When plotted against Reynolds number the hump characteristic occurs in the region of flow transition between laminar and turbulent flow profiles. The Turbulent flow profile was taken to mean Reynolds numbers greater than 10,000 and the laminar flow profile was Reynolds numbers less than 1200 (Miller 1983). A Reynolds number of 1000 corresponds to a velocity of approximately 20 mm/s. The hump characteristic is believed to be an artificial artefact related to the method of calibration of the flow meter. In the calibration process firstly the span is calibrated at a relatively high (turbulent profile) flow rate and secondly a relatively low (laminar profile) flow rate calibration is conducted. Within the transitional region the profile is by its very nature

transitional and neither turbulent nor laminar. Therefore as the calibration process attempts to remove errors from two very different velocity profiles the likely result is a hump characteristic within the transitional region.

The results for the reference flow meter are shown in figure 3.13.

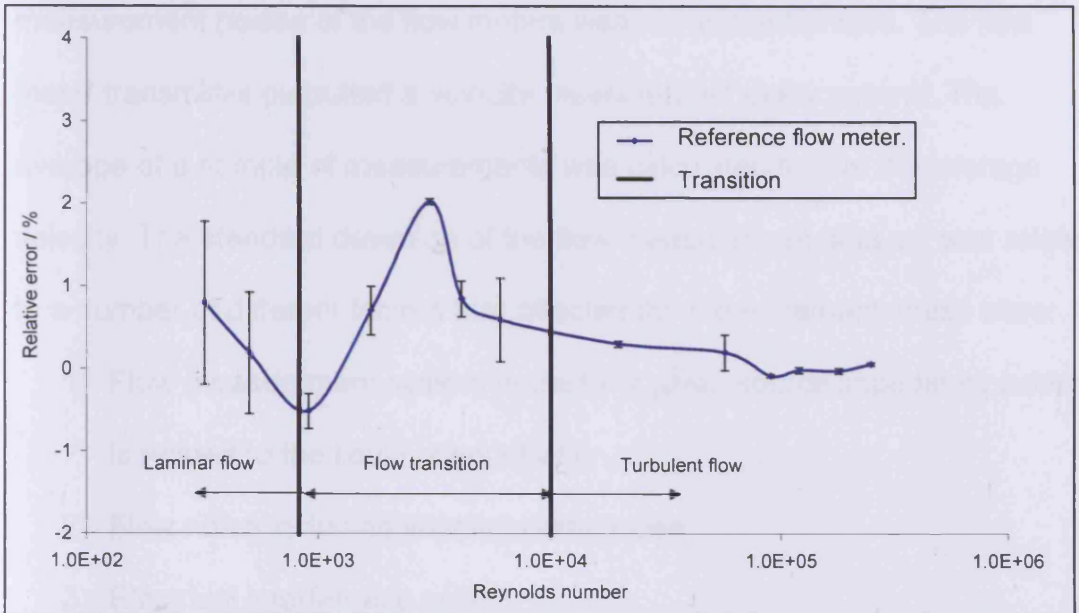

Figure 3.13. Reference flow meter, Measurement error v Reynolds number

The results in figure 3.13 show a very similar characteristic within the flow transition region to Turner's prototype. The profile sensitivity is an interesting characteristic of both flow meters, which will be investigated further in chapter 4.

The potential measured at the electrodes for the ABB reference flow meter and for Turner's prototype were 200 μV/m/s and 319 μV/m/s respectively. This means that Turner's prototype measures 60 % more signal at the electrodes for a given velocity compared with the reference flow meter.

3.4.5.2. Testing the flow meters using the demineralised water rig

The demineralised water rig was used to compare the performance of the flow meters when tested with different water conductivities. It was thought that as the conductivity reduces the measurement noise would increase but the signal level would remain constant. To make a comparison between the measurement noises of the flow meters was not straightforward. The flow meter transmitter outputted a velocity measurement every second. The average of a sample of measurements was calculated to give the average velocity. The standard deviation of the flow measurement data set was related to a number of different factors that affected the measurement, these were:

1) Flow measurement system noise for a given source impedance (which is related to the liquid conductivity)
2) Flow noise including impeller pump noise
3) Electrical interference noise
    a. Plant noise (Earthing related)
    b. Triboelectric noise generated within the liquid
    c. Electrostatic and electromagnetic interference
4) Changes in flow rate
5) Length of flow run

With the number of factors that can have a bearing on the standard deviation results it was felt that the testing should be conducted in a manner that ensured fair comparisons between flow meters could be made. It was decided that the flow meters should be tested simultaneously. By testing simultaneously the flow noise, plant noise and changes in flow rate can be negated as factors affecting the flow measurements, as they will be the same

for both flow meters. A flanged section of pipe work, which was 10 diameters long, was installed between the two flow meters. The sump of the rig was filled with tap water having an electrical conductivity of 404 μS/cm. A number of tests were performed to check that the flow meters did not interfere with each other before tests to compare the standard deviations of flow runs could be made. Once satisfied that the installation conditions did not detrimentally affect the performance of either flow meter flow runs were carried out and the data from each flow meter was collected simultaneously. Figure 3.14 is a graph showing the standard deviation data for flow runs conducted simultaneously.

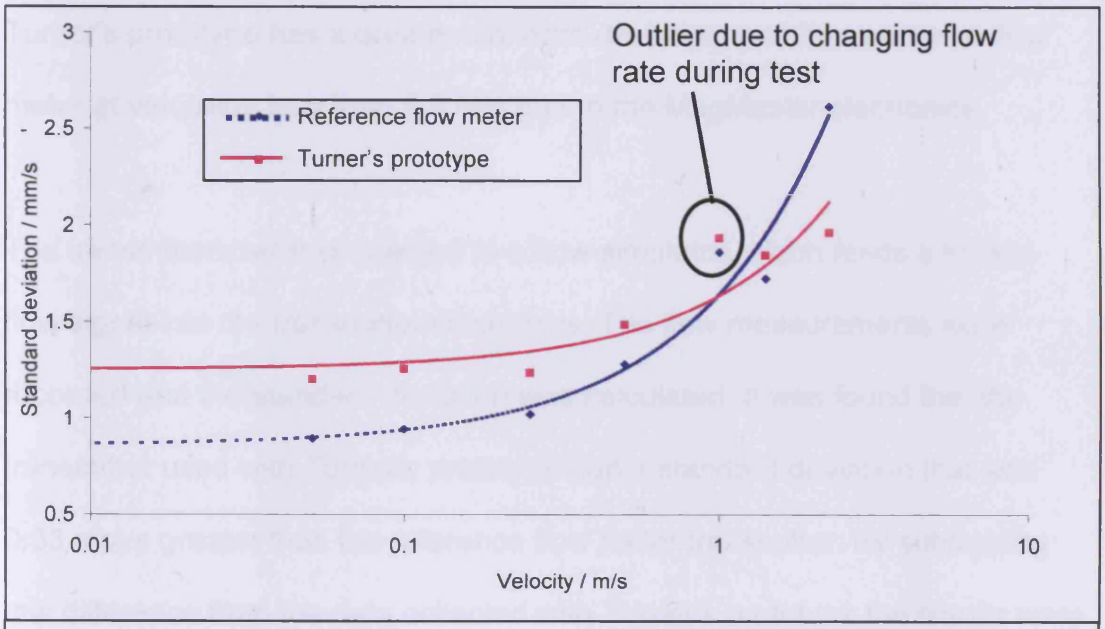

Figure 3.14. A comparison of the standard deviation for flow runs conducted on the demineralised water rig operating with water having an electrical conductivity of 404 μS/cm

Figure 3.14 shows that at velocities below 1 m/s the standard deviation results follow the trend lines quite closely, but as the velocity increases to 1 m/s and above the results do not follow the trend line very accurately. When the run data at the 1 m/s flow test was analysed the measurements appeared to show that the flow rate was decreasing throughout the flow run, therefore the standard deviation appears higher than expected for both flow meters. Turner's prototype has a higher standard deviation than the reference flow meter at velocities less than 0.5 m/s. It is believed that at low flow velocities (< 0.5 m/s) the measured standard deviation is due to system noise rather than the flowing liquid. As the flow rate is increased (> 0.5 m/s) the noise associated with the flowing liquid predominates over the system noise. Turner's prototype has a greater standard deviation than the reference flow meter at velocities less than 0.5 m/s due to the MagMaster electronics.

The transmitters were connected to a flow simulator, which feeds a known flow signal into the transmitter electronics. The flow measurements were recorded and the standard deviation was calculated. It was found that the transmitter used with Turner's prototype had a standard deviation that was 0.33 mm/s greater than the reference flow meter transmitter. By subtracting this difference from the data collected with Turner's prototype the results were re-plotted and are shown in figure 3.15.

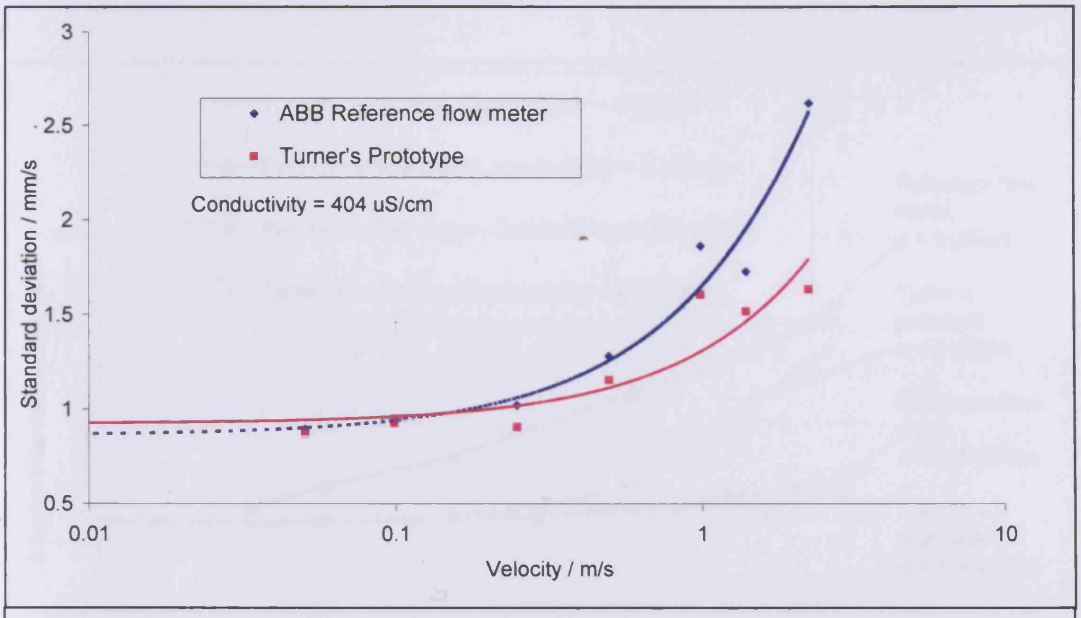

Figure 3.15. The standard deviation results presented in figure 3.14 with Turner's prototype results compensated for the difference in transmitter noise

Figure 3.15 shows that Turner's prototype has a similar standard deviation to the reference flow meter at velocities below 1 m/s.

3.4.5.3. Demineralised water testing

The tank was filled with demineralised water having an electrical conductivity of 5 µS/cm. The flow runs were conducted whilst the conductivity was monitored. The standard deviation data was plotted against velocity and the results, including the 400 µS/cm results are shown in figure 3.16.

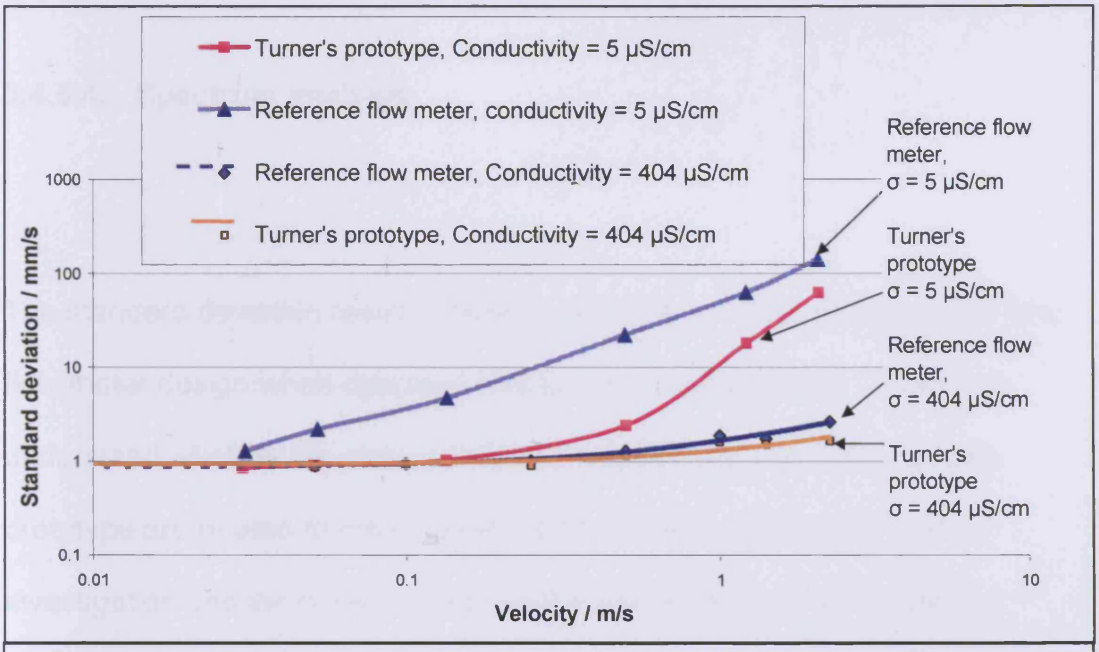

Figure 3.16. A comparison between the standard deviation of Turner's prototype and the reference flow meter measuring tap water and demineralised water

The results in figure 3.16 show that the testing on 404 µS/cm water produced a relatively flat standard deviation compared with the 5 µS/cm test results. The results suggest that at 5 µS/cm the flow noise dominates over the system noise at much lower flow rates. The standard deviation results for Turner's prototype operating with 5 µS/cm water were lower than the standard deviation results for the reference flow meter. These results suggest that having a long electrode and magnetic field reduces the standard deviation of the flow measurement when operated with low conductivity water. However the gradient of Turner's prototype is steeper than the reference flow meter suggesting that at velocities above 2 m/s there is no real advantage to having an elongate flow meter.

3.4.5.4. Spectrum analysis

The standard deviation results showed evidence of an advantage to the long flow meter design when operated with low conductivity water. To try and understand whether the reduced standard deviations seen with Turner's prototype are related to the long electrode or the long magnetic field an investigation into the noise present on the electrodes was undertaken. A Spectrum analyser program which operates with Labview® was used. The computer was fitted with a PC-LPM-16/PnP board, which is a low-cost, input / output board. An electrode was connected to the signal terminal of the input board and the earthing point of the flow meter was connected to the input board 0 Volt terminal. The coils were not energised during this experiment. A number of frequency sweeps were conducted at different flow velocities using both the reference flow meter and Turner's prototype. Figure 3.17 shows a graph of the raw spectra for the reference flow meter measured with water having an electrical conductivity of 0.7 μS/cm.

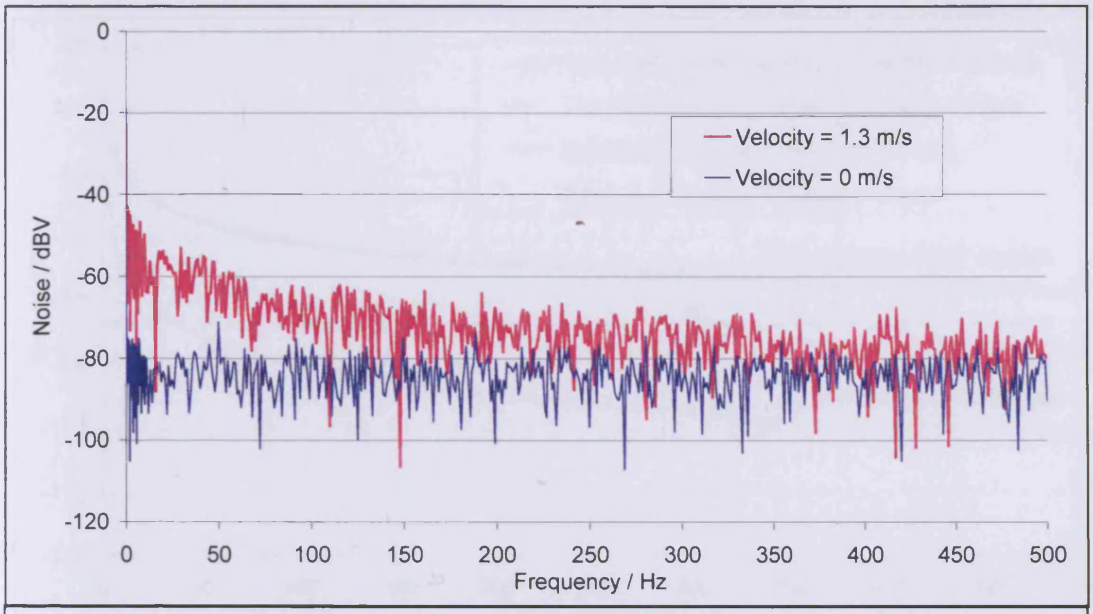

Figure 3.17. Spectrum analysis of the Reference flow meter flowing with demineralised water having an Electrical conductivity = 0.7 µS/cm

Two flow velocities are plotted on figure 3.17; they are zero flow and a velocity of 1.3 m/s. The plots show a great deal of scatter across the frequency range tested, this scatter is random noise and was different every time a frequency sweep was conducted. The zero velocity noise spectra was essentially flat over the frequency range tested. Figure 3.18. shows the spectrum analysis lines of best fit for both flow meters operated under the same flow conditions and electrical conductivity.

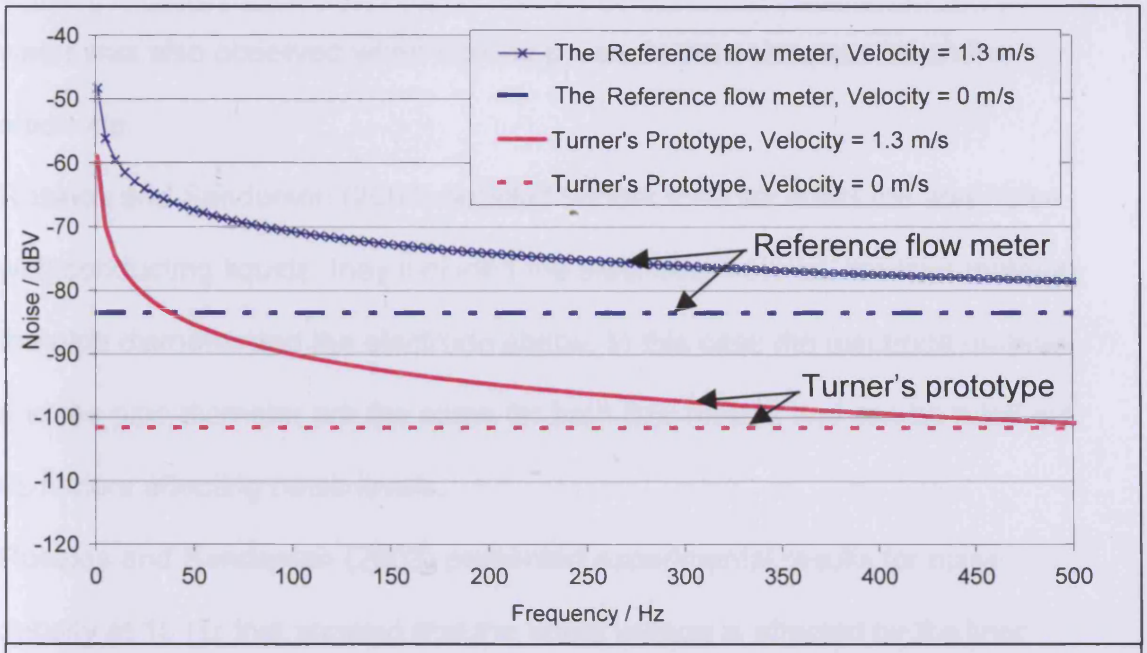

Figure 3.18. A graph comparing the noise present at the electrodes of both flow meters at two different flow velocities with water having an electrical conductivity = 0.7 µS/cm

At zero velocity the line electrode is quieter than the standard electrode by 18 dBV. At 1.3 m/s the noise predominates at the low frequency end of the spectrum and has a similar characteristic for both electrode geometries. The line electrode is more than 20 dBV quieter than the standard electrode at frequencies above 100 Hz.

This test has shown that the line electrode geometry in its own right has a clear advantage for flow measurements at low conductivities.

3.5. Discussion

In making comparisons between the conventional flow meter and the elongate flow meter it is clear that with demineralised water Turners' prototype provides a quieter measurement. The spectrum analysis work demonstrated that the

reduction in standard deviation seen during flow testing with demineralised water was also observed when looking purely at the noise present on the electrode.

Rosales and Sanderson (2003) detailed factors that can affect the flow noise with conducting liquids, they included the electrode material, the liner material, the pipe diameter and the electrode shape. In this case the electrode material and the pipe diameter are the same for both flow meters and can be ruled out as factors affecting noise levels.

Rosales and Sanderson (2003) presented experimental results for noise density at 10 Hz that showed that the noise voltage is affected by the liner material. They describe the zeta potential (ξ) as the potential drop between the pipe wall and the bulk liquid. It is a function of the average charge density at the wall (q_w), the molecular diffusivity of the liquid (D) and the electrical conductivity of the liquid (σ); see equation 3.7:

$$\xi = \frac{Dq_w}{\sigma} \qquad (3.7)$$

They claim that it is the change in zeta potential that affects the noise levels. As the molecular diffusivity and the conductivity of the liquid are unaffected by the wall material the noise levels must be dependent on the average charge density at the wall. Rosales and Sanderson (2003) produce a theoretical model of the noise levels expected from a given flow meter configuration and flow condition. They comment that for the theoretical model a value for the zeta potential was chosen to suit the experimental noise levels. Unfortunately there is a contradiction within the report by Rosales and Sanderson (2003) where they claim that there is an inversely proportional relationship between

the noise spectrum voltage V_0 and conductivity assuming the zeta potential remains constant. This assumption is not valid because the zeta potential as shown in equation 3.7 is inversely proportional to the conductivity, therefore the equations derived by Rosales and Sanderson (2003) will not be used to predict the noise levels.

Rosales and Sanderson (2003) conducted a theoretical noise comparison between a 1cm diameter electrode and a 1cm square electrode operating in a turbulent flow regime. They measured the noise spectrum of a circular electrode and then calculated the noise spectrum theoretically. The theoretical results gave good agreement with the experimental results. They then calculated the noise spectrum with a square electrode. They found that the noise spectrum of the square electrode was less than the circular electrode. They argued that in a flowing condition it is the length of the electrode in the axial direction that is important rather than the area of the electrode. They considered turbulent eddies (which contain charge) travelling axially along the pipe. As eddies pass over the surface of the round electrode, depending on their vertical position the transit time will differ. Figure 3.19 is a picture illustrating different length scales of a circular electrode compared with a square electrode.

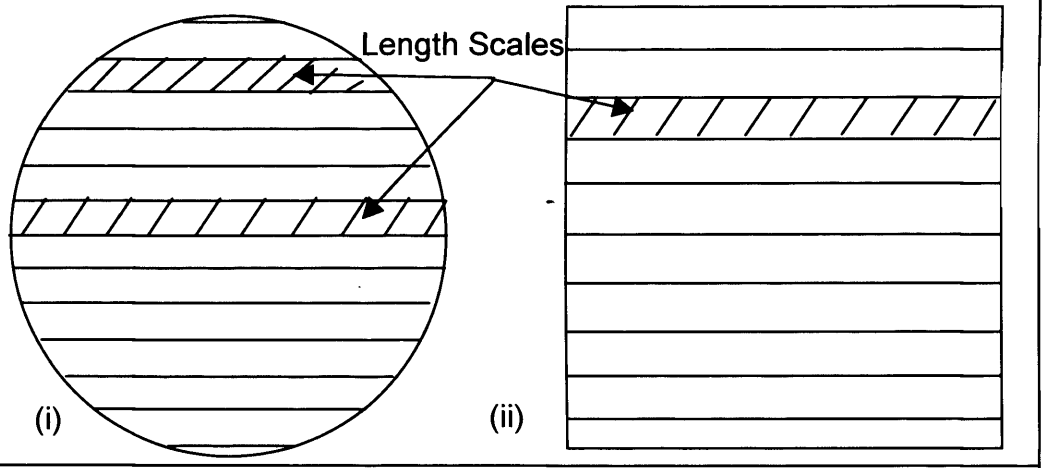

Figure 3.19. Examples of length scales over the surface of (i) circular and (ii) square electrode

Depending on the length scale the charge will be imparted onto the surface of the electrodes at different frequencies. The square electrode has only one length scale therefore assuming the eddies are all travelling axially along the pipe they will pass over the surface at a constant rate in all regions of the electrode. Eddies travelling at a constant rate over a square electrode surface could present a noise spectrum that is lower at higher frequencies compared with the circular electrode due to the position in which they pass over the surface (Rosales and Sanderson, 2003). From the spectra work conducted in this research the line electrode has a significantly lower noise output than the circular electrode. The elongate electrode was 18 dBV quieter with static flow and 20 dBV quieter at frequencies above 100 Hz with water flowing at a velocity of 1.3 m/s.

Although the tests conducted in this research are different to the theoretical analysis conducted by Rosales and Sanderson (2003) the 2 dBV additional noise reduction seen at frequencies greater than 100 Hz could be attributed to

the length scales of the line electrode compared with the circular electrode. However the additional noise reduction also supports Turner's (2002) theory regarding the elongate electrode averaging the effect of the turbulent eddies; as described in chapter 2.

Vickers (2004) analysed the noise sources that can be expected. The noise sources present at the electrodes can be either electrical noise or flow noise. The electrical noise comprises of Johnson noise, Pink noise and external noise. Johnson noise (Ballentyne & Walker 1958) is generated through the thermal vibrations of atoms and electrons within an electrical conductor. In this instance the electrode circuit comprises of the sensing electrodes, the liquid in the measuring section of the pipe, the electrode wiring and the amplifier circuitry. Johnson noise is white noise that is random by nature with components of equal magnitude at all frequencies. Pink noise (Vickers 2004), also known as 1/f noise, is where the noise output is proportional to the reciprocal of the frequency. Pink noise is commonly found radiating from and around electronic equipment. External noise relates to other electrical equipment and radio waves amongst others (Vickers 2004). The Zero flow noise spectrum is linear with a zero gradient, and like Johnson noise it is independent of frequency. The line electrode has a lower noise output than the circular electrode when the flow is static. In a static flow condition there are no eddies passing over the surface of the electrode and consequently the length in the axial direction plays no part in the magnitude or the frequency of the noise levels present at the electrode. When analysing the factors that may affect the noise levels at zero flow the only variable that has changed significantly is the area in contact with the liquid. A larger area electrode will

present a lower resistance path to the process liquid. Vickers (2004) presented the Johnson noise power equation (3.8):

$$P_n = 4k.T.b \quad (3.8)$$

Vickers (2004) described how the noise voltage could be calculated using equation 3.9:

$$V = \sqrt{(P_n.R)} \quad (3.9)$$

By substituting equation 3.8 into 3.9 there is a relationship between the noise voltage and resistance, thus showing that Turner's elongate electrode should produce a lower noise voltage. Turner derived two equations, 2.11 and 2.12, to calculate the resistance of any circular and any line electrode respectively with different liquid conductivities. The calculated resistances for water of conductivity 0.7 μS/cm are 46 kΩ for Turner's prototype and 1.8 MΩ for the reference flow meter. By substituting equation 2.11 and 3.8 into equation 3.9 an equation that estimates the Johnson noise voltage for a circular electrode with any liquid conductivity is derived, as shown in equation 3.10:

$$V = \sqrt{\frac{8kTb}{\pi\sigma d}} \quad (3.10)$$

For the line electrode equation 2.12 and 3.6 are substituted into equation 3.9 to give equation 3.11:

$$V = \sqrt{\left(\frac{4kTb}{\pi\sigma l}\right) log_e\left(\frac{2S}{d}\right)} \quad (3.11)$$

Using equations 3.10 and 3.11 the predicted noise voltages at zero flow with a bandwidth of 100 kHz (National Instruments Corp., 1996) are 8.6 μV (or – 101

dBV) for Turner's prototype and 54 μV (or – 85 dBV) for the Reference flow meter. Turner's prototype had an experimental noise voltage of – 101 dBV with static flow. The reference flow meter had an experimental noise voltage of – 84 dBV. Therefore the method used to predict the noise voltage of two different electrode configurations is valid and will allow different electrode designs to be analysed without requiring experimentation.

The successful test work conducted by Cushing (1962,1971) involved operating at an A.C. drive frequency between 1.5 kHz and 10 kHz; Amare (1995) was operating at a frequency of 1.5 kHz. The results in figure 3.7 show that at a frequency of 1 kHz the current normalised flux has dropped to 1.5 mT/A for Turner's prototype and 4.2 mT/A for the reference flow meter. This represents a drop in signal level for Turner's prototype and the reference flow meter of 81 % and 73 % respectively. The results in figure 3.8 show that the inductive impedance of the flow meters has increased to 460 Ω for Turner's prototype and 580 Ω for the reference flow meter. Assuming that an A.C. current of 0.5 A was required the voltage supply for Turner's prototype and the reference flow meter would be 230 V and 290 V. It is not practical to use such high voltages to drive the coils. It is therefore clear that neither flow meter is suitable for operating with A.C. frequencies of 1 kHz. To understand at what sinusoidal frequencies the flow meters may adequately operate at, a theoretical prediction of the likely signal levels with frequency was conducted. Using the pulsed D.C. system the signal level with a current of 0.5 Amps was 200 μV/(m/s) for the reference flow meter. Turner's flow meter had a signal level of 319 μV/(m/s). The signal level is proportional to a number of factors including the magnetic field strength, the magnetic field pattern, the distance

between the electrodes and the size of the electrode. Using the hysteresis measurements from section 3.4.4 the flux at 0.5 A was 4.2 mT for Turner's prototype and 8 mT for the reference flow meter. The signal level is directly proportional to the flux. By dividing the signal level by the 0.5 A flux measurements the signal levels can be calculated in terms of flux rather than current, giving 25 μV/(mT.m/s) for the reference flow meter and 100 μV/(mT.m/s) for Turner's prototype. To operate these flow meters with a sinusoidal waveform a power amplifier would be required to drive the current through the coils. A suitable power amplifier has a maximum supply voltage of ± 100 V (QSC Audio products inc., 2006). For this analysis it was assumed that the magnetic flux density was linear with D.C. current, this is not strictly true as the results in figure 3.9 show that the reference flow meter begins to saturate at currents above 0.4 A. However for performing direct comparisons between the flow meters it was reasonable to make such an assumption. Using the impedance measurements from the A.C. experiments detailed in section 3.4.3 the current supplied to the coils with frequency was calculated based on a voltage supply of ± 100 V. By multiplying the calculated current by the current normalised flux at each frequency measured, the flux with a 100 V supply was calculated. By multiplying the theoretical flux levels by the flux normalised signal levels the A.C. signal level with a 100 V supply was calculated. The results for both flow meters are shown in figure 3.20.

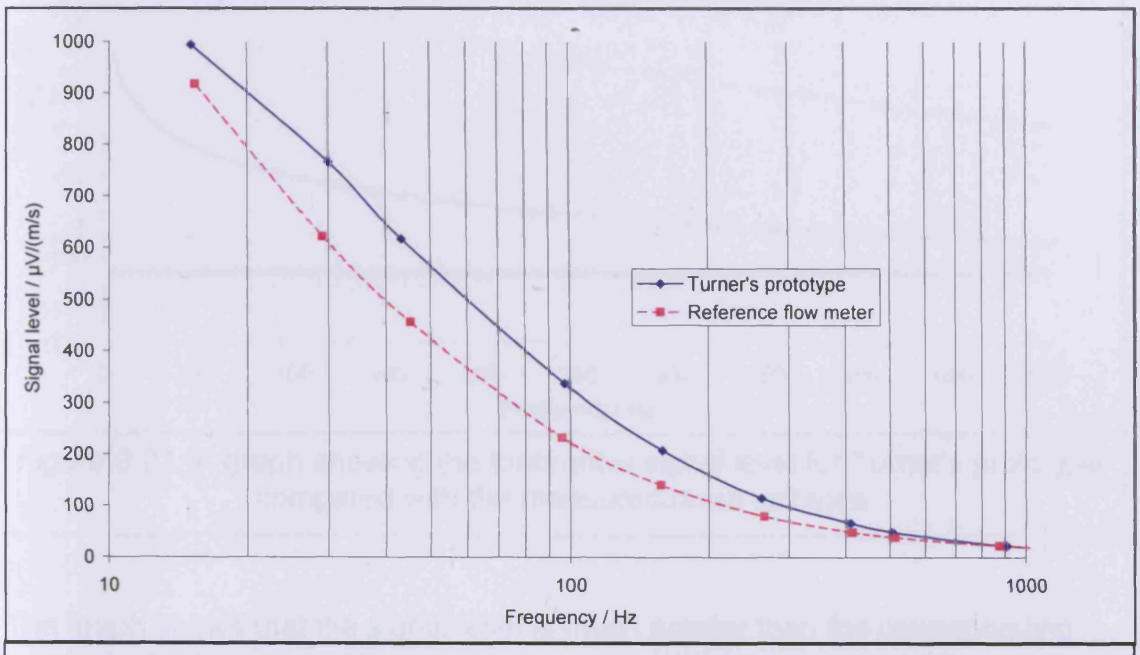

Figure 3.20. A graph showing the theoretical signal level of both flow meters when operated with an A.C. waveform using a constant supply voltage of 100 V pk-pk.

Figure 3.20 shows that Turner's prototype has more signal than the reference flow meter up to a frequency of 500 Hz but above this frequency the signal level for both flow meters is tending to zero.

The theoretical signal level at a flow velocity of 1.3 m/s was calculated and compared with the spectrum analysis data presented in figure 3.18. Figure 3.21 shows a graph of signal and noise voltages with frequency for Turner's prototype.

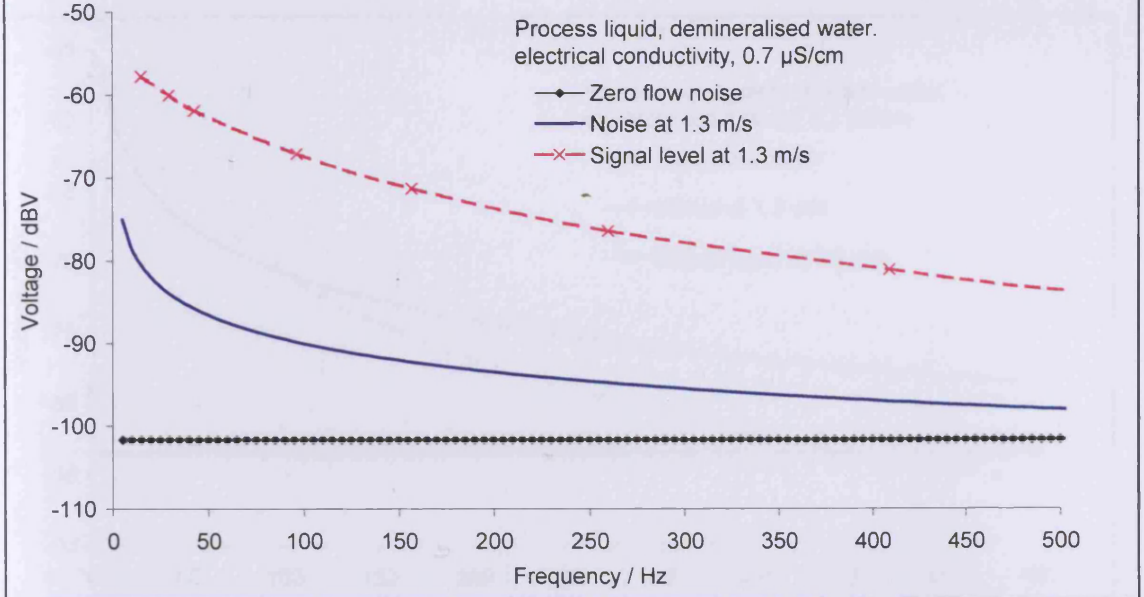

Figure 3.21. A graph showing the theoretical signal level for Turner's prototype compared with the measured noise voltages

The graph shows that the signal level is much greater than the corresponding noise level; therefore Turner's prototype could theoretically measure the flow of demineralised water using an A.C. waveform at frequencies up to 500 Hz.

Figure 3.22 is a graph showing the signal and noise levels with the reference flow meter.

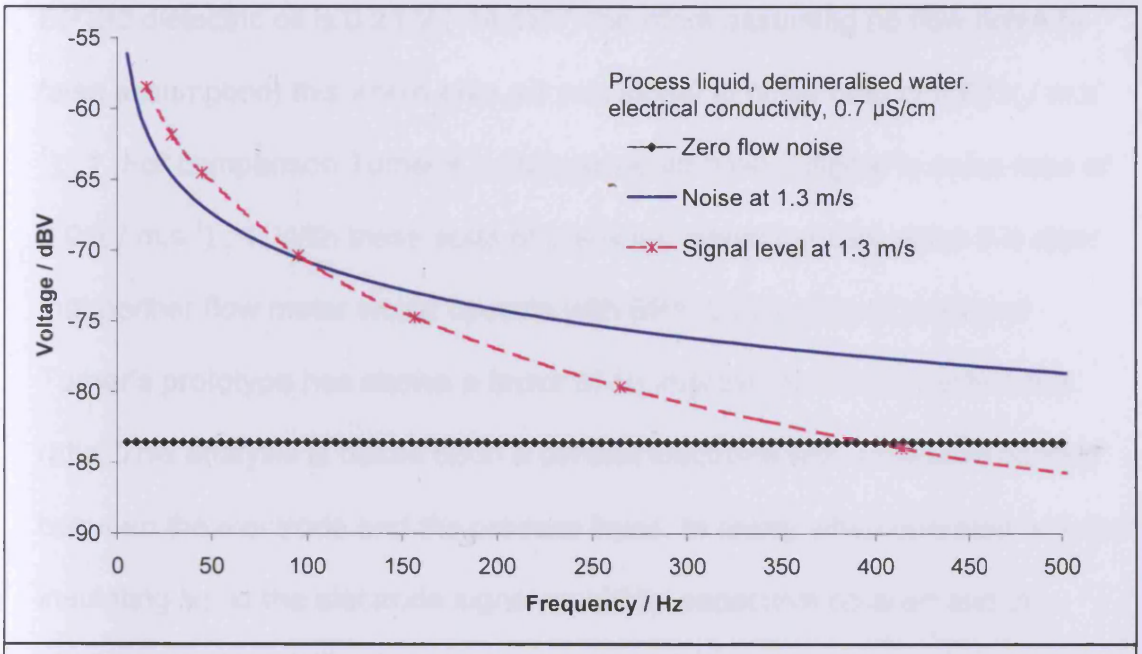

Figure 3.20. A graph showing the theoretical signal level for the Reference flow meter compared with the measured noise voltages

Figure 3.22 shows that the noise levels would be greater than the signal level at frequencies above 100 Hz, this would make it very difficult to resolve the signal from the noise. By comparing the results of figure 3.21 and 3.22 it is clear that Turner's prototype would operate much better than the reference flow meter with a sinusoidal waveform, however most of the improvements seen relate to the superior noise levels with the long electrode geometry.

If an electromagnetic flow meter were designed to operate with an insulating liquid then the performance should be at least as good as Turner's prototype operating with 0.7 µS/cm. The signal level operating at a velocity of 1 m/s and frequency of 6 Hz is –69 dBV, the noise level at this frequency was -75 dBV, therefore a signal to noise ratio of approximately 2 : 1 would be adequate. The

predicted static flow noise level for the reference flow meter operated with BP180 dielectric oil is 0.21 V (-14 dBV) therefore assuming no flow noise (a false assumption) this would give a 1 m/s signal to noise ratio of 0.001(/ $m.s^{-1}$) : 1. For comparison Turner's prototype would have a signal to noise ratio of 0.01(/ $m.s^{-1}$) : 1. With these sorts of predicted signal to noise ratios it is clear that neither flow meter would operate with BP180 dielectric oil, however Turner's prototype has shown a factor of 10 improvement in signal to noise ratio. This analysis is based upon a contact electrode with a resistive contact between the electrode and the process liquid. In reality when operated with an insulating liquid the electrode signal would be capacitive coupled and the resistance to the process liquid may not be so problematic.

In making comparisons with the Reference flow meter it is clear that Turner's prototype will reduce the noise levels when operated with demineralised water. However there is also a marked improvement in signal level. The signal level of Turner's prototype was 319 μV/m/s, using 300 ampturns of wire whereas the reference flow meter had a signal level of 200 μV/m/s using 740 ampturns. Hemp et al (2002) believed that a large area electrode increased the signal level. The electrode arrangement utilised by Hemp et al (2002) was a current sensing amplifier, therefore the larger the area the greater the current flow. With a voltage-sensing high input impedance amplifier no current flows into the electrode. The signal measurement is proportional to the potential generated between the electrodes. Therefore the length of the electrode will not contribute a larger flow signal. For a voltage sensing electrode the greater the distance between the electrodes the greater the potential between them. It is believed that the improvement in signal level is

related to the length of the insulating liner. In the reference flow meter the earthing planes are only 42.5 mm from the electrodes. Part of the potential generated across the pipe is probably leaking to ground.

This analysis shows that it will not be possible to operate either flow meter at the frequencies that were successfully used by Amare (1995) and Cushing (1962) to measure the flow of an insulating liquid. Based on this analysis a new flow meter is required to continue testing.

3.6. Conclusions

- Turner's prototype was not suitable for operation with insulating liquids.
- The line electrode produced a lower noise threshold than a circular electrode.
- The lower noise threshold was due to the area in contact with the liquid and the consequent reduction in resistance to the process liquid.
- The MagMaster electronics was not suitable for operation with insulating liquids.
- A new flow meter and transmitter is required to further analyse the performance of an elongate flow meter with low conductivity liquids.
- A method of predicting the zero flow noise level has been successfully developed and used to predict the performance of different contact electrode designs.
- The accuracy of both flow meters is affected by the velocity profiles they are trying to measure.

Chapter 4

Weight function Analysis

4.1. Introduction

The work conducted in chapter 3 showed that Turner's prototype and the reference flow meter behaved quite differently. The performance was affected in a number of ways, including the magnitude of the signal generated, the measurement performance with different axis-symmetric velocity profiles and the amount of noise present within the electrode measuring circuit. It was proven that the area of the electrode surface affects the resistance to the process liquid and consequently the measurement noise levels. A simple method of predicting the measurement noise voltage in static flow for any contacting electrode geometry with any liquid conductivity was derived. Shercliff (1962) designed a mathematical model that could be used to analyse flow meter performance. A similar model will be produced and a theoretical analysis of Turner's prototype and the reference flow meter will be undertaken. An investigation into the performance with different electrode geometries will be conducted in readiness for designing a new prototype. At the time of investigation there was a commercial interest within ABB in developing a flow meter that could measure the flow accurately regardless of the flow profile. It was proposed that the technique developed should be used to help ABB in their development of a profile insensitive flow meter.

4.2. A Review of the Work of Others in Predicting the Performance of Electromagnetic Flow meters

Since the electromagnetic flow meter was invented scientists have been trying to predict and understand the performance of the electromagnetic flow meter under different design configurations and flow conditions (Shercliff 1962; Rummel, Ketelsen 1966; Bevir 1969; Hussain, Baker 1984; Wada, Ichiro 1992). Shercliff (1962) conducted some of the early work in this field and developed two-dimensional mathematical models to predict how simple flow meter designs would behave under different flow conditions.

4.2.1 The Weight Function Concept

The work published by Shercliff (1962) analysed the behaviour of a number of different flow meter configurations. He introduced the idea of a weight function vector and produced a two-dimensional graph showing contours of weight function (figure 4.1). The contours of weight function represent how sensitive the flow meter will be to the velocity of the fluid at all positions within the measuring section.

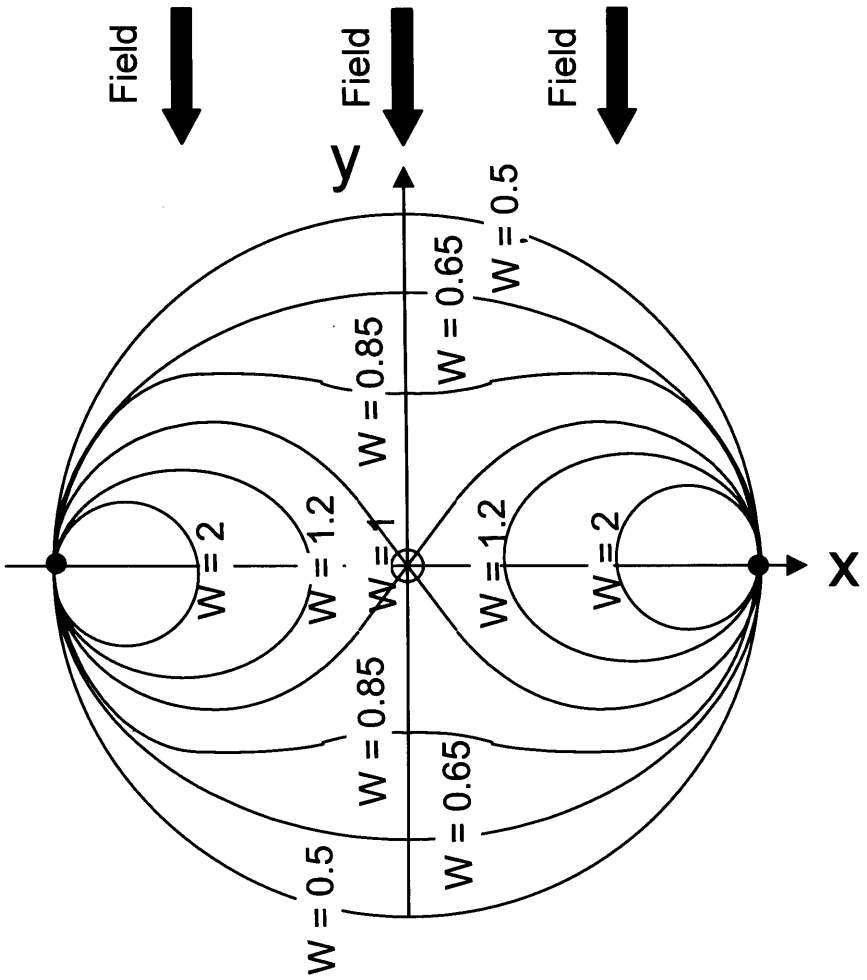

Figure 4.1. Weight Function for a point electrode flowmeter with a uniform magnetic field

From figure 4.1 it can be seen that if the velocity profile is asymmetric then the flow meter may not accurately determine the average velocity. The induced voltage between two electrodes is given by equation 4.1(Bevir 1969):

$$V = \oint \underline{W} \bullet \underline{u}\, d\tau \qquad (4.1)$$

where the weighting vector $\underline{W}$ is given by:

$$\underline{W} = \underline{B} \times \nabla G \qquad (4.2)$$

∇G was invented to help understand the behaviour of an electromagnetic flow meter, it represents the current distribution that is generated when unit

current is injected onto one electrode and out of the other. Using this idea and generating plots of weight function contours (figure 4.1) scientists are able to predict how a particular flow meter configuration may respond under different hydraulic conditions.

4.2.2. Development of the Weight Function Process

Shercliff's (1962) analysis predicted the performance of an infinitely long uniform magnetic field with infinitely long electrodes. One of the configurations he analysed had a rectangular duct with electrodes covering the walls of two sides of the duct and a uniform magnetic field. The analysis concluded that this design of flow meter would accurately measure the average velocity of any flow profile. Shercliff named this particular design of flow meter an ideal flow meter. Rummel and Ketelsen (1966) expanded on Shercliff's (1962) analysis to include magnetic fields that were finite in length and included point contact electrodes. They found that in practical flow meter configurations the weight function prediction was inaccurate. From the description of their analysis they produced a computer model that calculated the weight function distribution in the electrode plane and at a series of planes along the pipe axis. Rummel and Ketelson's (1966) analysis found that cylindrical flow meters with non-uniform magnetic fields were better able to measure the average liquid velocity of different axis-symmetric velocity profiles. Bevir (1969) conducted an exhaustive theoretical analysis with a view to designing ideal cylindrical flow meters. His research concluded that for cylindrical ducts with point contact electrodes it was not possible to produce an ideal flow meter. It would have been useful however if he had described how close to an

ideal flow meter this particular configuration could be made. Instead he focused on the geometry of cylindrical flow meters with rectangular saddle coils and point contact electrodes operating with axisymmetric velocity profiles. He produced two simulated axisymmetric velocity profiles, a flat turbulent profile and a laminar parabolic profile and calculated the electrode potential for both profiles. When the ratio of these two profile potentials approximated one the flow meter was deemed immune to axisymmetric flow profiles. Bevir produced a series of tables giving the profile ratios for different pipe diameters and a range of saddle coil geometries. These tables have been used until very recently by ABB. Research by scientists and manufacturers into producing cylindrical flow conduit flow meters that are less susceptible to asymmetric flow profiles has continued. Al-Khazraji and Baker (1979) performed a weight function analysis on large area electrodes within a cylindrical flow conduit using two field-generating coils. The electrodes analysed ranged in dimensions from $\beta = 45°$, $l = 0.77D$ to $\beta = 40°$, $l = 0.7D$. Their analysis concluded that depending on the magnetic field pattern the weight function could be less uniform than a good point contact electrode flow meter. However with the right field pattern the large area electrode weight function could be made to look like the flow meter had four point electrodes. Hussain and Baker (1985) later reported how a large area electrode flow meter was tested with an asymmetric flow profile produced by an orifice plate positioned 2.5 diameters upstream of the flow meter. The flow results were in error by as much as 0.6%, proving that increasing electrode angle does not necessarily produce an ideal flow meter. Hussain and Baker (1984) produced a capacitive electrode prototype with a series of elongate electrode strips as

illustrated in figure 4.2. A flow signal will be generated on each strip; the size of the flow signal will depend upon the location of each strip relative to the uniform magnetic field direction.

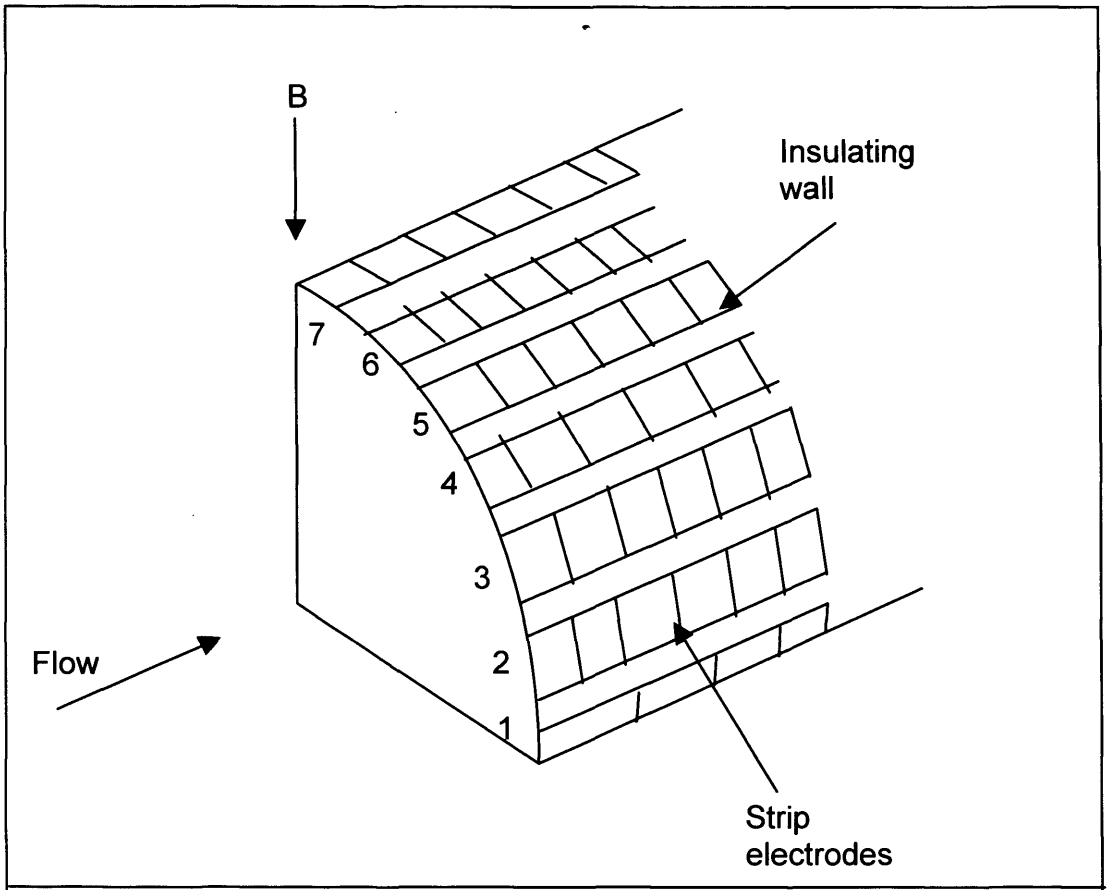

Figure 4.2. A representation of Hussain and Bakers (1984) prototype flow meter with a series of capacitive strip electrodes of the same size.

Hussain and Baker (1985) have used the weight function technique to predict how much weighting they should apply to each strip in calculating an overall measurement. For example strip 1 should represent 62 % of the overall measurement whereas strip 7 only 5 %. By weighting the output of each strip in this manner they produced a flow meter that was significantly more accurate at measuring asymmetric flow profiles.

Based on the work conducted by others it is clear that the weight function method can be used to give qualitative results that will aid in predicting the performance of any flow meter geometry and configuration.

4.3. Development of a Graphical FEA model of the weight function technique

Using equation 4.2 the weight function vector product in Cartesian coordinates is:

$$\underline{W} = \boldsymbol{i}\left(B_y G_z - B_z G_y\right) - \boldsymbol{j}\left(B_x G_z - B_z G_x\right) + \boldsymbol{k}\left(B_x G_y - B_y G_x\right) \qquad (4.3)$$

By assuming that the magnetic field and the virtual current field do not vary in the z-direction and that the velocity is rectilinear (as shown in figure 4.3);

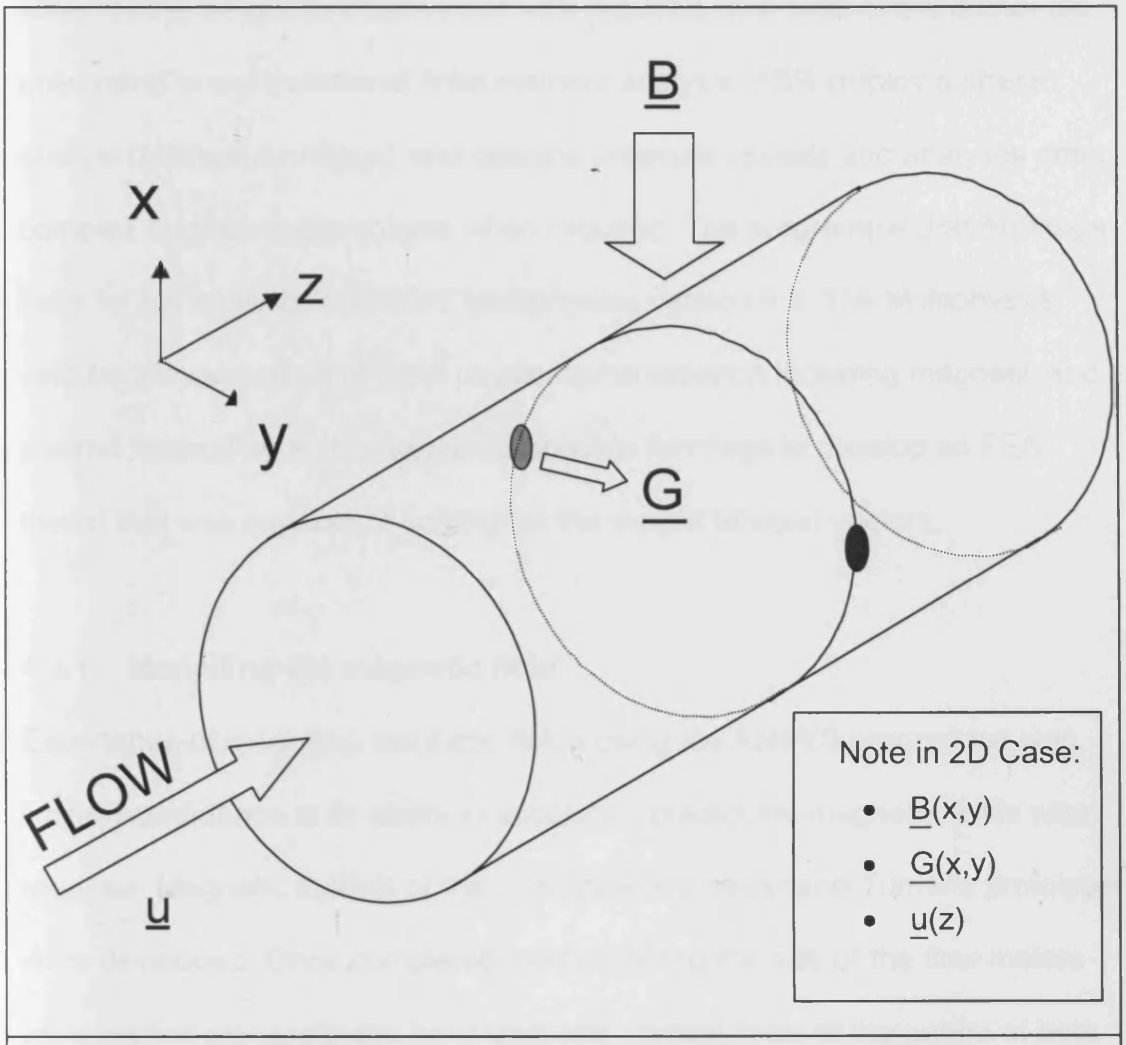

Figure 4.3. The geometry of a cylindrical flow meter

equation 4.3 can be simplified to:

$$\underline{W} = \boldsymbol{k}\left(B_x G_y - B_y G_x\right) \qquad (4.4)$$

By substituting equation (4.4) into equation (4.1) the electrode potential becomes:

$$V = \oint u_z \left(B_x G_y - B_y G_x\right) d\tau \qquad (4.5)$$

An FEA model that can predict the magnetic and electric field behaviour and solve for the weight function vector was required. The skills of the author did not extend to computational finite element analysis. ABB employ a stress analyst (Michael Armitage) who designs pressure vessels and analyses other complex engineering problems when required. The programme that Armitage uses for his analysis is ANSYS Multiphysics version 9.0. The Multiphysics version allows models of most physical phenomenon including magnetic and electric fields. The author worked alongside Armitage to develop an FEA model that was capable of solving for the weight function vectors.

4.3.1. Modelling the magnetic field

Experience of modelling magnetic fields using the ANSYS programme was limited; confidence in its ability to accurately predict the magnetic fields was required. Magnetic models of the reference flow meter and Turner's prototype were developed. Once completed the field along the axis of the flow meters were plotted along with the horizontal and vertical fields at the centre of both flow meters. The results were then compared with the experimental data presented in Chapter 3, section 3.4.1. Figures 4.4 and 4.5 show graphs of the experimental and theoretical magnetic fields within Turner's prototype.

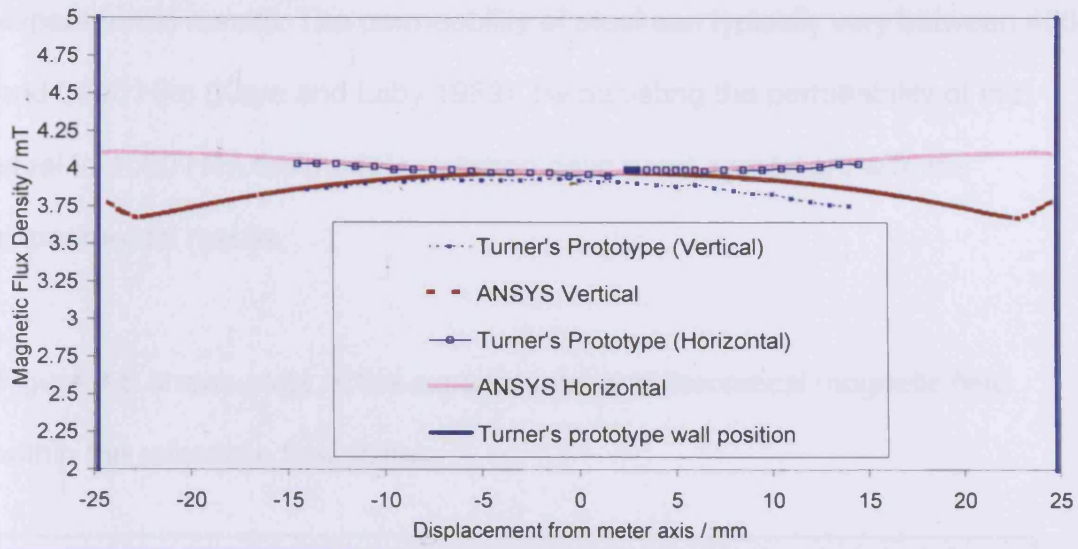

Figure 4.4. A comparison between the theoretical prediction and the experimental measurements of the field at the centre of Turner's prototype in the vertical and horizontal planes

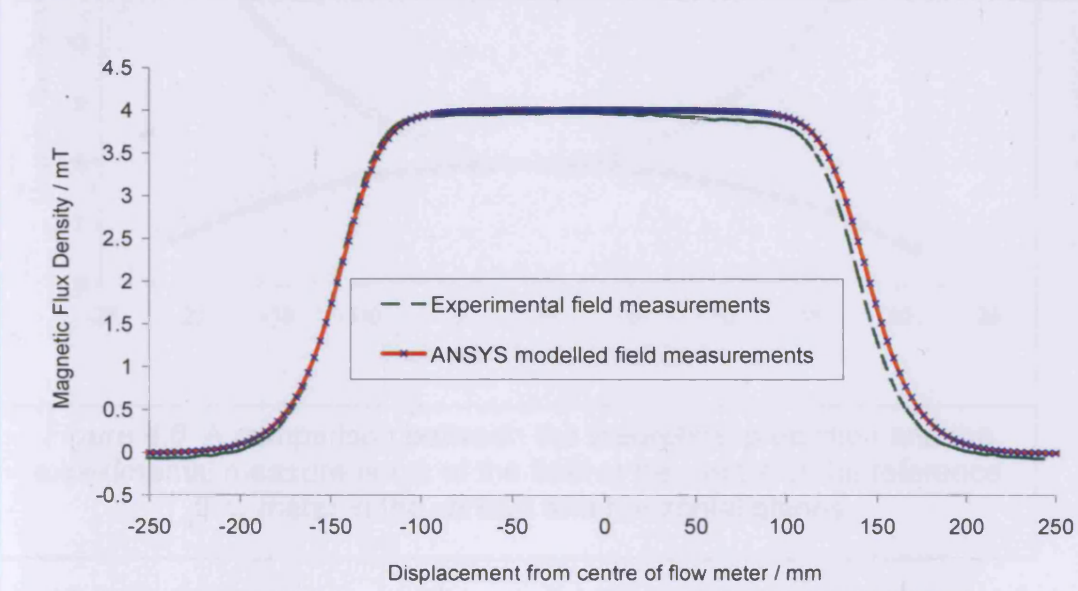

Figure 4.5. A comparison between the theoretical prediction and the experimental measurements of the field along the centre of Turner's prototype

Figures 4.4 and 4.5 show that the ANSYS model has correctly predicted the shape of the magnetic field within Turner's prototype. Initially the magnitude of

the flux calculated by the ANSYS model did not exactly match the experimental results. The permeability of steel can typically vary between 400 and 3000 H/m (Kaye and Laby 1989). By adjusting the permeability of the steel to 1000 H/m the model prediction gave good agreement with the experimental results.

Figure 4.6 shows plots of the experimental and theoretical magnetic field within the reference flow meter.

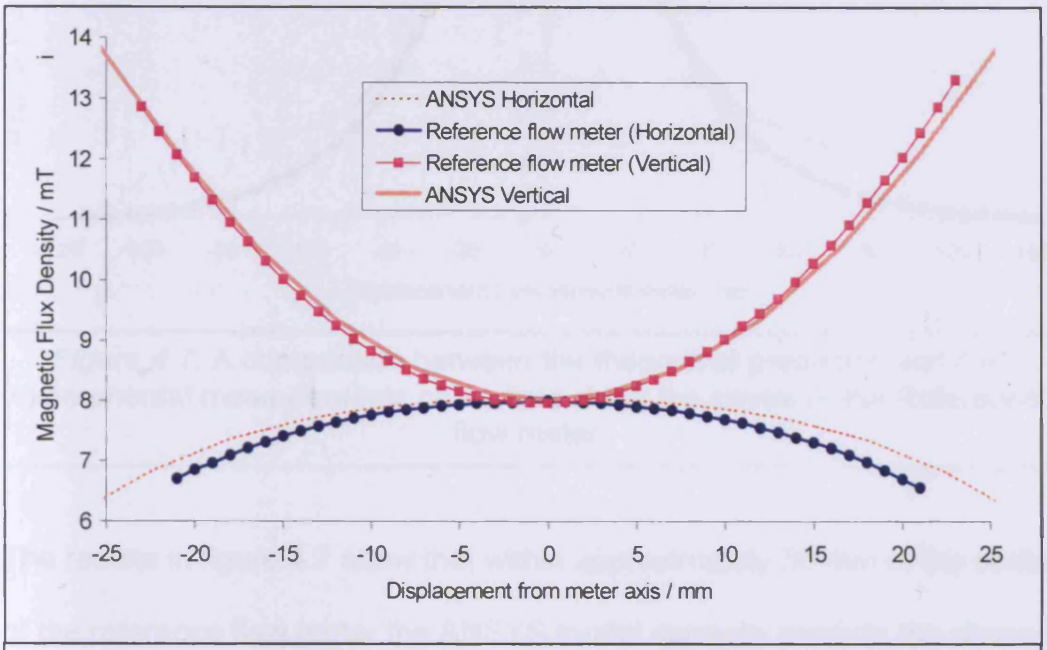

Figure 4.6. A comparison between the theoretical prediction and the experimental measurements of the field at the centre of the reference flow meter in the vertical and horizontal planes

Figure 4.6 shows that the ANSYS model has correctly predicted the shape of the magnetic field within the flow meter. As with Turner's model the permeability of the steel was adjusted to ensure the magnitudes of the flux matched.

Figure 4.7 shows the ANSYS predicted flux along the centre of the reference flow meter along with the experimental measurements.

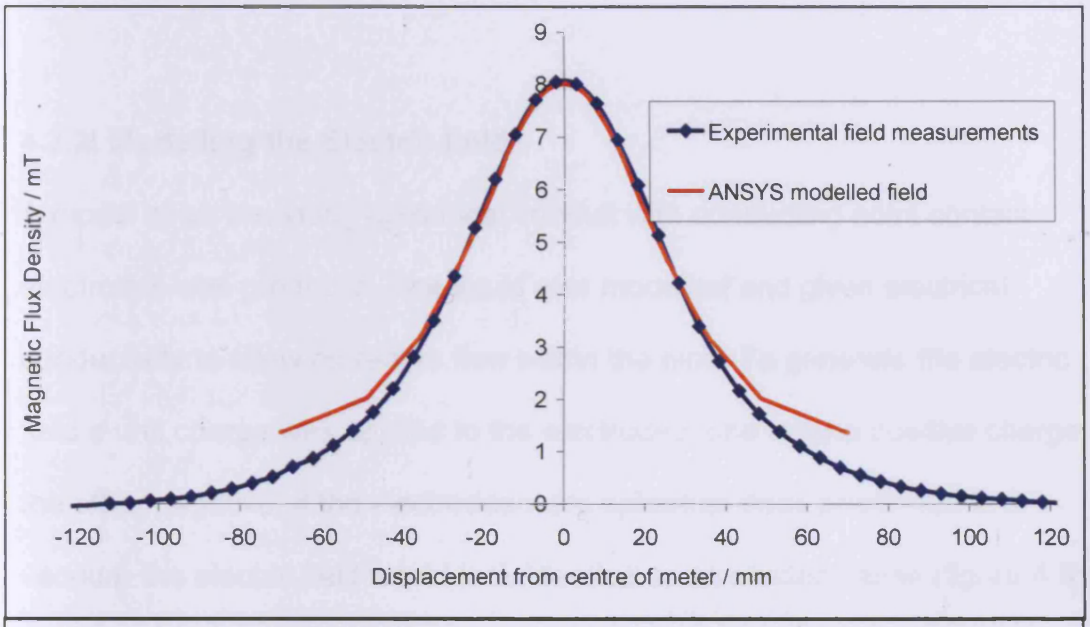

Figure 4.7. A comparison between the theoretical prediction and the experimental measurements of the field along the centre of the Reference flow meter

The results in figure 4.7 show that within approximately 30 mm of the centre of the reference flow meter the ANSYS model correctly predicts the shape of the magnetic field. At displacements greater than 30 mm the model over estimates the amount of flux. The ANSYS model was only 70 mm long, at the edge of the model a boundary condition was applied that would assume that all flux would be parallel at the edge of the model. A similar problem was experienced with the model of Turner's prototype, by extending the model a better prediction of the field was produced. If the model of the reference flow

meter were extended to say 140 mm then the field prediction would greatly improve.

4.3.2. Modelling the Electric field

A model of an insulating cylindrical conduit with conducting point contact electrodes was produced. The liquid was modelled and given electrical conductivity to allow current to flow within the pipe. To generate the electric field a unit charge was applied to the electrodes, one having positive charge the other negative. If the electrodes were spherical discs positioned in a vacuum the electric field would look identical to an electric dipole (figure 4.8).

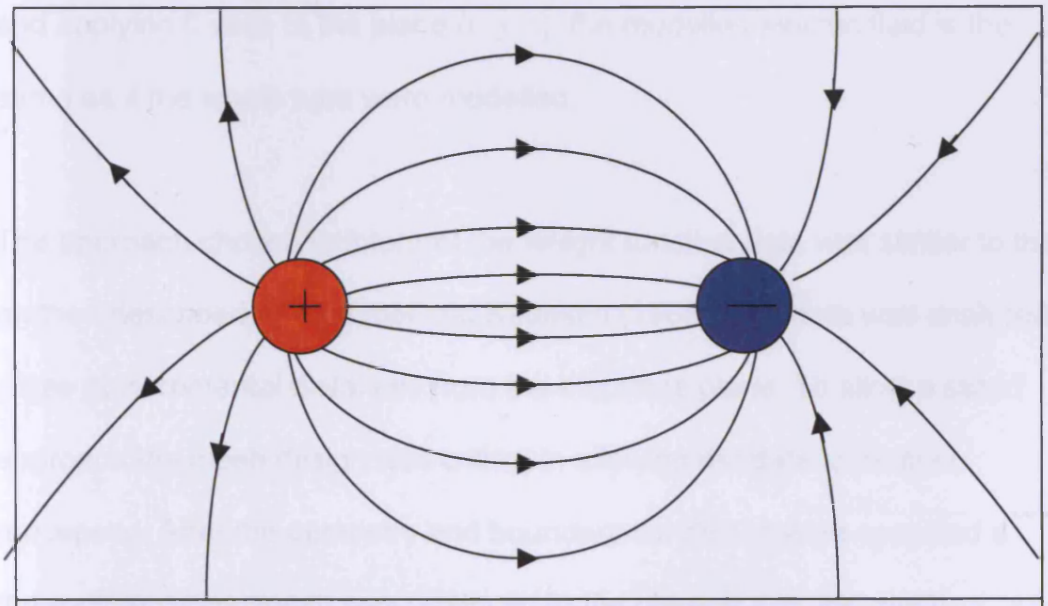

Figure 4.8. An Electric Dipole

4.3.3. Combining the electric and magnetic field models to produce a weight function model

Having modelled the virtual current potential and the magnetic field vectors separately, the experience required in using ANSYS as a tool to predict the relevant fields was gained. A combined model was now required to allow ANSYS to calculate the weight function vectors at each element within the model. The symmetrical nature of the problem allowed the model to be simplified so that only one quarter of the tube was modelled, as shown in figure 4.9. By applying symmetry boundary conditions along the plane $(x, 0, z)$ and applying 0 volts to the plane $(0, y, z)$, the modelled electric field is the same as if the whole tube were modelled.

The approach chosen to interpret the weight function data was similar to the method described by Rummel and Ketelsen (1966). The data was analysed in slices at incremental distances from the electrode plane. To allow a sliced approach the mesh design was critical in allowing the data to be post processed. After the geometry and boundary conditions were specified a three-dimensional mesh was produced in the plane $(x, y, 0)$, the mesh consisted of 4-sided shapes, as shown in figure 4.9.

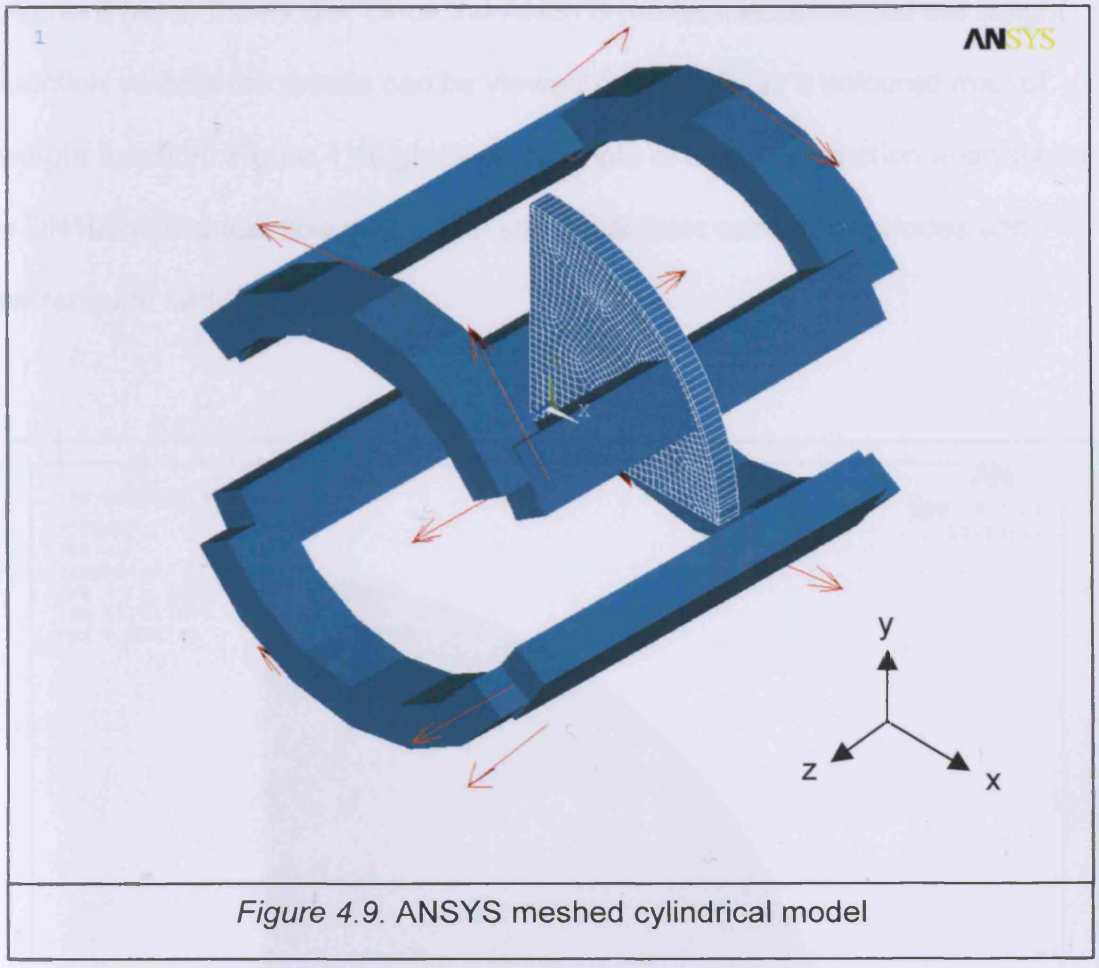

Figure 4.9. ANSYS meshed cylindrical model

Once a suitable three-dimensional mesh was defined the mesh was then extruded along the length of the model. This style of meshing allowed bricks of a certain defined length to be produced thus allowing the data to be analysed at a series of known positions throughout the length of the model. The model is solved for the virtual current potential and the magnetic field vectors. The mesh is identical for both solutions and so each element or brick contains at its centre vectors of magnetic field and virtual current potential. Once the ANSYS model has solved for both magnetic and electric fields the FEA analysis is complete. The ANSYS program is then used to post process

the data to calculate the weight function vector, $\underline{W} = \boldsymbol{k}\left(B_x G_y - B_y G_x\right)$, for each element within the model. Once the ANSYS model has calculated the weight function vectors the results can be viewed graphically as a coloured map of weight function. Figure 4.10 gives an example of a weight function analysis on a DN100 cylindrical flow meter with small diameter contact electrodes and rectangular saddle coils.

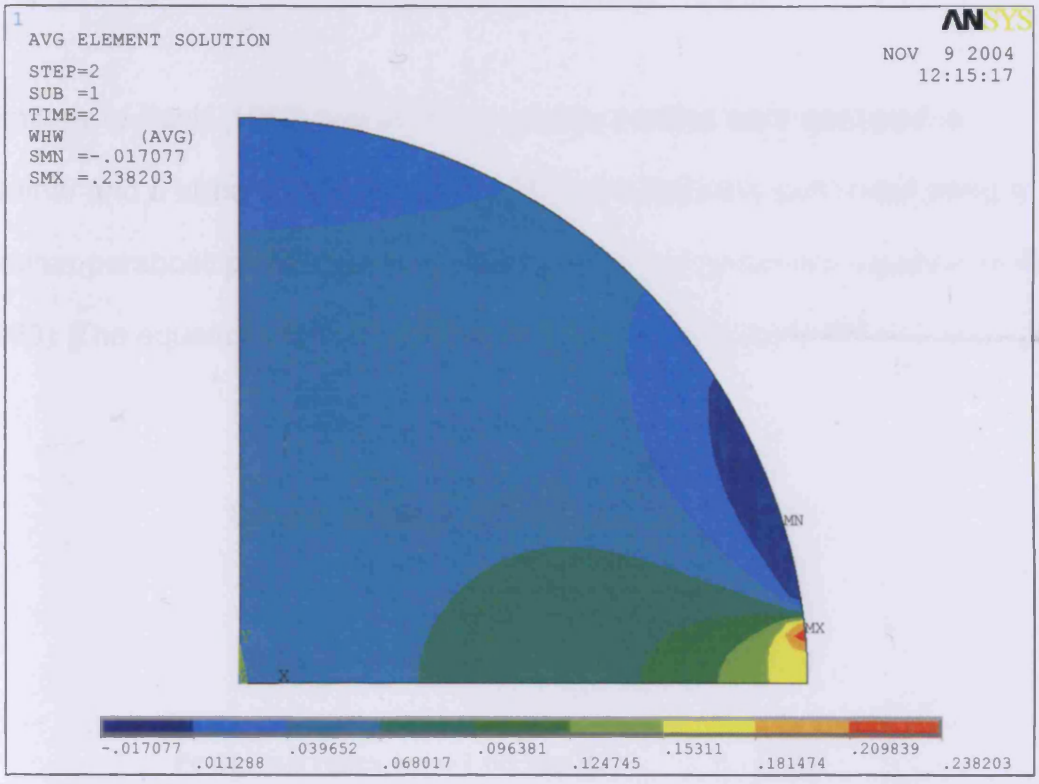

Figure 4.10. Weight function coloured map of a DN100 flow meter

Similar plots to figure 4.10 can be displayed for each slice throughout the model, thus giving an indication of how far from the electrode plane the measuring section extends.

4.3.4. Post processing the weight function F.E.A. data

To analyse the performance when the flow meter is subjected to a flowing condition further post processing of the ANSYS results was required. The weight function vectors were exported one layer at a time into Microsoft Excel. The exported results included the calculated weight function vector within each brick element, the volume of each individual brick and its relative Cartesian coordinates.

Similarly to Bevir (1969) two different velocity profiles were analysed, a laminar and a turbulent velocity profile. The profiles were generated using a laminar parabolic profile and the turbulent empirical power law equation (Miller 1983). The equations for both profiles are given in equations 4.6, 4.7 and 4.8.

$$\text{Laminar profile}: u_{Lam} = \hat{u}\left(1-\left(\frac{y}{r}\right)^2\right) \qquad (4.6)$$

$$\text{Turbulent profile}: u_{turb} = \hat{u}\left(1-\frac{y}{r}\right)^{1/n} \qquad (4.7)$$

$$\text{Power law index}: \; n = 1.66.\log(\text{Re}) \qquad (4.8)$$

To allow direct comparison between the calculated electrode potentials the profiles were designed so that the mean average velocity for each profile was constant. The velocity profiles are shown in figure 4.11.

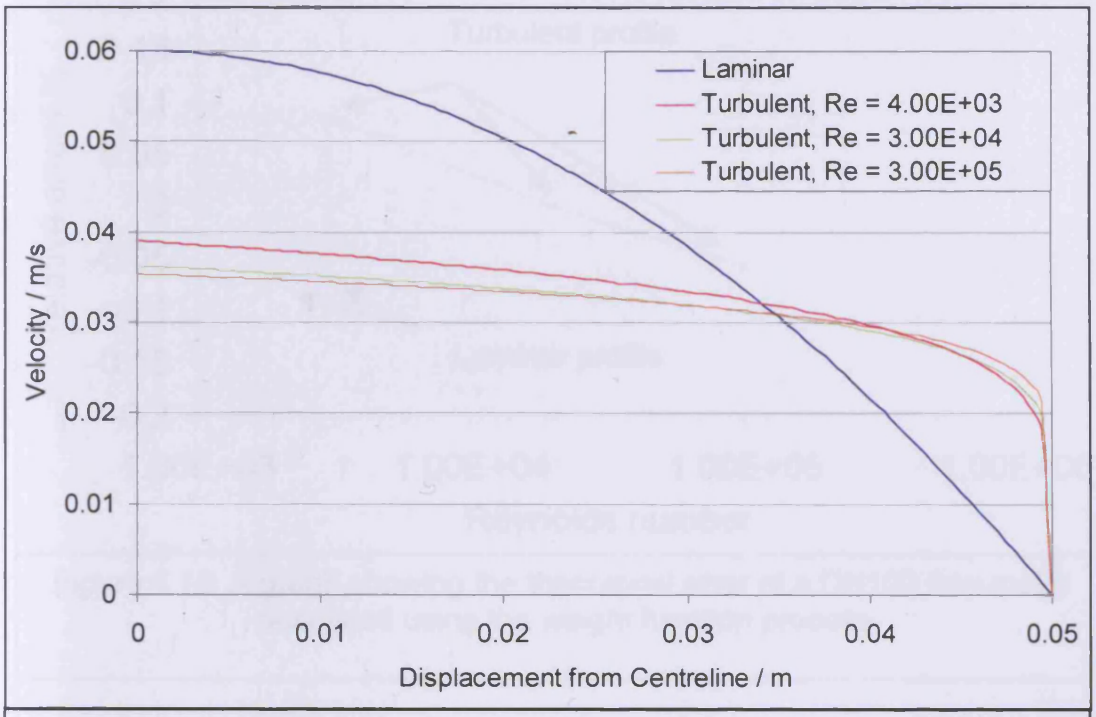

Figure 4.11. A comparison between theoretical and experimental Magnetic flux density measurements

The local velocity at each element location was calculated using its relative Cartesian coordinates. The potential of each slice was calculated using equation 4.5 and the volume used for the integral was based upon the volume of each slice. Flow meters are calibrated by performing a span calibration at a relatively high velocity (4 m/s, Turner's prototype); the performance at lower velocities (0.5 m/s and 0.1 m/s) is then checked. Similarly to the actual calibration of a flow meter the weight function process was used in the same manner. For example if the voltages generated for Reynolds numbers of 1 x 10^5, 2 x 10^4, 3000 and 2000 are calculated, the voltage error relative to the 2 x 10^4 profile can be plotted on a graph, as shown in figure 4.12.

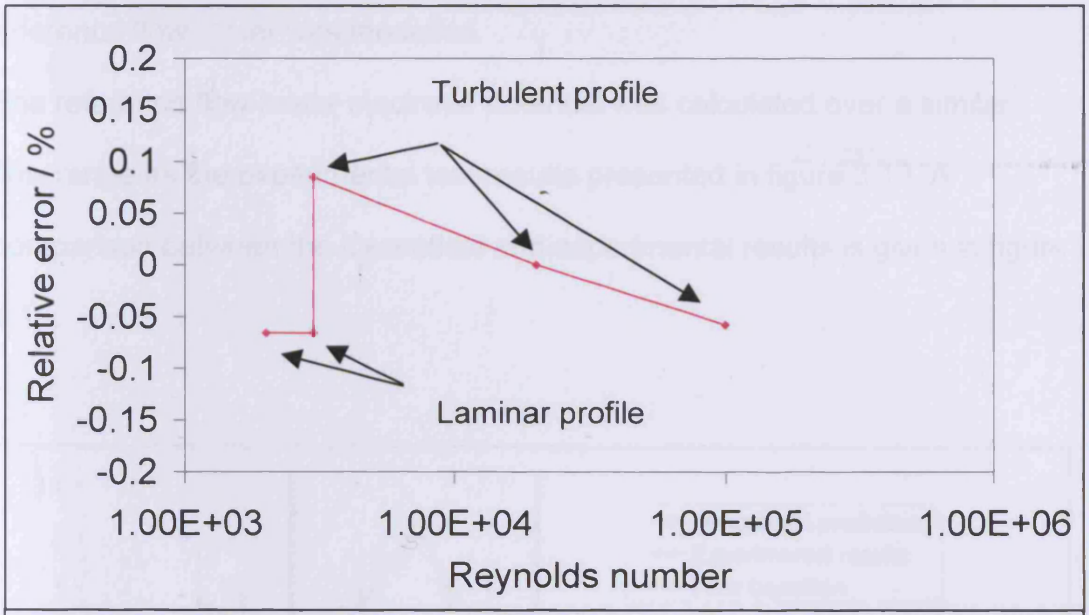

Figure 4.12. A graph showing the theoretical error of a DN100 flow meter calculated using the weight function process

The relative errors used in the figures within this chapter show the difference between measured and calibrated output using standard error technique. The results in figure 4.12 show that there are two error values at the same Reynolds number. To allow a continuous line throughout the calibration region the turbulent profile was calculated at a value that is within the transition region. The laminar profile at the same Reynolds number was also calculated. This completes a description of the weight function process developed as part of this project. The next section will detail the work undertaken in verifying how the theoretical error compares with the experimental results.

4.4. Experimental verification of the theoretical weight function model

4.4.1. Modelling the reference flow meter

Using the ANSYS weight function technique described in section 4.3 the reference flow meter was modelled.

The reference flow meter electrode potential was calculated over a similar flow range as the experimental test results presented in figure 3.13. A comparison between the theoretical and experimental results is given in figure 4.13.

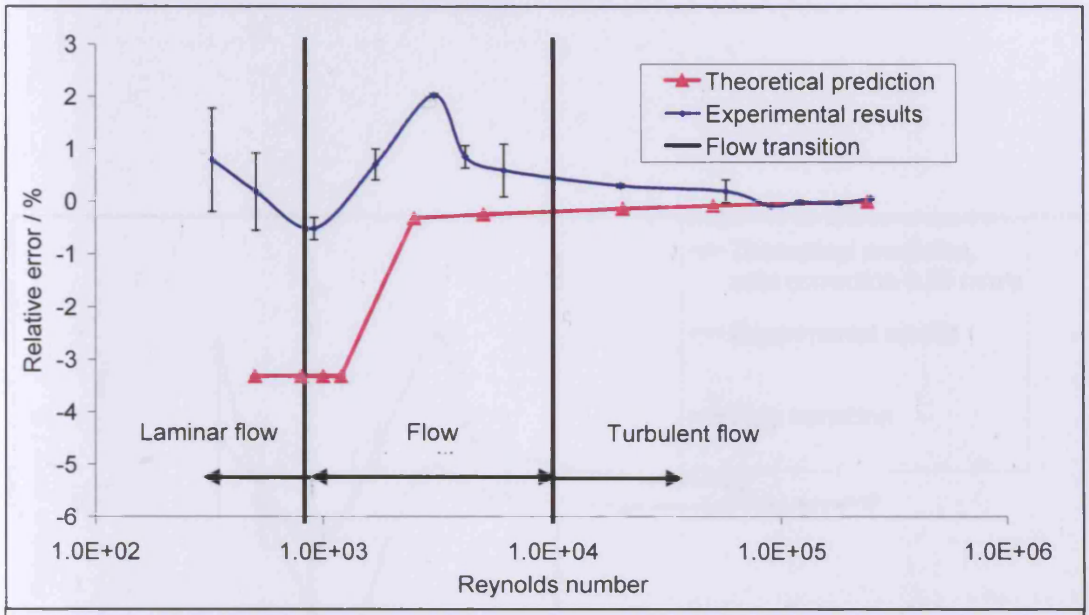

Figure 4.13. A comparison between the experimental results and the theoretical weight function results for the reference flow meter

Figure 4.13 shows that the weight function process has predicted the change in performance between the laminar and turbulent flow regimes. The performance within the flow transition region has been predicted by testing the model with a laminar profile in a region where it would be transitional and also with a turbulent profile with a Reynolds number that would be transitional. The

results show that the theoretical model predicts that the performance will change as the velocity profile changes from laminar to turbulent. When the reference flow meter was calibrated a small zero correction was made to improve the low velocity performance, the exact shift in calibration corresponded to 0.05 mm / s. By applying a zero correction of 0.4 mm/s the theoretical results become very similar to the experimental results as shown in figure 4.14.

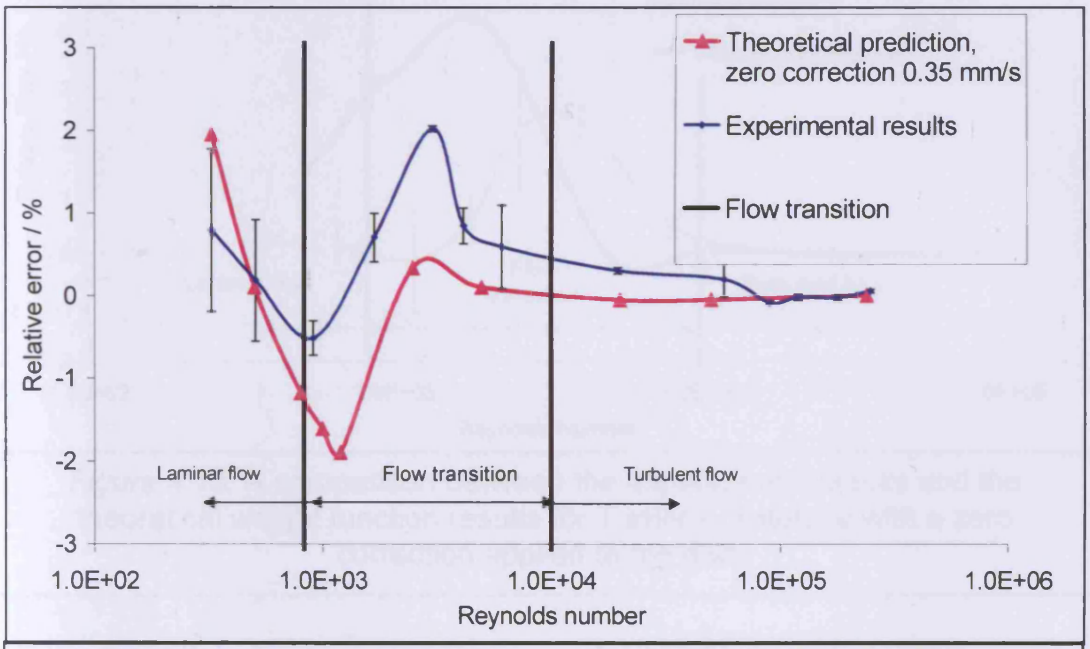

Figure 4.14. A comparison between the experimental results and the theoretical weight function results for the reference flow meter with a zero correction applied to the data.

4.4.2. Modelling Turner's prototype

The electrode potential for Turner's prototype was calculated over a similar flow range as the experimental test results shown in figure 3.12. A comparison between the theoretical and experimental results is shown in figure 4.15.

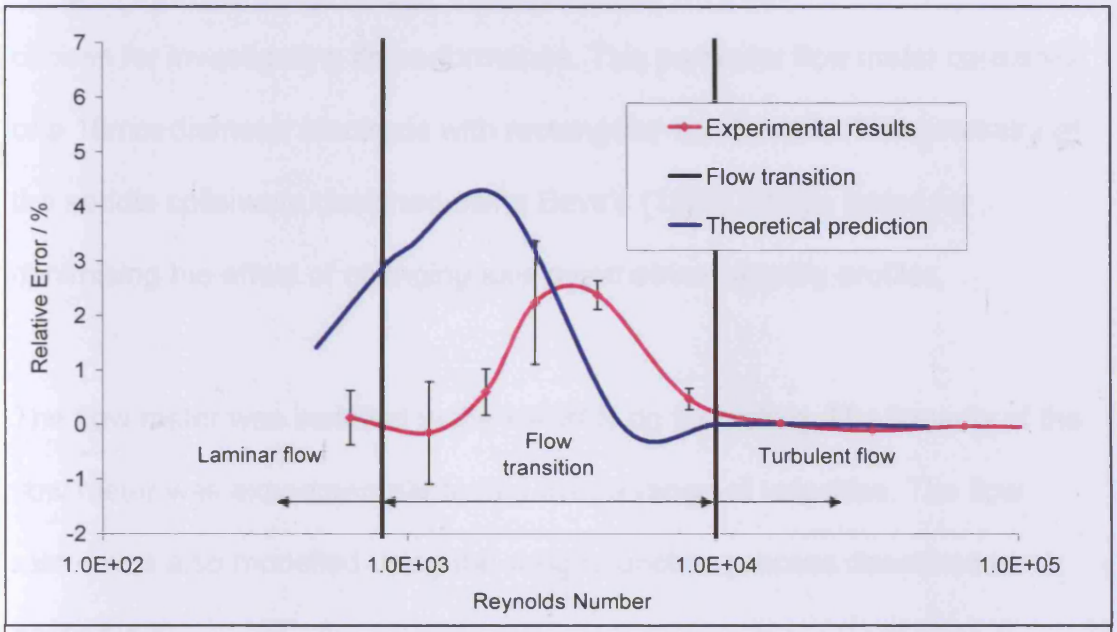

Figure 4.15. A comparison between the experimental results and the theoretical weight function results for Turner's prototype with a zero correction applied to the data.

The results in figure 4.15 show that the weight function process has not predicted the correct location of the transition region. This is probably due to simplifications made to the model. The electrodes on Turner's prototype are positioned proud of the wall of the flow tube. In the model they were modelled as flush with the pipe wall.

4.5. Developing an Ideal Flow meter for ABB

4.5.1. An Investigation into the performance of a conventional flow meter with asymmetric velocity profiles

As Bevir (1969) had not indicated how poorly the conventional geometry flow meter might perform with asymmetric flow profiles an experiment was designed to do this. An ABB manufactured DN100 'Hiflo' flow meter was chosen for investigating its performance. This particular flow meter consisted of a 10mm diameter electrode with rectangular saddle coils. The geometry of the saddle coils were designed using Bevir's (1969) design tables for minimising the effect of changing axis-symmetrical velocity profiles.

The flow meter was installed in the NAMAS rig for testing. The linearity of the flow meter was experimentally tested over a range of velocities. The flow meter was also modelled using the weight function process described in section 4.3.

A comparison between the theoretical and experimental test results is given in figure 4.16.

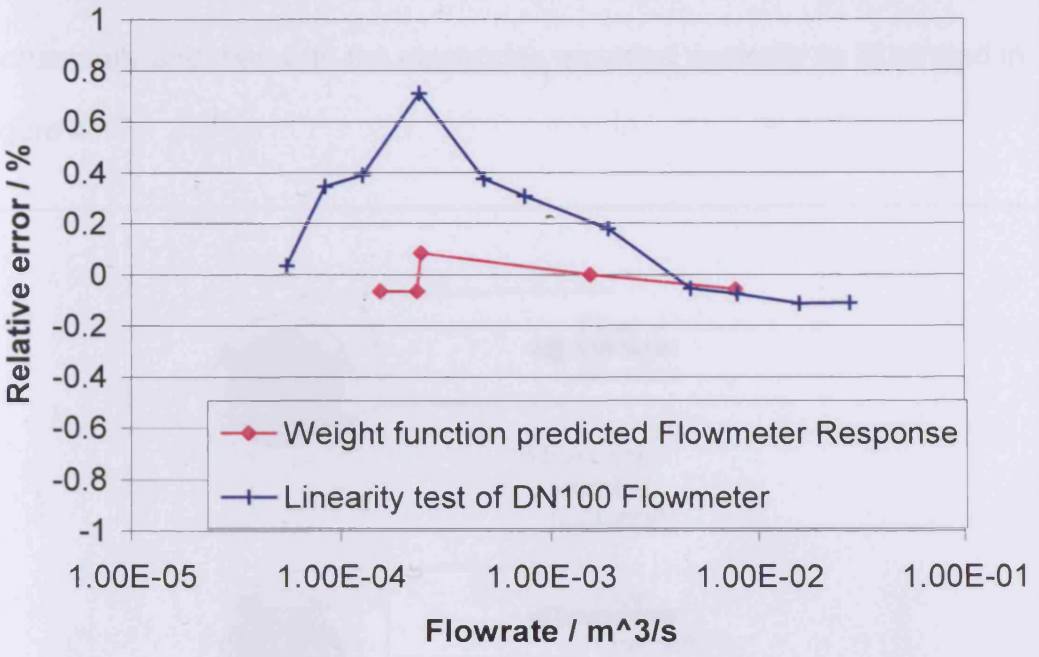

Figure 4.16. A comparison between the theoretical and experimental flow performance of a DN100 'Hiflo' flow meter

By comparing the results in figure 4.16 with those in figure 4.15 and 4.16 the DN100 flow meter is less susceptible to changes in velocity profile than the reference flow meter and Turner's prototype. The theoretical modelling has correctly predicted a change in performance in a similar position to the experimental results. The weight function process has under predicted the magnitude of the errors found experimentally. This suggests that either the model does not represent the actual flow meter or that the experimental data is in error.

The DN100 flow meter was then installed with a 90 Degree elbow upstream and five diameters of straight pipe work downstream to ensure the flow was fully developed. Flow tests were then performed at a range of velocities.

The flow meter was installed with the measuring electrodes positioned horizontally and then with the electrodes mounted vertically as illustrated in figure 4.17.

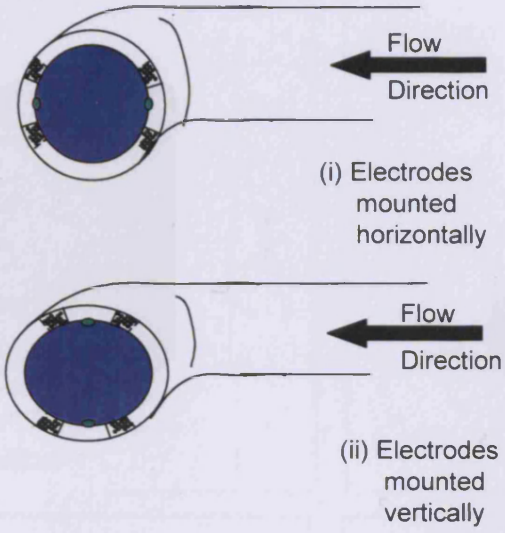

Figure 4.17. Elbow test installation configurations

The elbow was used, as it is a good method of creating a skewed profile (Sierra-Espinosa, 1997 and Miller, 1990). A very crude skewed profile was created using a spreadsheet with IF logic in Cartesian coordinates. The boundary layer was generated using the logical equation 4.9.

$$v(x,y) = IF((\sqrt{x^2 + y^2} - r) < \delta, 0, 1) \qquad (4.9)$$

where $\delta = 0.002\ m$

The skewed profile was created using equation 4.10.

$$v(x) = IF(x \geq 0, 0.7, 1.4) \qquad (4.10)$$

To change the orientation of the skewed profile the variable x was replaced by the variable y in equation 4.10.

The three dimensional velocity profiles together with the plots of the three-dimensional potentials are shown in figure 4.18.

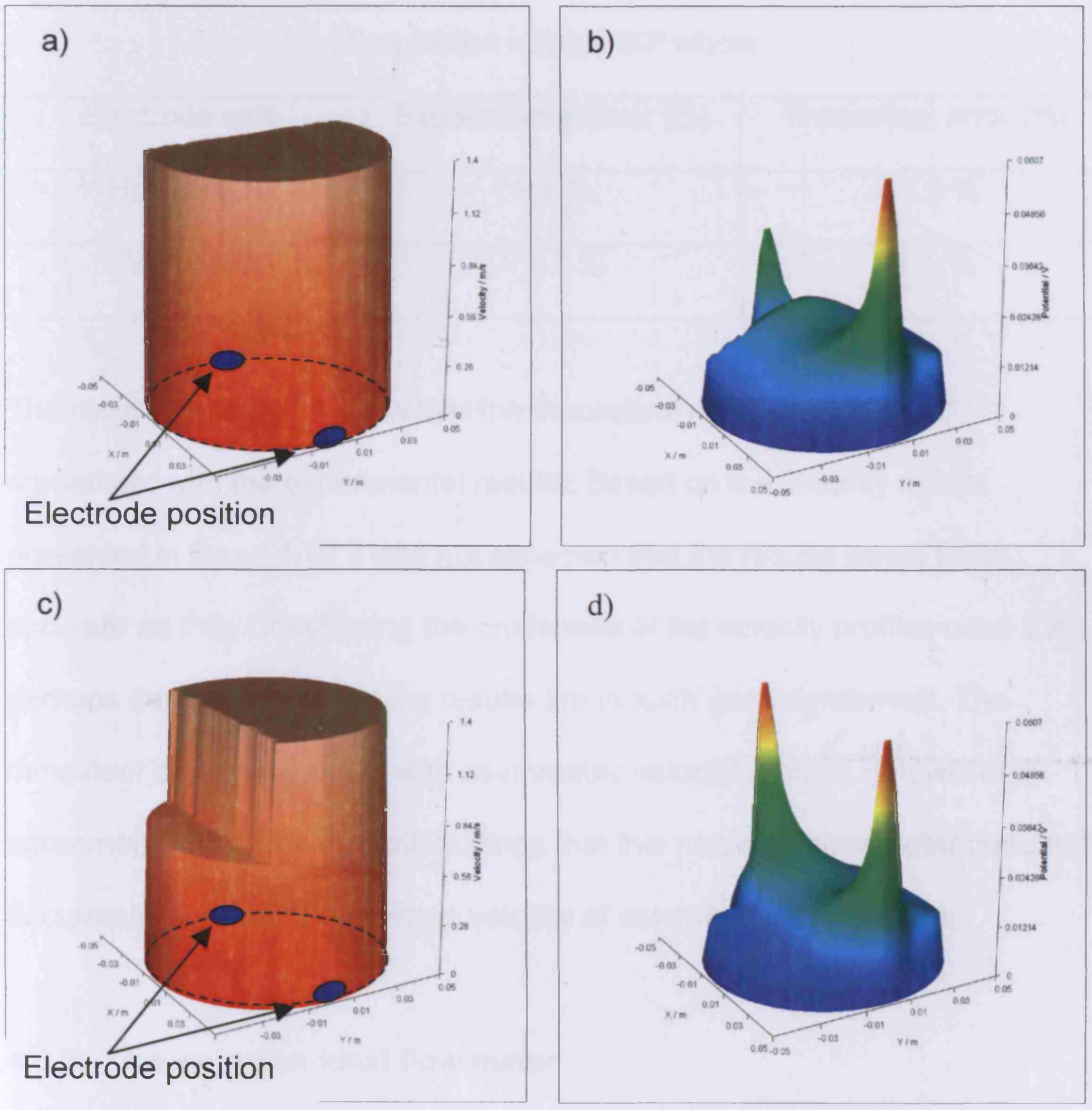

Figure 4.18. 3D plots of the skewed profiles along with the potentials predicted by the weight function process,
a) Vertical velocity profile, horizontal electrodes
b) Vertical potential profile, horizontal electrodes
c) Horizontal Velocity Profile, horizontal electrodes
d) Horizontal potential profile, horizontal electrodes

The theoretical and experimental results are shown in table 4.1.

Table 4.1. A comparison between theoretical and experimental error when flow tested using a 90° elbow

Electrode axis	Experimental error (%)	Theoretical error (%)
Horizontal	+ 2 %	+ 2.9 %
Vertical	- 1.7 %	- 1.4 %

The results in table 4.1 show that the theoretical results are in good agreement with the experimental results. Based on the linearity results presented in figure 4.16 it was not expected that the results would be as accurate as this. Considering the crudeness of the velocity profiles used it is perhaps serendipitous that the results are in such good agreement. The behaviour of the flow meter with asymmetric velocity profiles is however in agreement with Bevir's (1969) findings that this particular flow meter does not accurately measure the average velocity of asymmetric flow profiles.

4.5.2. Designing an Ideal flow meter

Bevir (1969) had presented weight function contour plots for cylindrical conduits with circumferential line electrodes subtending different angles. The results suggested an improvement in performance was possible over point contact electrodes, but Bevir (1969) acknowledged that performance was not ideal. Toshiba released a flow meter that claims ideal performance using a

cylindrical flow conduit and point contact electrodes. The patent (US 5125276 1992) describes how four coils are used to produce a specific magnetic field that allows any velocity profile to be accurately measured. This is similar to some of the ideas explored by Bevir (1969) where a matching magnetic field was used to improve the weight function contours. The coils represent one of the major costs associated with manufacturing flow meters therefore for ABB a flow meter with more than two coils was not a viable solution. The proposed solution for ABB involved creating a flow meter that was somewhere in between a rectangular ideal flow meter and a conventional flow meter. The proposed design is shown in figure 4.19.

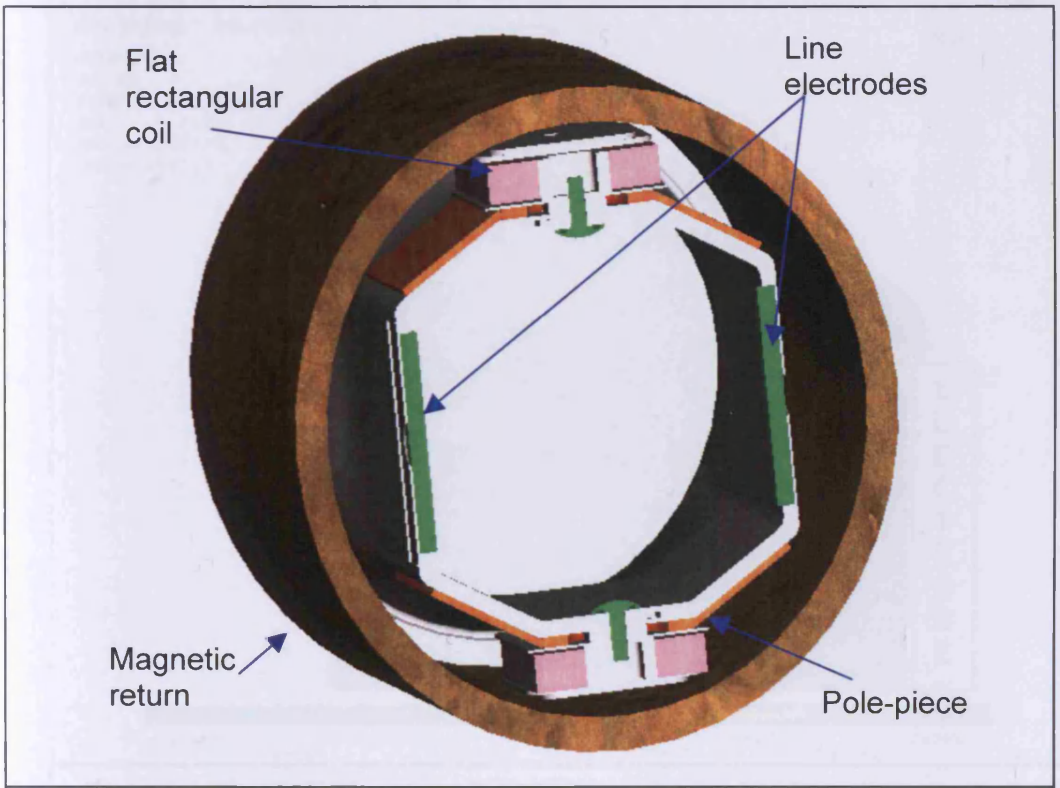

Figure 4.19. A picture illustrating the basic design of the proposed ideal flowmeter

From the ANSYS modelling work carried out it became clear that the electrode geometry would have to change to allow the flow meter to achieve its objective. The electrode geometry was changed to a line electrode (as shown in figure 4.19), which covered the vertical surface of the conduit. The ANSYS model was used to design a magnetic field that would give as close to a uniform weight function in all regions of the measuring section. By having a constant weight function vector at all positions within the duct the flow meter will accurately measure the average velocity of any velocity flow profile.

The ANSYS weight function model with as uniform a weight function as possible is shown in figure 4.20.

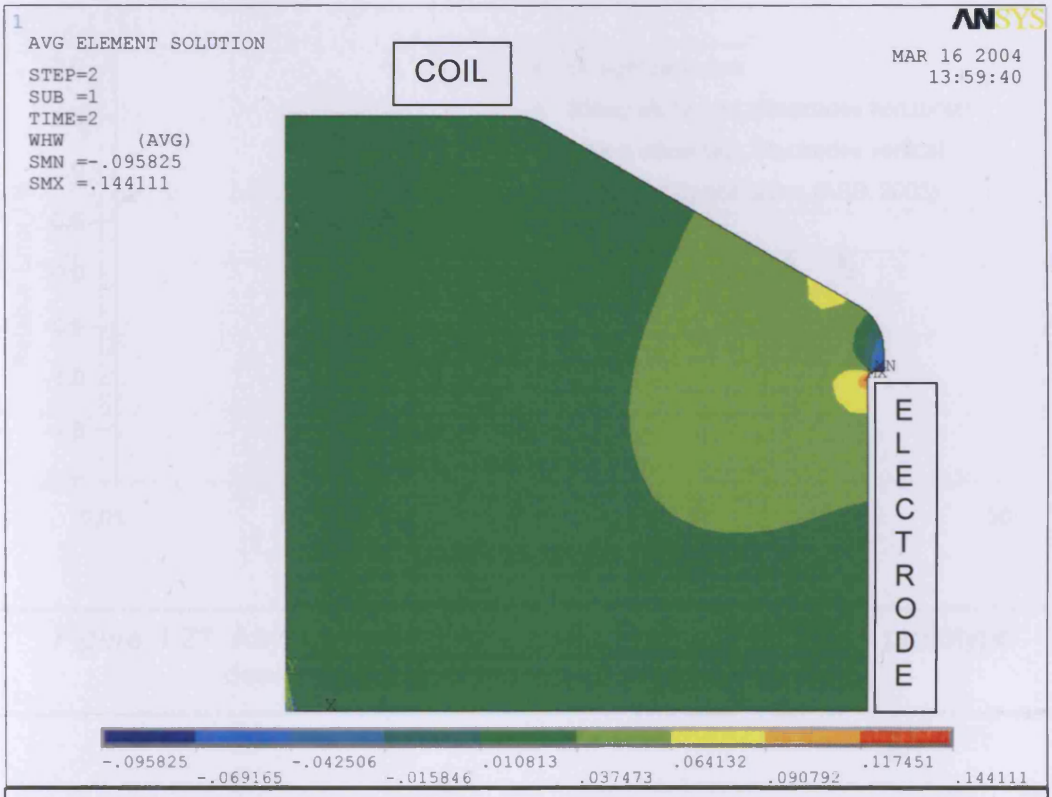

Figure 4.20. ANSYS weight function results for ¼ of the flow conduit of a DN100 flow meter.

The results in figure 4.20 show that the weight function is uniform over most of the flow duct. At the edge of the electrode strip the weight function reaches a vector maximum because the orientation of the electric field leaving the electrode is perfectly perpendicular to the magnetic flux in that region. As a consequence the velocity measurement at the top and bottom edge of the electrode will have a greater weighting than the velocity in other regions of the duct. The design has been optimised as far as possible in the aim of producing a uniform weighting throughout the conduit. A prototype was built and the 90°-elbow test was used as the test for ideal behaviour. The results are shown in figure 4.21.

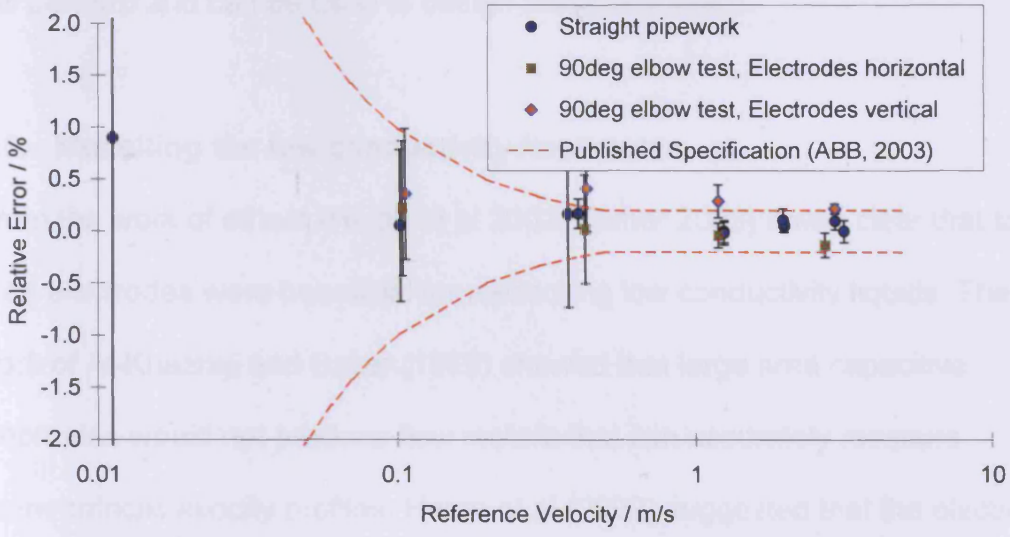

Figure 4.21. Asymmetric velocity profile testing of a DN100 prototype designed for near ideal flow meter behaviour

The results in figure 4.21 show that the flow meter performance with straight pipe work is within the published accuracy specification. The performance

with the electrodes horizontal and the 90-degree elbow directly upstream (refer to figure 4.17 (i)) show that the actual flow measurements were within the specification and very similar to the straight pipe work results. The performance with the electrodes positioned vertically (refer to figure 4.17 (ii)) is outside of the specification and has caused the flow meter to measure higher than the actual flow rate. The results in comparison to the DN100 Hiflo flow meter are much better. By referring to table 4.1 the measurement error for the DN100 Hiflo flow meter was approximately ± 2 % whereas the results in figure 4.21 show that the near 'ideal' prototype flow meter was accurate to within ± 0.5 %. This is a great improvement in performance and is further proof that the weight function process correctly predicts how the flow meter will perform and can be used to design real flow meters.

4.6. Modelling the low conductivity flow meter

From the work of others (Hemp et al 2002; Turner 2003) it was clear that large area electrodes were beneficial for measuring low conductivity liquids. The work of Al-Khazraji and Baker (1979) showed that large area capacitive electrodes would not produce flow meters that can accurately measure asymmetrical velocity profiles. Hemp et al (2002) suggested that the electrode half angle should be increased to 90° to increase the signal amplitude measurement (with a current sensing electrode arrangement). This is a simplistic solution to a complex problem because although the signal amplitude will be increased the flow meter performance will be significantly affected by the hydraulic conditions, both axis-symmetric and asymmetric. A small gap between the two electrodes is also required to ensure the

generated signal is not shorted out. Within this gap position the electric field between the two electrodes is very strong and the contribution of this area to the overall output of the flow meter will be large compared with the general level of signal present at other parts of the electrode. With this situation the flow meter effectively becomes a 2- point velocity-measuring device and it is unlikely to be able to accurately infer flow rate with different velocity profiles. To understand what the likely affect in performance might be the weight function process was used to compare the performance of different electrode angles with different axis-symmetrical velocity profiles. A model was created for a DN50 flow meter using a set electrode length of 8 mm, the batch file used to create the ANSYS model is given in appendix A. The magnetic circuit consisted of two rectangular saddles coils, which were shaped to follow the radius of the DN50 pipe. Surrounding the coils was a cylindrical mild steel pipe, which acted as the magnetic return path. The electrode angle was increased from a half angle of 4.6° up to 88°. The performance with different velocity profiles was then calculated. A graph of profile ratio against electrode half angle is shown in figure 4.21.

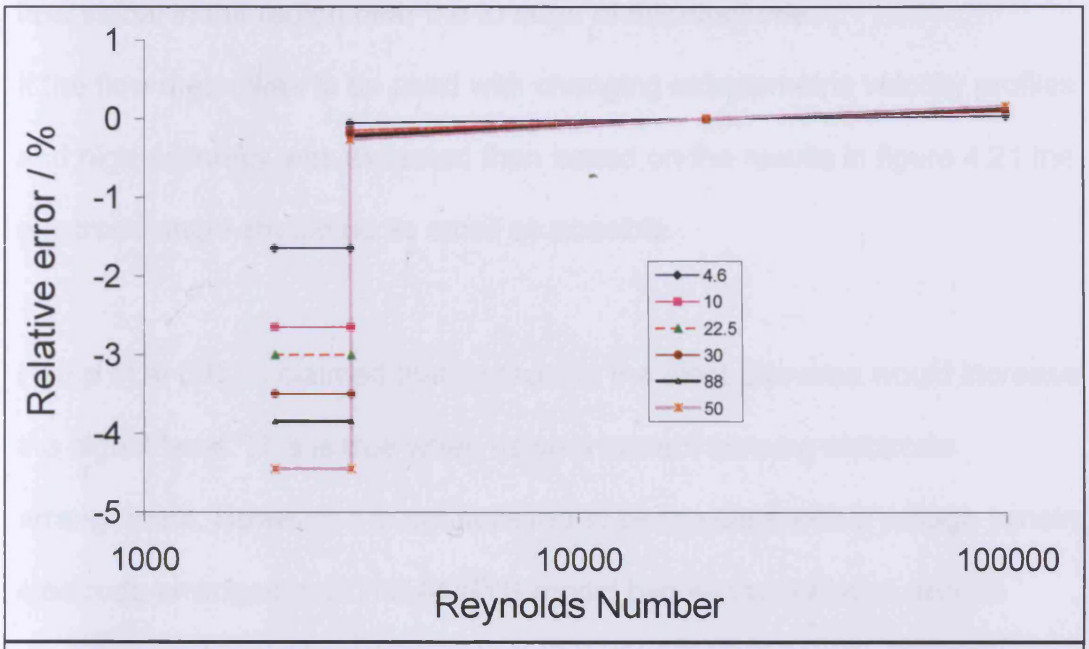

Figure 4.21. A theoretical analysis of the performance of a DN50 flow meter with different electrode angles and different velocity profiles

The results in figure 4.21 show that the electrode angle has a major affect on the flow meter performance when tested with different velocity profiles. With the saddle coil arrangement modelled the results show that generally the smaller the electrode the better the performance. However the results predict that the 88° electrode half angle will more accurately measure changing velocity profiles than the 50° electrode half angle. Further investigations found that the flow meter was unusually sensitive to changes in electrode half angle around the 40° - 50° angle position. For example the laminar error at 45° was – 10 %, whereas at 44° and 46° the laminar errors were – 5 % and – 5.5 % respectively. The reason for these measurement errors was related to the location of the coil bundle relative to the edge of the electrode. Small changes in electrode angle had a large impact on the cross product of the electric field

and the magnetic field locally to the electrode edge, thus generating a large flow signal in the region near the to edge of the electrode.
If the flow meter was to be used with changing axisymmetric velocity profiles and high accuracy was expected then based on the results in figure 4.21 the electrode angle should be as small as possible.

Hemp et al (2002) claimed that increasing the electrode area would increase the signal level. This is true when using a current sensing electrode arrangement. However it is not believed to be the case with a voltage sensing electrode arrangement. The ANSYS model had so far not been used to predict the potential magnitudes and it was not known whether the ANSYS results would produce answers that were based on current sensing or voltage sensing. With high impedance potential sensing electrodes the potential developed across the pipe will be related to the size of the magnetic field and the velocity of the liquid passing through it. Therefore the length of the electrode will not influence the size of the potential generated across the pipe. A test using the ANSYS model of Turner's prototype was devised whereby the electrode length was reduced in decrements and the weight function output was recorded for each length. It was found that as the electrode length decreased the weight function output potential also dropped. This result indicated that the ANSYS weight function process was predicting the behaviour of current sensing electrode designs. To make the ANSYS model behave like a high impedance voltage-sensing electrode the boundary conditions applied to the electrode surface were changed from constant voltage to constant current. When the electrode length was changed the

ANSYS model did not show any change in weight function potential. The line electrode results for both boundary conditions are shown in figure 4.22.

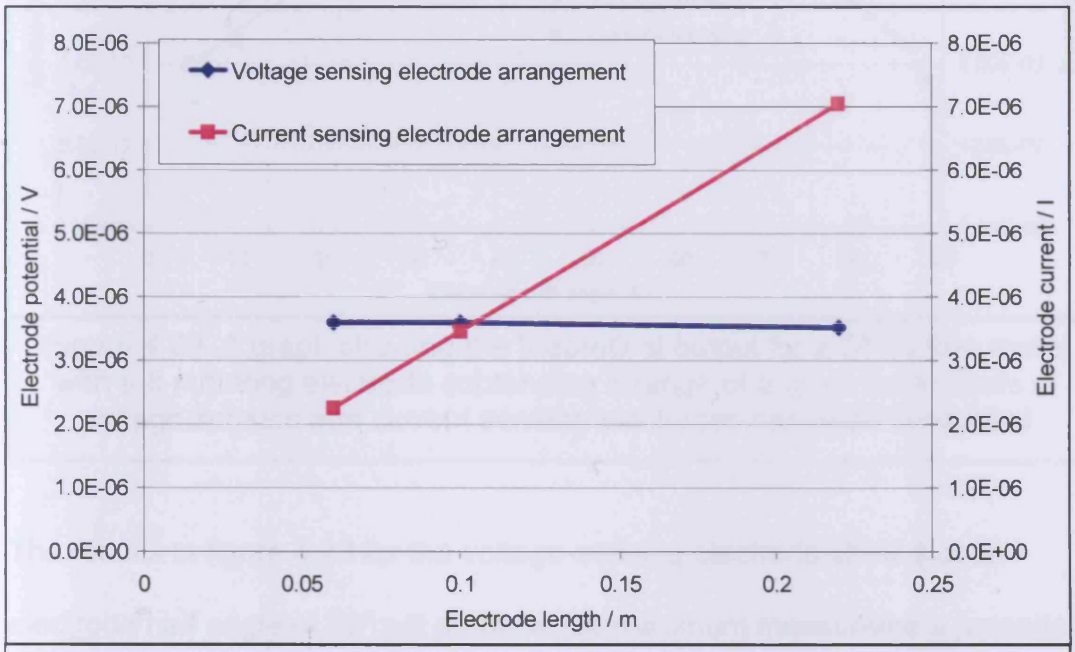

Figure 4.22. A graph showing the ANSYS weight function predictions for Turner's prototype with different length electrodes when operated with either a current sensing or with a voltage sensing electrode arrangement

With the ANSYS weight function process producing results that are in line with expectations the affect of increasing the electrode angle was explored. Using the DN50 model created to examine the velocity profile performance the weight function potential was calculated with the different electrode angles. The test was conducted using both of the described boundary conditions at the electrode surface. The results are shown in figure 4.23.

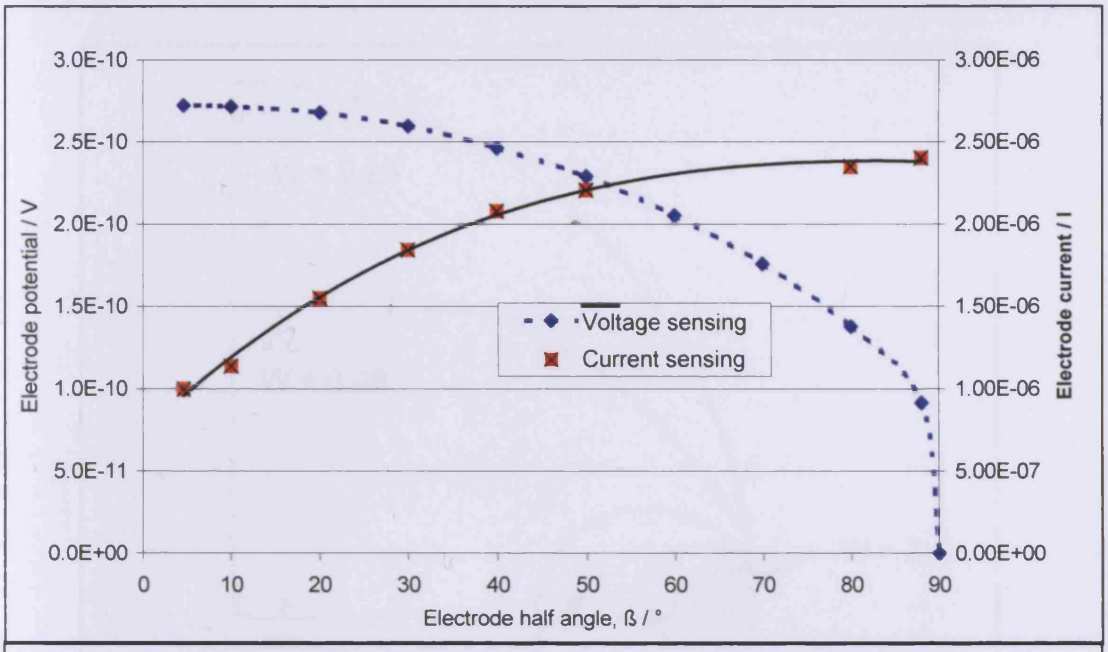

Figure 4.23. A graph showing the theoretical output for a DN50 flow meter with a 8 mm long electrode subtending a range of angles. An analysis of voltage sensing and current sensing electrodes has been conducted

The results in figure 4.23 for the voltage-sensing electrode show that an electrode half angle of 60° will produce the maximum measurement potential, above this value the potential begins to drop. With the current sensing electrode arrangement as the electrode angle increases the measurement potential also increases, but as the half angle tends towards 90° the amount of signal collected reaches a maximum. Intuitively this looks to be correct as once the electrodes are covering the entire diameter of the pipe no more current can be collected. The weight function contour maps for the different electrode angles were plotted to help understand the behaviour. The current sensing results for three different electrode angles are shown in figures 4.24, 4.25 and 4.26.

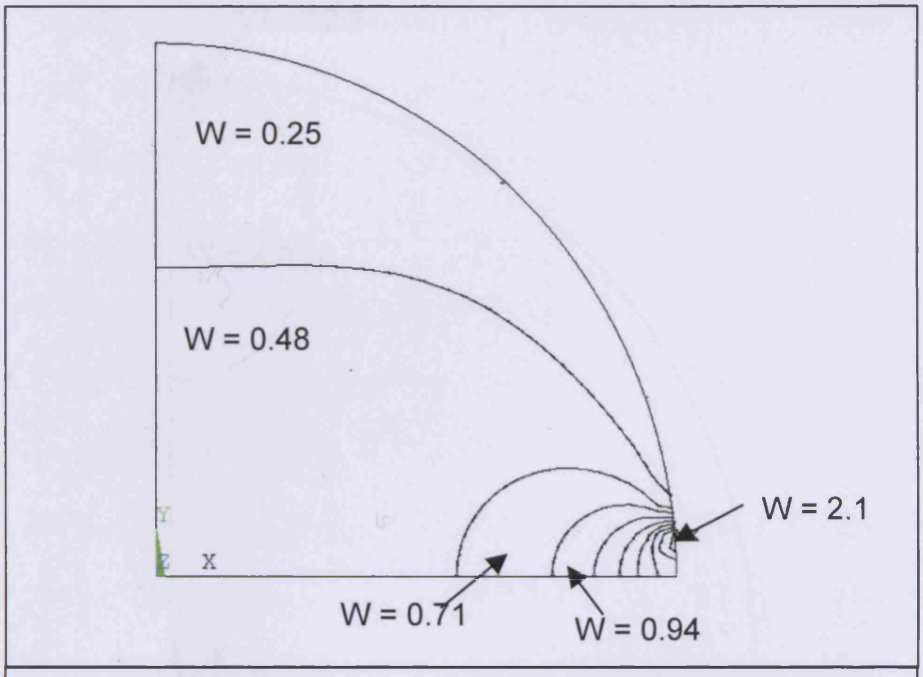

Figure 4.24. Weight function contour plot for ¼ of a DN50 flow meter with an electrode half angle β =4.6°

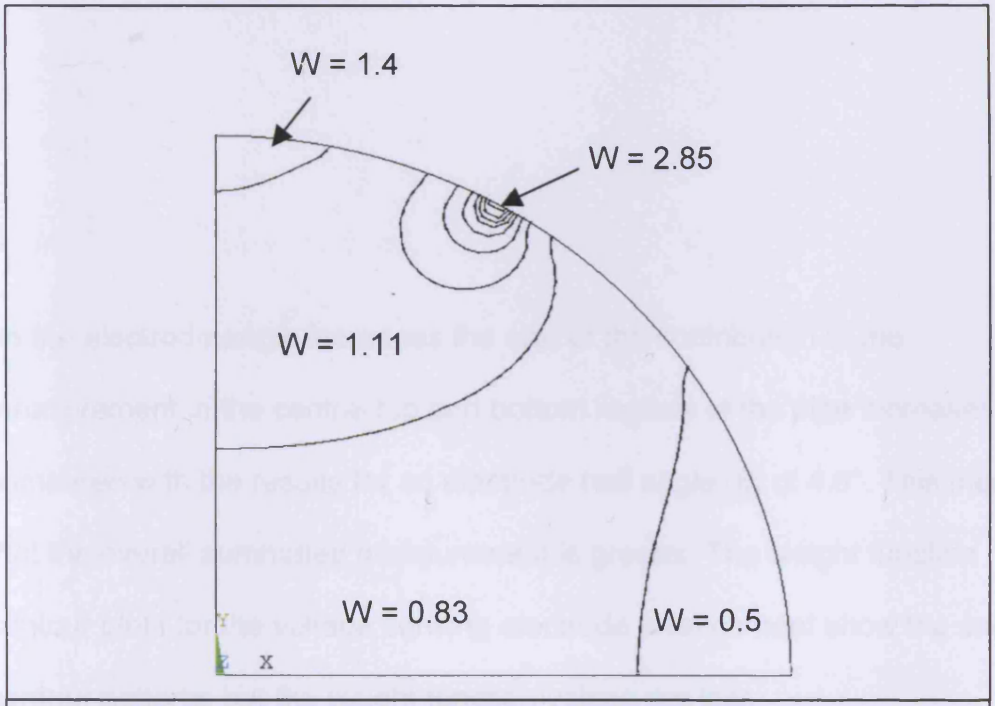

Figure 4.25. Weight function contour plot for ¼ of a DN50 flow meter with an electrode half angle β =60°

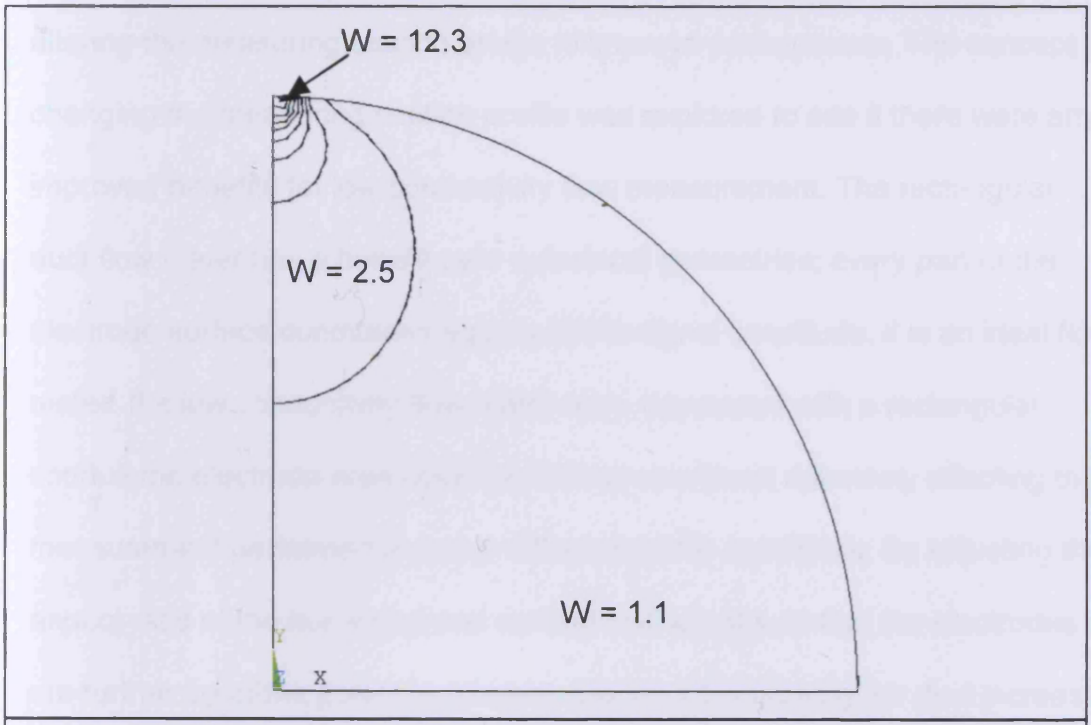

Figure 4.26. Weight function contour plot for ¼ of a DN50 flow meter with an electrode half angle β =88°

As the electrode angle increases the size of the contribution to the measurement in the central top and bottom regions of the pipe increases compared with the results for an electrode half angle (β) of 4.6°. This means that the overall summated measurement is greater. The weight function contour plots for the voltage sensing electrode arrangement show the same contour patterns but the weight function values are less.

The work carried out in developing an ideal flow meter for ABB involved altering the measuring section profile to improve performance. The concept of changing the measuring section profile was explored to see if there were any improved benefits for low conductivity flow measurement. The rectangular duct flow meter has a benefit over cylindrical geometries; every part of the electrode surface contributes equally to the signal amplitude, it is an ideal flow meter. If a low conductivity flow meter were developed with a rectangular conduit the electrode area could be increased without adversely affecting the measurement performance under different profile conditions. By adjusting the aspect ratio of the horizontal and vertical wall lengths so that the electrodes are further apart the potential generated across the rectangular duct increases and consequently so does the signal level.

4.7. Discussion

Development of the weight function process has allowed the performance of Turner's prototype and the reference flow meter to be modelled. The flow meter performance with different velocity profiles can be predicted with reasonable accuracy.

The likely signal level with different electrode geometries has been analysed. By changing the boundary conditions within the model the results indicate performances similar to those expected with current sensing and voltage sensing amplifier designs.

The performance with different velocity profiles and electrode angles was analysed and showed that increasing the electrode angle did not necessarily improve the flow meter performance when measuring different velocity profiles. Hemp et al (2002) claim that for low conductivity flow measurement the electrode area is key to successful performance. The limitations of large area cylindrical electrodes has demonstrated to the author that development of a rectangular duct flow meter would allow large area electrodes to be used without impeding flow performance.

The technique developed by Lincoln and Armitage used an off the shelf FEA package. At the early stages of this development a custom made programme using Visual Basic was considered, this idea was abandoned because of the complexity of the problem and the time available. By using a versatile FEA package, which could already model electric and magnetic fields, the time taken to develop the models and prove the process was significantly shortened compared with starting from scratch. Only once the process was started were the benefits of using such a package realised. Lincoln and Armitage are still developing the ANSYS weight function process, some of the areas of development include, the purchase of a CFD package. The CFD package will allow different velocity profiles to be modelled, this will be especially useful for modelling flow conduits that are not round.

It is also planned that the effect of eddy currents within the conductive parts of the flow meter will be researched. Modelling the effect of eddy currents will allow the performance with different AC frequencies to be analysed.

At the time of writing the number of boundary conditions within the model was being increased to analyse the shunting effect of earthing planes at either end of the magnetic field.

Chapter 5

Development of a new flow meter and measurement system

5.1. Introduction

The literature survey has shown that the noise voltages present when measuring a dielectric liquid are a major cause for concern. Amare (1995), Durcan (1998) and Cushing et al (1962, 1964 and 1965) designed flow meters to operate at frequencies greater than 1 kHz, as the noise voltages present at these frequencies were much less than at lower frequencies. To operate a flow meter at 1 kHz and higher the materials of construction were somewhat different to those used in conventional flow meters. One of the main differences related to the material used for the pressure containment tube. Instead of using a lined stainless steel tube (as is common practice (ABB, 2002)), Amare (1995) and Durcan (1998) used a Perspex tube. Cushing et al (1962) used a fibreglass wound tube. These tubes are insulators and do not generate eddy currents that may affect the magnetic field generation. Their flow meters (Cushing et al (1962) and Amare (1995)) also used capacitive electrodes with a fish bone design (see figure 2.3), in an attempt to reduce the generation of eddy currents.

From the test work conducted in Chapter 3, it was clear that an elongated electrode and coil arrangement produced a lower noise voltage than a conventional design of flow meter. The testing of Turner's prototype showed that it would not be able to efficiently operate at high frequencies.

The work conducted in Chapter 4 showed that a large area electrode can be used to increase the signal level when current sensing, as claimed by Hemp et al (2002). It was also found that the performance with different velocity profiles was affected as the area of the electrode was increased.

Based upon the experience gained from experimenting and through reviewing the work of others the development of a new flow meter will now be described. A brief review of the electronics and software used to operate the flow meter will also be given. Finally the process of combining the flow meter and electronics to produce a stable flow measuring system will be discussed.

5.2. The Flow meter Design

The next prototype needed to be easily assembled and disassembled to allow for modifications to the electrodes and the magnetic circuit. This section will give an overview of the flow meter design and also explain and justify some of the major design decisions.

The intention of this prototype was to operate at as high a frequency as possible, but lower than Amare (1995), Durcan (1998) and Cushing et al (1962, 1964 and 1965). By aiming to operate at a frequency of approximately 500 Hz the problems associated with zero stability will be less restrictive upon performance. The increased length of electrode will reduce the measured noise levels; consequently a lower frequency of operation should be possible.

5.2.1. The Flow Conduit Design

Based on the weight function work conducted as part of this project (Chapter 4) a rectangular flow duct was considered the optimum shape for making a low conductivity flow meter. A rectangular duct will accurately measure the flow rate regardless of the velocity profile. Despite having clear advantages in performance rectangular structures make very weak pressure vessels compared with cylindrical structures. As a compromise a square duct flow meter was designed. A square duct is stronger than a rectangular duct as the length of each side is equal meaning that the peak stresses and strains within each side are less when compared with a rectangular duct. To reduce the stresses placed on the tube when under pressure the square duct was designed with radii on the inside and outside corners of the square duct. A square duct flow meter with electrodes covering the entire length of the sidewalls has the advantage of being an ideal flow meter. As appreciated in chapter 4 an ideal flow meter will accurately measure the flow rate regardless of the velocity profile it is presented with.

Turner's prototype had a 50 mm nominal bore with a magnetic field length of approximately 300 mm. Theoretically the longer the magnetic field and the closer the electrode separation the lower noise voltage (see equation 3.9). A 25 mm square flow tube was chosen for this prototype as the magnetic field can be made a similar length to Turner's prototype but the electrode separation distance will be halved, consequently the noise voltage will be reduced. If the flow meter were installed in DN50 pipe work then for an incompressible liquid the velocity in the measuring section would be greater

than that in the surrounding pipe work. For example if the velocity in the pipe work is 1 m/s then by continuity the velocity in the measuring section will be 3.14 m/s. Therefore the flow meter will measure 3.14 times more signal than a standard cylindrical DN50 diameter flow meter.

The options for manufacturing the flow conduit are to produce an insulating liner that can act as the pressure containment or to build a pressure containment tube and then line it with an insulating liner. Lining a square stainless steel conduit would be very difficult due to the cross section and length of the measuring section. With metallic lined flow tubes the design can suffer from signal degradation by capacitive losses through the lining, also eddy current losses can be problematic. Producing an insulating liner that could act as the pressure containment was favoured. The flow meter will be tested on water, demineralised water, glycols and mineral/synthetic oils therefore careful selection of the wetted parts was required to ensure chemical compatibility.

5.2.1.1. A Flow conduit manufactured from Glass Fibre Reinforced Plastic

The first material identified as chemically resistant to the liquids specified was Glass fibre reinforced plastic (GRP). An 'off the shelf' GRP fibreglass tube was purchased and a small-scale prototype was assembled for evaluation. When pressure tested water began to leak through the sidewall of the tube as shown in figure 5.1.

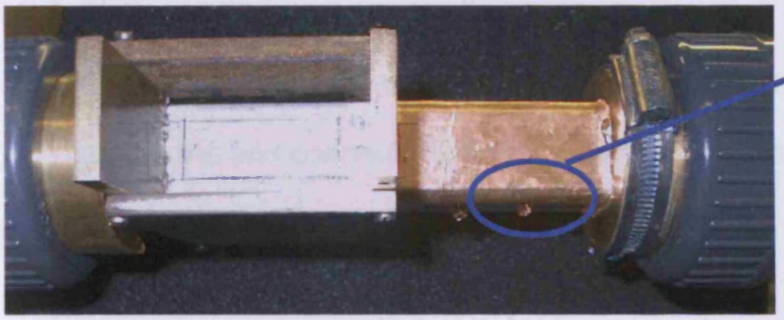

Figure 5.1. A photograph showing the prototype GRP flow conduit leaking

GRP tubes are manufactured by spraying strands of epoxy and glass fibre onto a mandrel. The resulting structure has an excellent strength to weight ratio but can have a tendency to be porous, especially when placed under strain. The idea of sealing the internal surfaces with a secondary layer was considered but deemed unlikely to work and so the use of GRP as a flow conduit was abandoned due to this problem.

5.2.1.2. An Extruded boro-silicate glass conduit

The next concept considered involved the manufacture of an extruded boro-silicate glass tube. Glass has excellent chemical resistance and for this laboratory research it can be designed to withstand 1 bar internal line pressure, which is sufficient. The dielectric constant of borosilicate is between k = 4 and 5, the volume resistivity is 10^{12} Ω.m (Kaye & Laby, 1989). This means it is not as good an insulator as PTFE for example, where k = 2.1 and

the volume resistivity = $10^{15} - 10^{19}$ Ω.m (Kaye & Laby, 1989). The tube manufacturing drawing is given in appendix B.

5.2.2. Flow conduit end connection means

Having a square glass tube presented itself with a problem in how to manufacture the end connections to the mating pipe work and seal the process liquid.

5.2.2.1. Joint connection method 1

The first design involved welding a DN50 to DN25 stainless steel reducer cone to a DN25 PN16 flange and then potting the end of the glass tube into the cone, see figure 5.2.

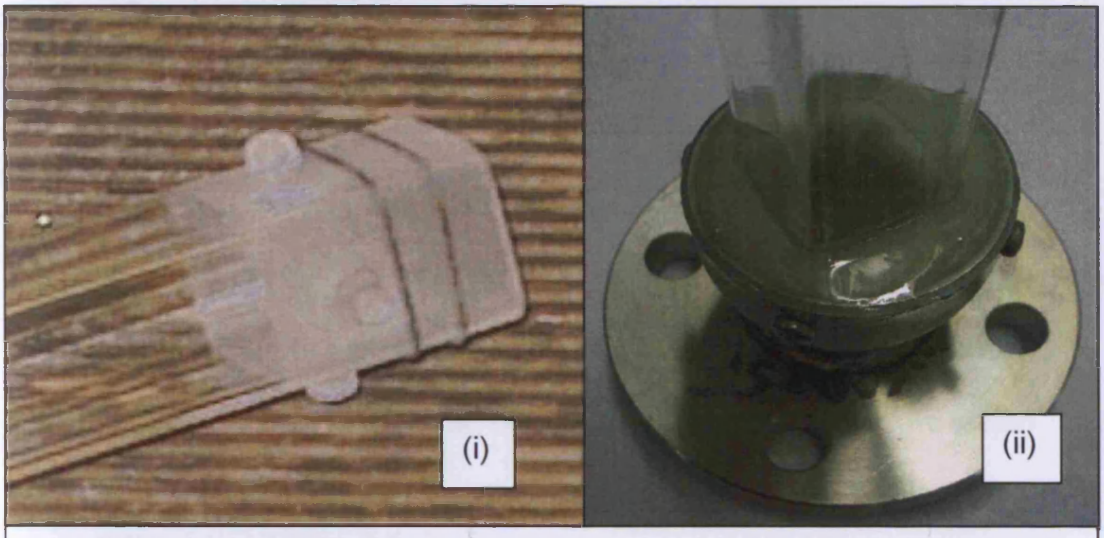

Figure 5.2. Epoxy potting end sealing connection method showing:
(i) Glass tube pre-prepared for bonding.
(ii) Glass tube potted in position creating sealed joint.

To improve bond strength the ends of the glass tube had glass rods melted to the surface and the surface was bead blasted to increase the surface roughness, as shown in figure 5.2, (i). The finished potted assembly is shown in figure 5.2, (ii). The chosen epoxy had a thermal expansion coefficient very similar to that of the glass but despite this the curing process caused the glass tube to crack in one of its corners. The epoxy was constrained by the steel and consequently when the epoxy expanded during the 70 °C curing process the majority of expansion would have been directed inwards causing the tube to crack. This connection method was abandoned.

5.2.2.2. Joint connection method 2

The method of creating the end connection to the next glass tube involved producing a brass component with a square hole for the tube to locate into. The square hole in the brass tube was 2 mm oversized compared with the glass tube and the gap was filled using a flexible silicone sealant. Silicone is elastic enough to extrude itself out of a gap when it expands rather than place the rigid glass under high stress concentrations; it also cured at room temperature. Once the tube had been assembled it was pressure tested. The flow tube was installed into a section of plastic pipe work; the plastic pipe work was in turn connected to flexible hosing. As the pressure increased it caused the flexible hosing to move and lift the upstream pipe section, the movement caused the very rigid glass tube to fracture, as shown in figure 5.3.

Figure 5.3. A picture showing the fractured glass tube assembly

With future prototypes the glass tube and the surrounding pipe work was constrained so that no movement could take place.

5.2.3. Designing and building a support structure to hold the glass tube

The joint method used on the last prototype successfully sealed the ends of the glass, but it did not allow the pipe work to be rigidly fixed. A new tube was assembled with the same brass components but this time inserted onto DN50 Stainless steel flanges. The flanges were mechanically fixed to a metal plate using M8 Machine screws. The final design of tube with all of its support structure is illustrated in figure 5.4.

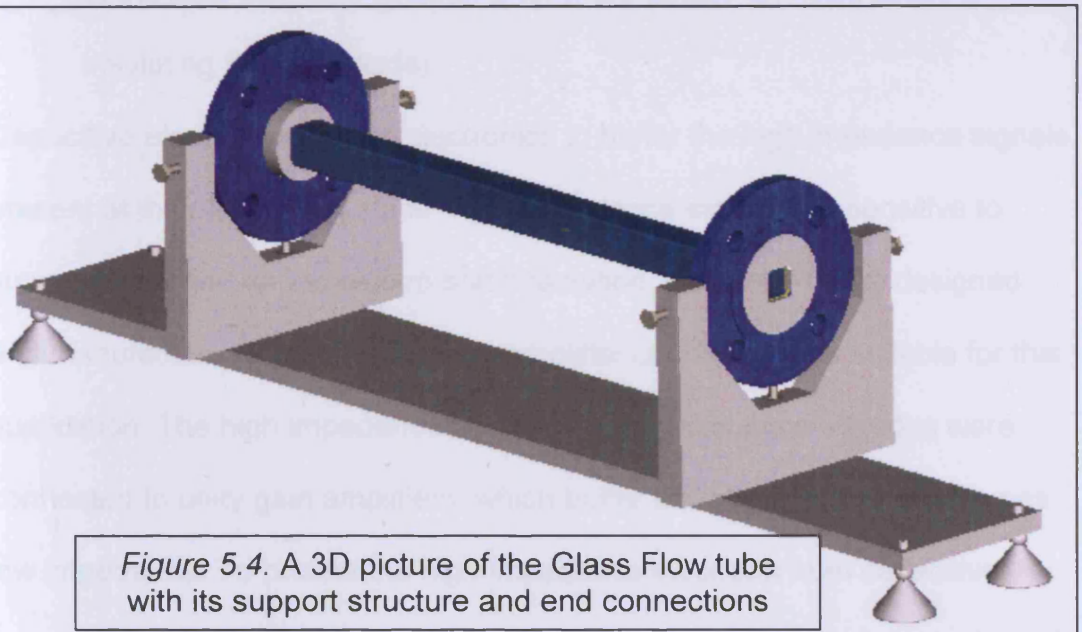

Figure 5.4. A 3D picture of the Glass Flow tube with its support structure and end connections

5.2.4. The electrode design

Based on the literature review and the theoretical analysis undertaken in Chapter 4 the decision to use capacitive electrodes was made.

The reasons for this decision are given below:

1) Producing a large area thin metal electrode possibly similar to that in figure 2.3 would be difficult to assemble within the duct of a small pipe and securely hold in position.
2) Capacitive electrodes positioned on the outside of the flow duct will be easier to modify.
3) Contacting electrodes are capacitive coupled to an insulating liquid anyway because there are no free ions present to produce conduction currents, only displacement currents.
4) Placing the electrodes on the outside of the flow conduit provides a buffer between the unwanted noise amplitudes present on the interior

of the pipe wall (see Chapter 2 for more details on noise present in insulating flowing liquids).

Capacitive electrodes require electronics to buffer the high impedance signals present at the electrode surface. High impedance signals are sensitive to stray capacitance and to electro-static radiation. Asquith (2003b) designed and manufactured a voltage sensing amplifier circuit that was suitable for this application. The high impedance signals measured at the electrodes were connected to unity gain amplifiers, which buffer the signal so that it becomes low impedance. To protect the high impedance electrode from capacitive losses a metallic screen was positioned near to the electrode. A proportion of the buffered electrode signal was then connected to the metallic screen, a technique that is known as "boot strapping" (Asquith, 2003b). The metallic screen (known as a driven screen) was larger than the electrode so that it can protect the electrode from electro-static radiation. The proportion of signal used to boot strap the driven screen was 100 %. It is unusual that 100 % boot strapping was possible as stability problems usually occur when the boot strapping is more than approximately 99 % (Asquith, 2006)

The circuit diagram is given in figure 5.5.

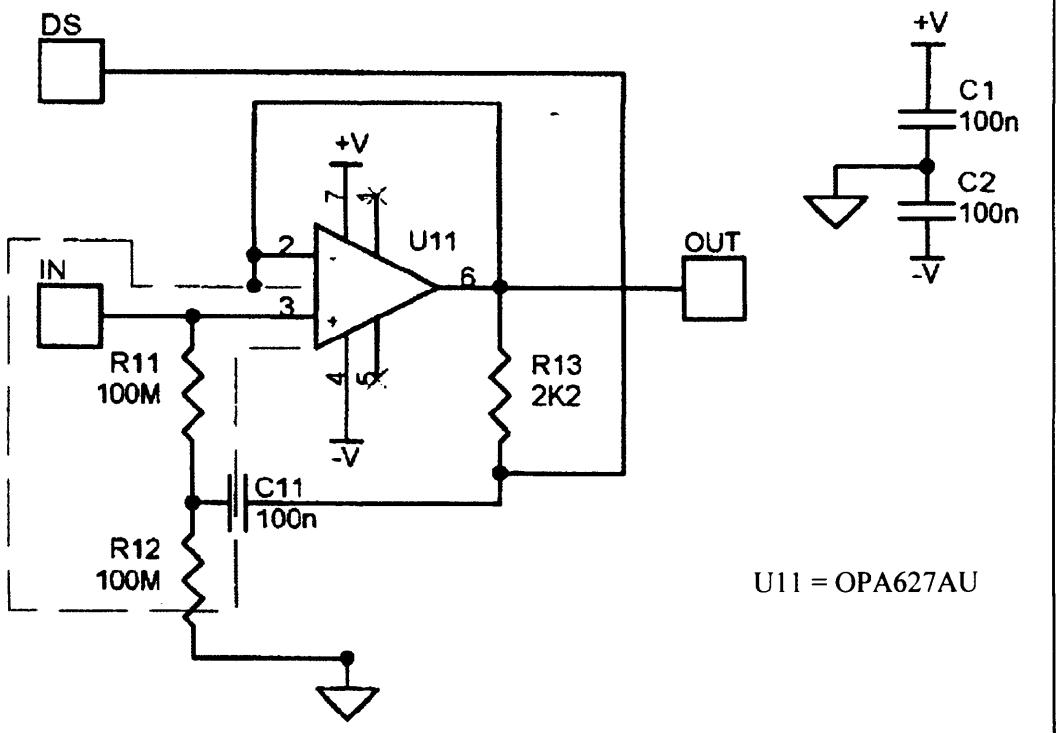

Figure 5.5. Buffer amplifier design for voltage sensing with capacitive electrodes (Asquith, 2003b)

Cushing et al (1962) and Amare (1995) both used electrodes similar in construction to figure 2.6. When operating at frequencies of 1 kHz it is essential to reduce eddy current generation where possible. The eddy currents generate a reaction magnetic field, which can affect the flow potential generated within the pipe. Also having unwanted currents or potentials circulating on the electrode surface may affect the measured potential. To check whether the electrode needed to be similar in construction to figure 2.6 a prediction of the eddy current generation was required. Eddy currents predominate on the surface layer of conductive material. From Stoll's (1974)

analysis of one-dimensional eddy current flows the eddy current skin depth is given by equation 5.1.

$$e = \left(\frac{2}{\omega.\sigma.\mu_0.\mu_r} \right)^{1/2} \qquad (5.1)$$

The skin depth is a measure of how thick a material is required to be to allow eddy currents to propagate efficiently. If the material thickness is much less than the eddy current skin depth then eddy currents are not considered to be problematic. For copper the skin depth thickness at a frequency of 500 Hz is 2.95 mm. A copper foil of thickness 35 μm was identified as a suitable thickness. For a one-dimensional semi-infinite plate Stoll derived an equation for the eddy current power loss as given in equation 5.2.

$$P_e = \frac{1}{3}.\omega^2.\sigma.\mu_o^2\mu_r^2 H^2 a^3 \qquad (5.2)$$

By assuming a magnetic field strength of 8 $A.m^2$ the power loss at a frequency of 500 Hz is 0.002 W. If the power required to generate the magnetic field strength was 250 W, the eddy current losses would represent 0.008 % of the total power used, which is a negligible loss. The 35 μm copper foil was used for both the electrode and the driven screen, see figure 5.6 for dimensional information.

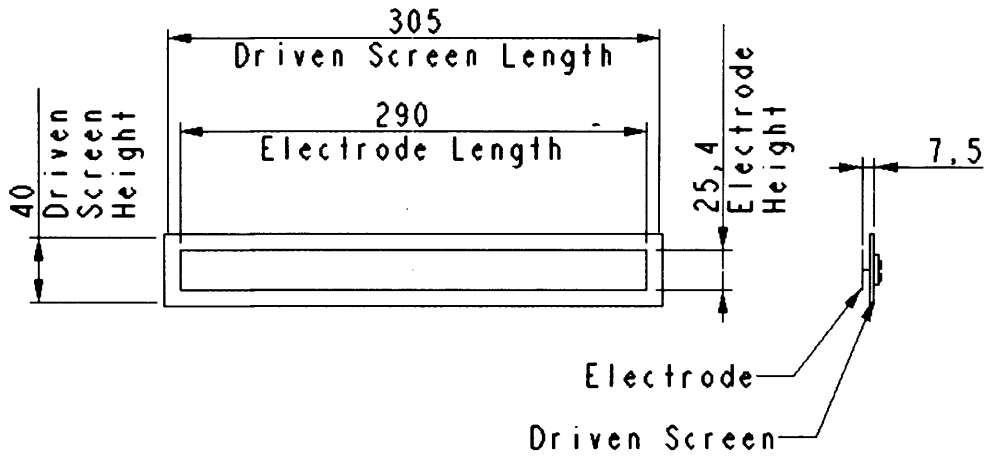

Figure 5.6. Electrode dimensions (in mm) for the new prototype

5.2.5. The magnetic circuit

The magnetic circuit for this flow meter was required to generate a uniform field in all regions of the measuring section. Amare (1995) used an air cored magnetic circuit as he was operating at a frequency of 1.5 kHz. An FEA program called Quickfield was used to model an air cored coil and it was found that it could not generate a uniform field over the length required. Cushing and others (1962) produced a flow meter that operated at 10 kHz; they used a powdered iron circuit to reduce eddy current losses. A powdered iron magnetic circuit was investigated. A supplier was sourced in the US who produced cylindrical powdered iron cores in the diameter (200 mm) required. To produce the length of magnetic circuit required the material costs were in

excess of £3000, which is too expensive for a commercial product. If purchased these cores would require machining to make them suitable for this application. Machining powdered iron cores requires special extraction due to the fine metal particles that would be given off. Machining powdered iron was also not recommended by the core manufacturers. Based on the problems with machining and the high costs associated with manufacturing a powdered iron magnetic circuit this idea was abandoned. The remaining practical option was a laminated iron circuit; Khanna (2006) stated that conventional iron circuits do not operate well at frequencies above 200 Hz due to eddy current losses. The skin depth of mild steel driven at a frequency of 500 Hz and 50 Hz is 0.14 mm and 0.45 mm respectively. For this application it was not practical to use laminations that are significantly thinner than 0.14 mm and in fact 0.5 mm was the thinnest that could be viably manufactured. The original intention was to operate at frequencies up to 500 Hz, it was decided that through building and testing the highest practical operating frequency would be used for testing. The laminated iron circuit design was constructed from E-cores made from carbon steel. To produce the required length magnetic field 1,100 laminations were screwed together and then welded in four positions to ensure each lamination could be electrically grounded. The coils were designed to fit within the E-core and were rectangular coils consisting of 75 turns of 1 mm diameter copper wire. Figure 5.7 is a sectional view through the centre of the flow meter and shows how the magnetic circuit is positioned relative to the flow conduit.

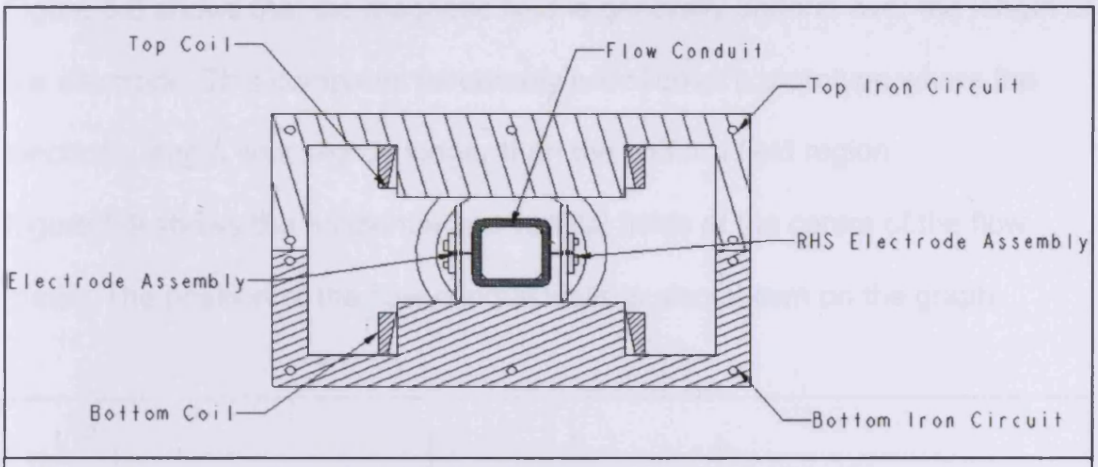

Figure 5.7. A sectional view of the proposed prototype design showing the field generating and sensing parts of the flow meter

Before flow testing could begin the performance of the magnetic circuit was required.

Using the method described in section 3.4.1 the magnetic field within the new magnetic circuit was measured. The field measured along the axis of the flow meter is shown in figure 5.8.

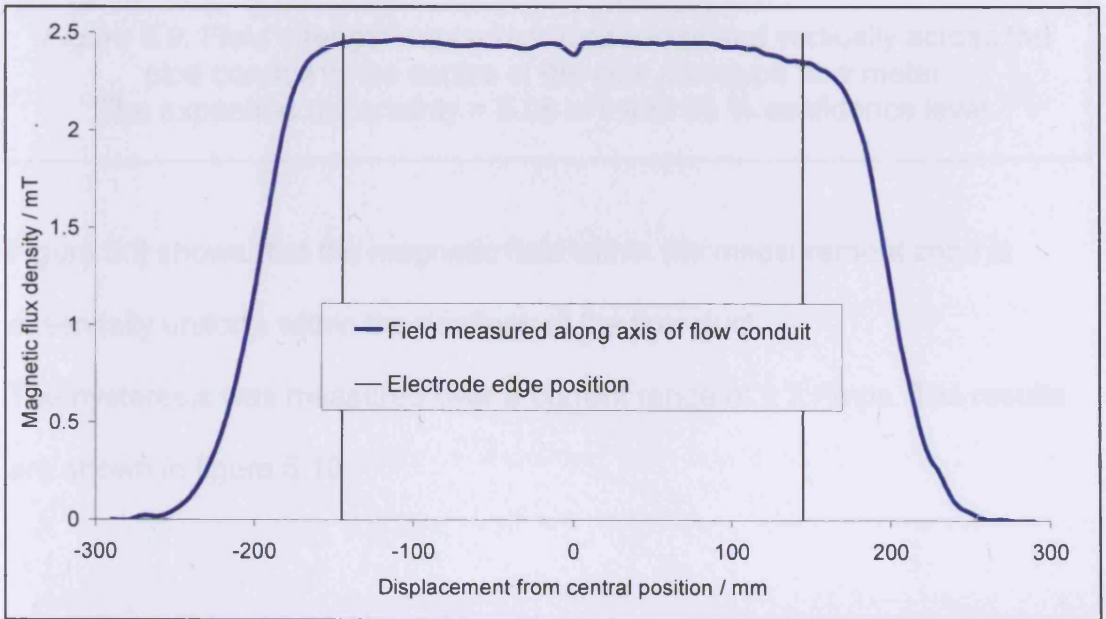

Figure 5.8. A Field plot along the pipe axis of the new magnetic circuit design. The expanded uncertainty = 0.08 mT with 95 % confidence level.

Figure 5.8 shows that the magnetic field is generally uniform over the length of the electrode. This compares favourably with Turner's prototype where the electrode length was slightly longer than the uniform field region.

Figure 5.9 shows the horizontal and vertical fields at the centre of the flow meter. The position of the flow conduit walls is also shown on the graph.

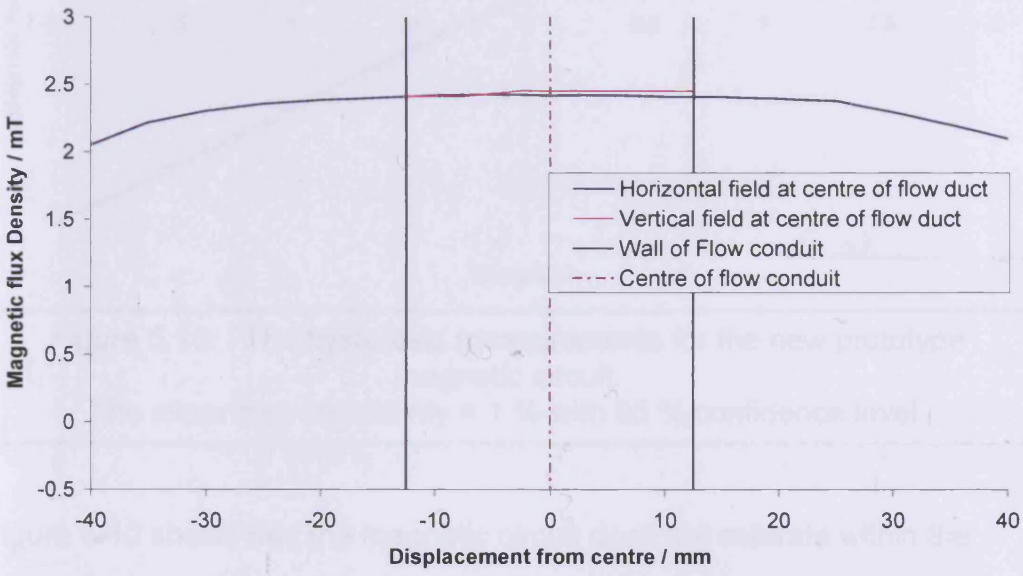

Figure 5.9. Field strength measured horizontally and vertically across the pipe conduit at the centre of the new prototype flow meter.
The expanded uncertainty = 0.08 mT with 95 % confidence level.

Figure 5.9 shows that the magnetic field within the measurement zone is essentially uniform within the confines of the flow duct.

The hysteresis was measured over a current range of ± 2 Amps. The results are shown in figure 5.10.

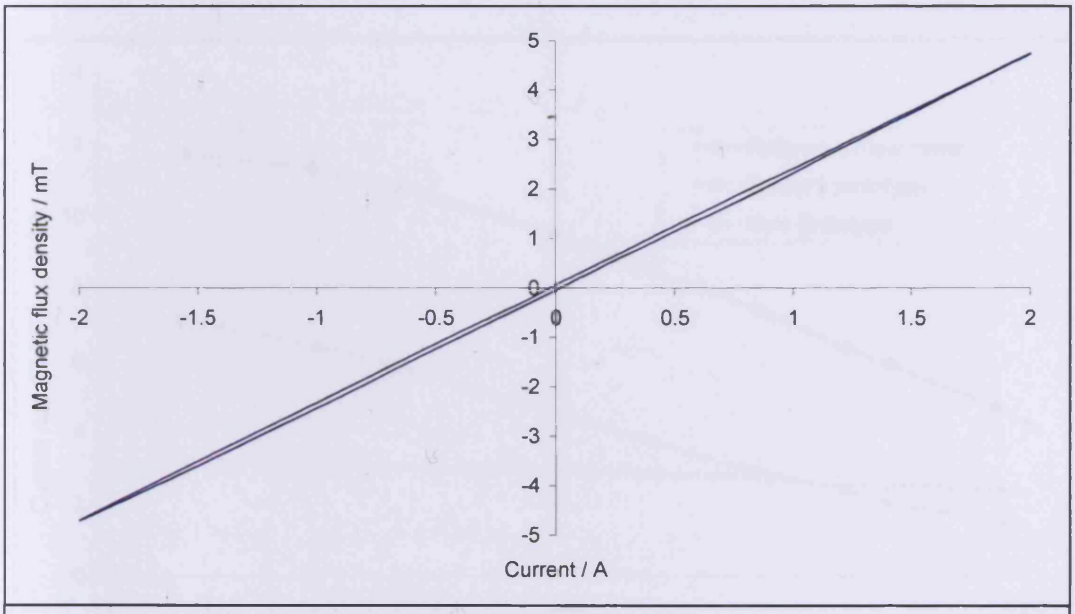

Figure 5.10. The hysteresis measurements for the new prototype magnetic circuit.
The expanded uncertainty = 1 % with 95 % confidence level.

Figure 5.10 shows that the magnetic circuit does not saturate within the current range tested. The level of magnetisation (or remanence) was 0.12 mT, this compares with Turner's prototype, which had a remanence flux density of 0.5 mT. For A.C. operation the smaller the remanence the better as it represents the energy lost during the complete cycle. A value of 0.12 mT is significantly less than Turner's prototype and shows that the magnetic circuit in the new prototype will be more efficient during operation.

To measure the A.C. response of the flow meter a search coil wound around the top field-generating coil was used. Using a signal generator the coils were energised with an A.C. waveform. At a range of frequencies the voltage in the search coil was measured. The voltage and current in the flow meter coils was

also recorded. From these measurements the current normalised magnetic flux density was calculated and the results are shown in figure 5.11.

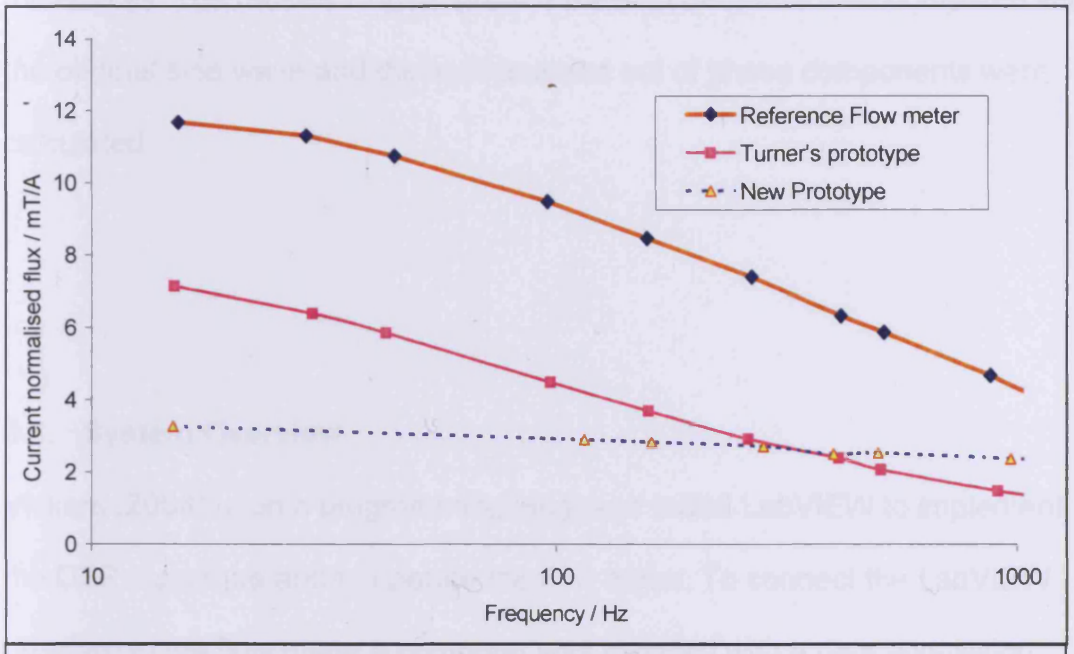

Figure 5.11. A.C. Field Strength for the new prototype compared with Turner's prototype and the reference flow meter

The results in figure 5.11 show that the new iron circuit does not generate as much flux per unit current as the previous flow meters tested. The current normalised flux gradient for the new prototype is shallower than Turner's prototype and the reference flow meter indicating that it is better suited for operation with A.C. waveforms.

5.3. The Electronics for operating the flow meter

There were no existing electronics within ABB that could be used to operate with an A.C. drive wave of variable frequency. Vickers (2004) conducted research into the suitability of different digital signal processing techniques for use with a flow meter. The signal processing technique employed for this

application was known as a cross correlation method. The cross correlation system generated a sine wave, which could be outputted to the power the flow meter coils. The received signal (from the electrodes) was then compared with the original sine wave and the in-phase and out of phase components were calculated.

5.4. System Overview

Vickers (2004) used a programming language called LabVIEW to implement the DSP technique and to operate the flow meter. To connect the LabVIEW program to the flow meter a computer was installed with a data acquisition card (PCI-6035E) and the NI-DAQ software necessary for communicating with LabVIEW. The software can be programmed to operate at any A.C. frequency. The generated sine wave was outputted to a QSC Audio PLX1202 power amplifier. The power amplifier was connected to the flow meter coils, which were connected in series. The capacitive electrodes measure the flow signal, quadrature and other noise amplitudes present within the system. Unity gain amplifiers (see figure 5.5. for circuit diagram) positioned close to the source of the signal buffer the high impedance electrode signals. The buffered signals were connected to a differential amplifier, an adjustable gain amplifier and also a high frequency filter. The circuit diagram is shown in figure 5.12.

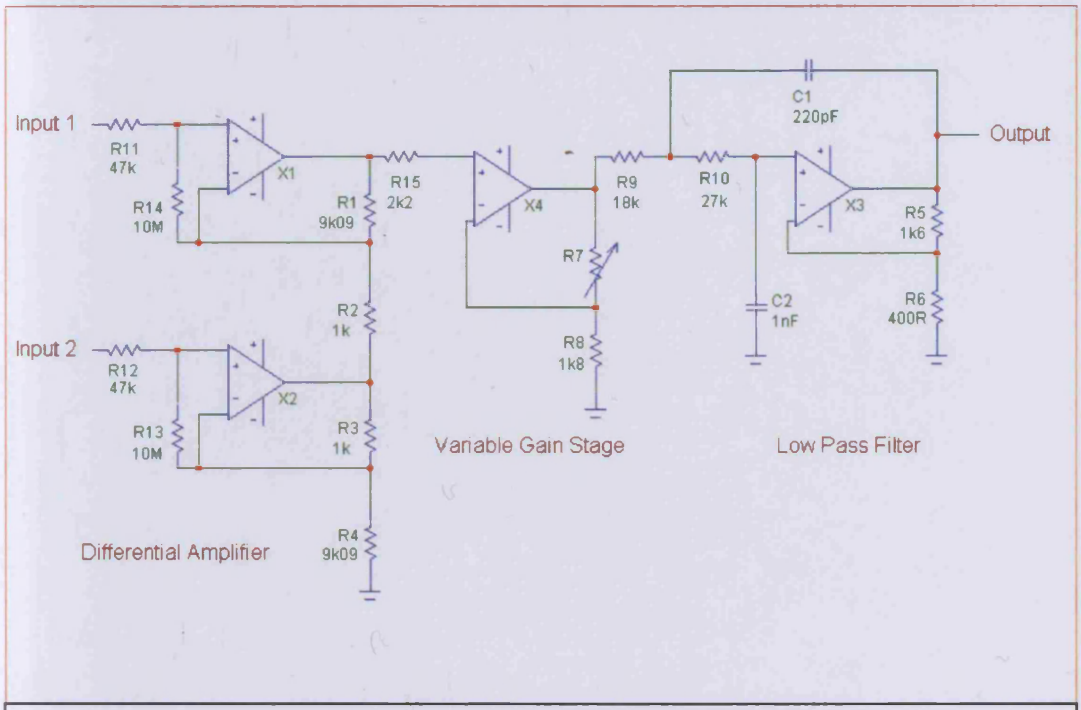

Figure 5.12. Circuit diagram of the electrode amplifiers

The amplified signal was connected to the input channel of the data acquisition card where an analogue to digital converter sampled the electrode signal. The software calculated the sine and cosine components of the collected sample and compared them to the original generated waveform. The LabVIEW program then outputted the magnitude of the sine and cosine components and plotted the results on a graph. The raw data was also outputted in a text format.

Figure 5.13. is a schematic diagram of the system set-up.

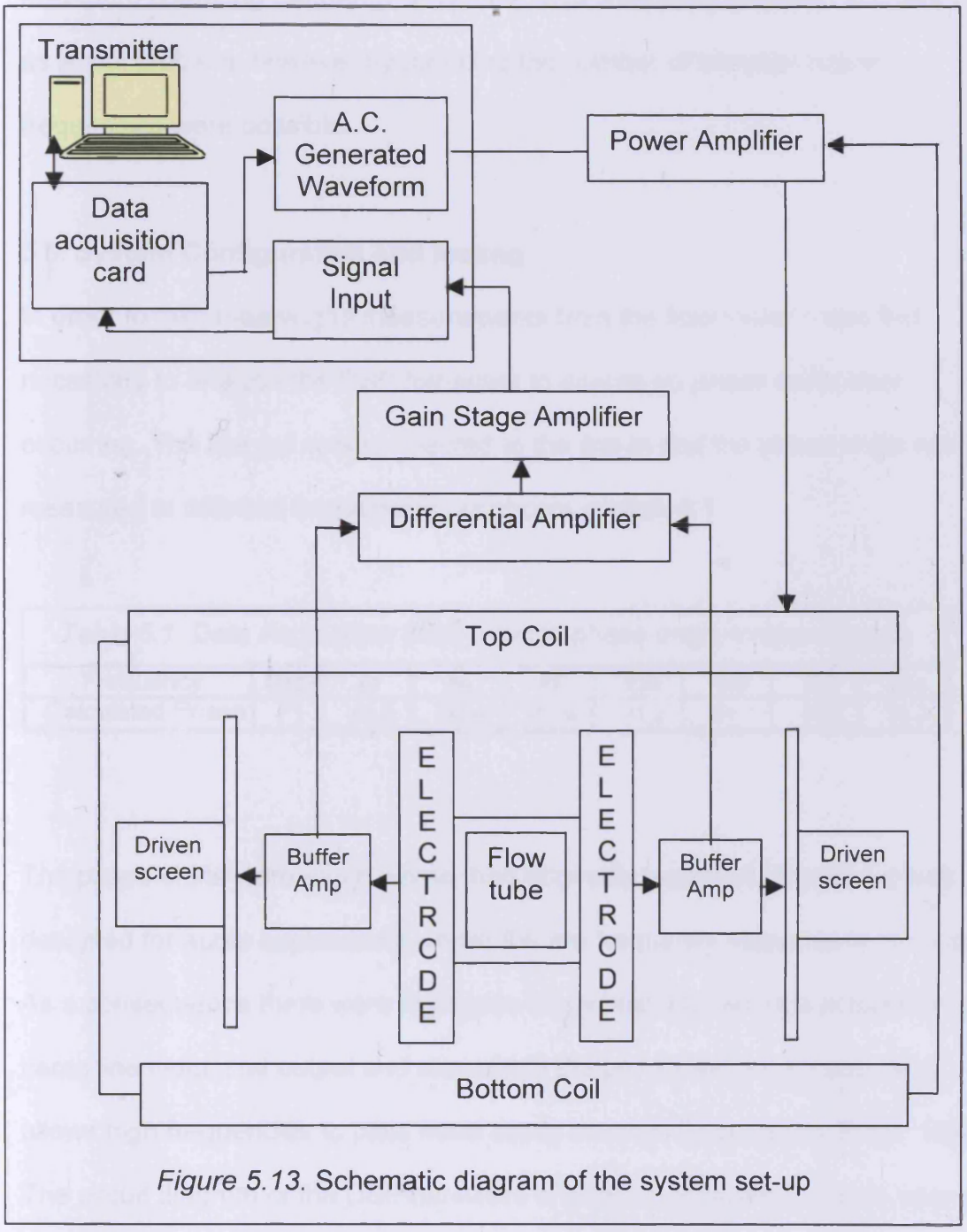

Figure 5.13. Schematic diagram of the system set-up

Vickers (2004) outlined the hardware limitations of the PC based system. The data acquisition card, PCI-6035 writes to the analogue output at 1 kHz, with the requirement for 8 samples per cycle and a Shannon limit of 500 Hz, the maximum operating frequency is 125 Hz. This frequency limitation was seen as a real problem, however by reducing the number of samples higher frequencies were possible.

5.5. System Configuration and testing

In order to take meaningful measurements from the flow meter it was first necessary to analyse the DSP hardware to ensure no phase shifts were occurring. The line out was connected to the line in and the phase shifts were measured at different frequencies, as shown in table 5.1.

Table 5.1. Data Acquisition Card internal phase angle measurements

Frequency	(Hz)	40	60	80	120	160	320	640
Calculated Phase	(°)	-98.2	-88.6	-81.9	-71.2	-61.7	-27.4	38.2

The phase shifts were much worse than originally expected. The circuit was designed for audio applications where the low frequency response is not critical. As a consequence there were high pass filters built into the data acquisition cards line input, line output and also within the processor. A high pass filter allows high frequencies to pass more easily than low frequencies (Plant, 1990). The circuit diagram of the DSP hardware is given in appendix C. As an example of a high pass filter the components R40 and C85 shown in appendix C have a frequency cut off at 2.2 Hz. This will affect the voltage gain up to a frequency of

approximately 150 Hz. To reduce this problem a number of components were changed to improve the low frequency response; the changes are listed in table 5.2.

Table 5.2. Component Changes to 'ANALOG DEVICES ADSP-21065EZ-LAB' Data acquisition card

Component ID	Original Value	New Value
C112	1 μF	10 μF
C113	1 μF	10 μF
C79	1 μF	100 μF
R40	5.1 kΩ	51 kΩ
C85	1 μF	470 μF

By changing these components the new frequency cut off on the line input will be 0.033 Hz and the voltage gain will only affect frequencies below 2 Hz.
After repeating the frequency response test with the changes in components the phase shifts were still present. It was realised that the CODEC (which manipulates the data prior to sending to the LabVIEW program) has an internal digital filter, which introduces a time delay between the signal out and the signal in. There was little that could be done except to calculate the time delay and subtract this from the phase before analysing the data. The internal digital

filtering time delay was 0.56 ms. By converting the time delay into a phase angle related to frequency the effect of the internal phase shifts can be removed with post processing. Figure 5.14 shows the frequency response with the time delay subtracted before and after the circuit board modifications were made.

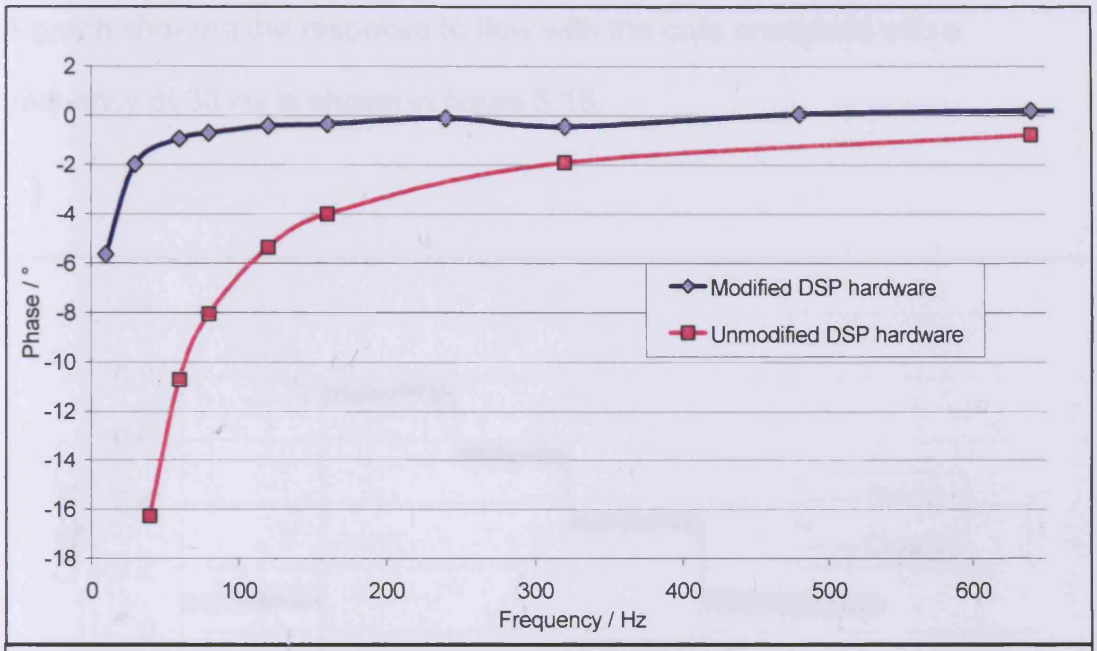

Figure 5.14. DSP Internal Phase Shifts with an imposed time delay of 0.56 ms

The results show that after modification the phase shifts were relatively small and mainly affect the measurements in the frequency range up to 100 Hz. By knowing what the phase shifts were their affect can be subtracted during the post processing of the results.

5.6. Flow Data Post Processing

The LabVIEW program outputted the magnitudes of the sine and cosine components of the electrode signal. It was found that both the sine and cosine components related to the flow velocity as the measurements changed when the flow velocity was adjusted.

A graph showing the response to flow with the coils energised with a frequency of 30 Hz is shown in figure 5.15.

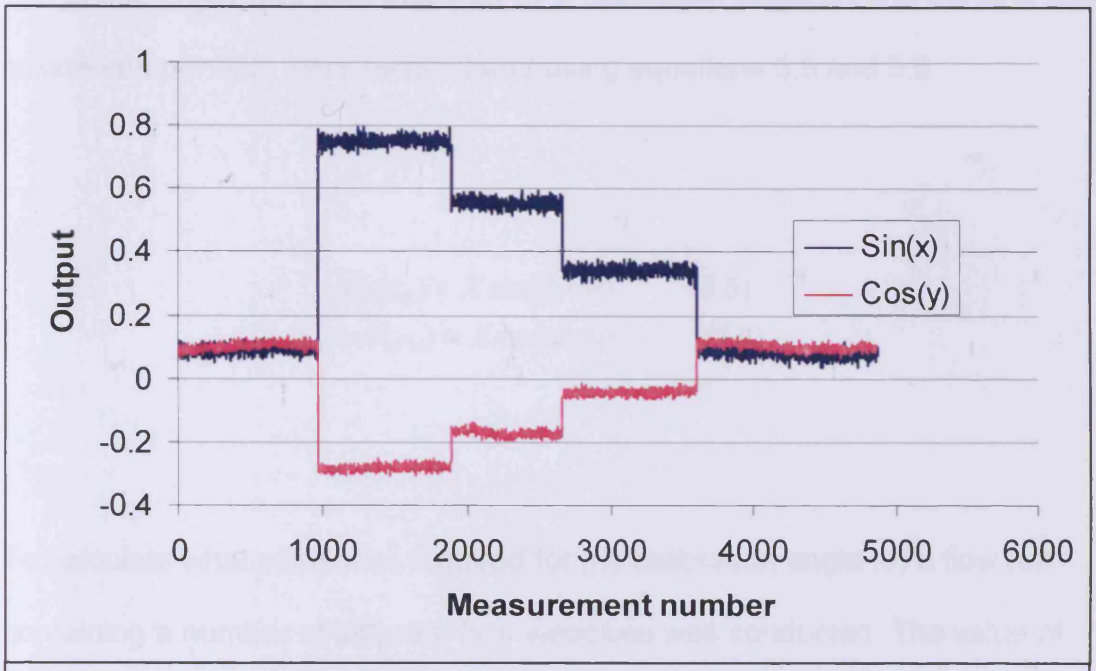

Figure 5.15. The DSP outputted Sine and Cosine transforms

Theoretically the unwanted quadrature signal should be 90° out of phase with the flow signal (Turner, 1985). The sine component should represent the flow signal, as it should be in phase with the flow signal. Keech (2004) believed that by rotating the sine and cosine components by a certain angle the flow

signal could be removed from the cosine transform. Using the sine and cosine transforms (x_1 and x_2) the signal magnitude was calculated using equation 5.3.

$$X = \sqrt{(\sin(x_1))^2 + (\cos(x_2))^2} \qquad (5.3)$$

The phase angle between the sine and cosine components was calculated using equation 5.4.

$$\phi = \tan^{-1}\left(x_1 / x_2\right) \qquad (5.4)$$

The phase angle was then adjusted by a calibration angle (θ) and the sine and cosine components were recalculated using equations 5.5 and 5.6.

$$\sin(x_\theta) = X \sin(\phi + \theta) \qquad (5.5)$$
$$\cos(y_\theta) = X \cos(\phi + \theta) \qquad (5.6)$$

To calculate what value was required for the calibration angle (θ) a flow run containing a number of different flow velocities was conducted. The value of $\cos ine(x_1)$ was calculated for each measurement within the flow run. The angle θ was adjusted until no velocity data were present on the $\cos ine(x_\theta)$ flow trace. An iterative process of reviewing the flow trace between manual adjustments to the calibration angle was initially used to calibrate the flow meter. Later the standard deviation of $\cos ine(x_\theta)$ was calculated and

automatically minimised using a solver program in Microsoft Excel. Once rotated the Sine and Cosine data in figure 5.15 is shown in figure 5.16.

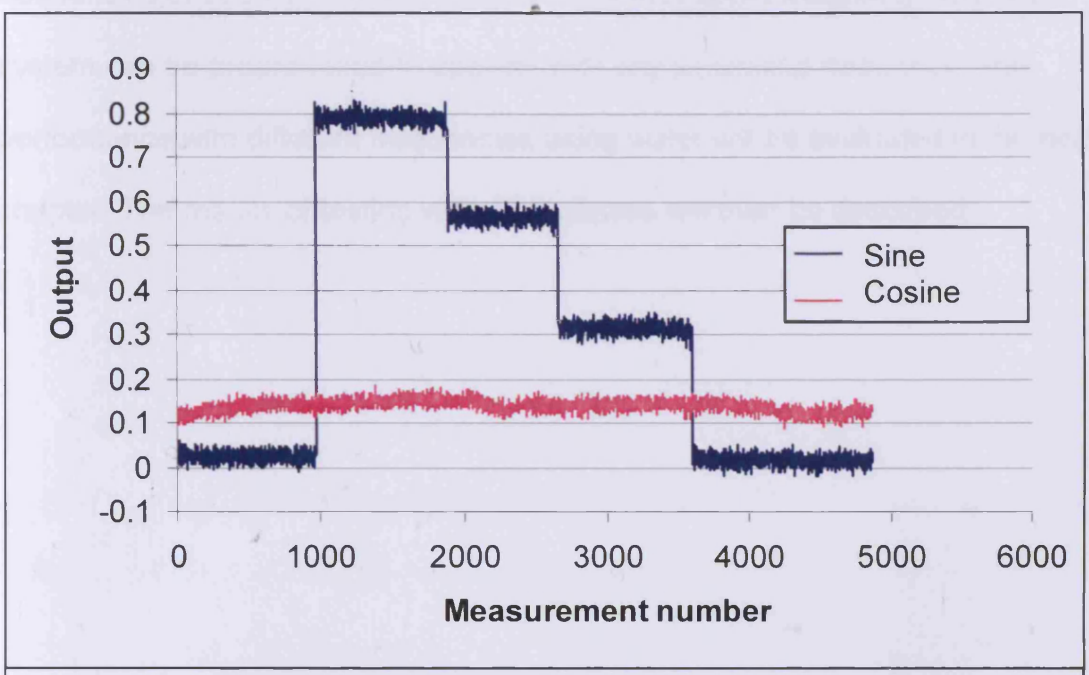

Figure 5.16. The rotated sine and cosine data

Figure 5.16 shows that the cosine data now represents the unwanted quadrature signal and the sine data the flow signal.

5.7. Discussion

This concludes a description of the design and development of the new flow meter system, including its electronics and the DSP system used to operate it. As described the design of the new flow meter system suffered from a series of compromises. It was found that designing a flow meter to operate at high frequencies was not straightforward. There were two insurmountable problems that affected the maximum operating frequency of the flow meter. The DSP

system was only designed to operate efficiently up to a frequency of 125 Hz. The iron circuit was manufactured from 0.5 mm thick laminations of mild steel, which was approximately 0.4 mm thicker than wanted for operation at frequencies of 500 Hz. Despite the problems with upper frequency limit, the system can be programmed to operate with any sinusoidal frequency. The performance with different frequencies using water will be evaluated in the next chapter. The results of testing with other liquids will then be described.

Chapter 6

Flow testing the New Prototype

6.1. Introduction

With the new flow meter system completed the intention was to evaluate its performance with low conductivity liquids. To test the flow meter with liquids of different conductivities a specialised flow rig was required. As part of this project a closed loop flow rig that could safely circulate and measure the flow rate of different liquids; such as glycols, alcohols and oils was designed. For details of the flow rig design and manufacture see appendix D. Once the flow meter was manufactured and the flow rig commissioned evaluation of the flow meter could begin.

6.2. System stabilisation through testing with water

The flow meter was installed in the flow rig with DN50 pipe work connected either side of the flow meter. The glass tube was designed to withstand a maximum operating pressure of 1 bar. Once installed in the flow rig the pipeline was filled with tap water. With the upstream valve closed a pressure test was conducted up to a pressure of 1 bar. The flow tube passed the

pressure test however for flow testing the line pressure would be kept below 0.5 bar. This was a necessary precaution based on the time taken to build the flow meter and the potential project delays related to breaking the flow tube. With a maximum operating pressure of 0.5 bar it was found that the maximum achievable flow rate caused cavitation upstream of the flow meter. The variable speed driver, which controlled the pump speed, was used in conjunction with the downstream flow control valve to identify the maximum flow rate whilst maintaining the 0.5 bar line pressure. The maximum flow rate without observing any cavitation was 0.81 l/s. This flow rate approximated to an average velocity of 1.3 m/s within the flow meter test section. For flow testing a number of flow rates were chosen that could be used with different system parameters to compare performance. The flowrates and the average velocity within the DN50 pipeline and the flow meter test section are given in table 6.1.

Table 6.1. The test flow rates and corresponding average velocities within the pipe work and prototype measuring section

Flow rate / l/s	Average velocity / m/s	
	DN50 Pipe work	Measuring section
0.81	0.41	1.3
0.58	0.30	0.9
0.30	0.15	0.5
0.00	0.00	0.0

These flow rates were attained by keeping the downstream control valve constant and adjusting the speed of the variable speed driver. The line pressure reduced with decreasing flow rate.
Once the flow rates had been chosen the performance of the flow meter system could be evaluated.

It was found that a number of factors affected the flow meter performance, these were:

- Operating frequency
- Coil drive voltage
- Environmental conditions
- Quadrature voltages

6.2.1. Operating frequency

Based on the work conducted in designing and building the flow meter the maximum operating frequency was expected to be less than 500 Hz. The performance with different frequencies was assessed based on zero stability over the length of a flow run. It was found that as the frequency increased the flow measurement stability deteriorated. The maximum frequency that could be reliably used without suffering from zero stability issues was found to be 160 Hz. The performance with higher frequencies could not sustain a stable flow measurement over the duration of the flow test. A typical example of the stability problems experienced with a higher frequency is shown in figure 6.1.

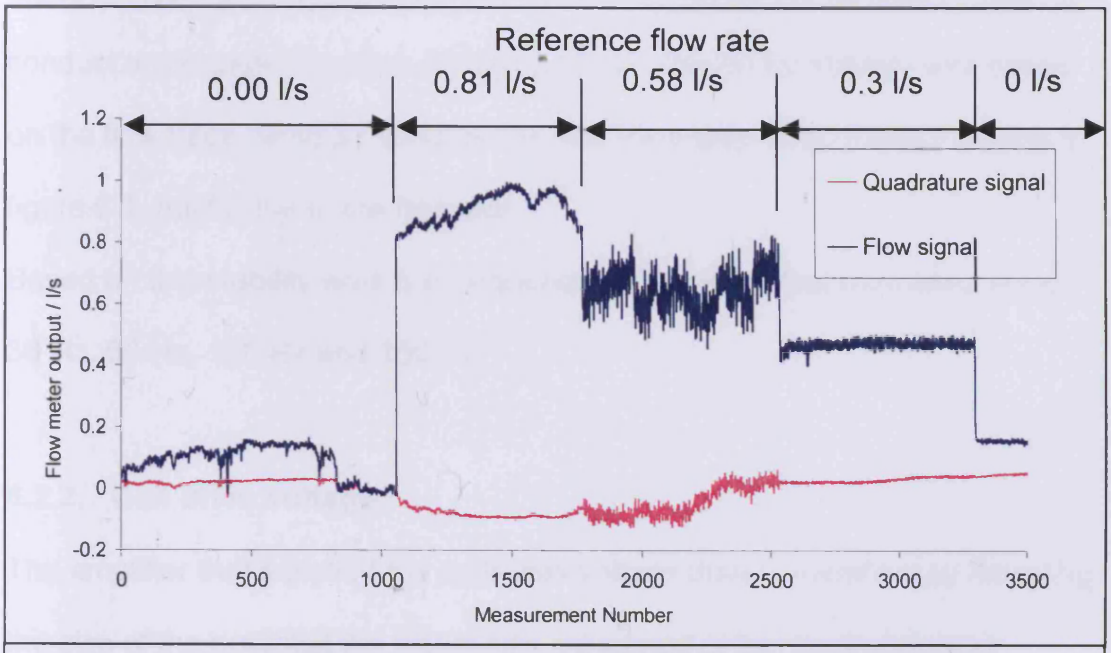

Figure 6.1. Flow testing the new prototype, Coil drive frequency = 240 Hz, Coil current = 0.7 A pk-pk, Liquid under test = water

Figure 6.1 shows that the zero stability is poor for the first 2500 measurements of the flow test. The first 1000 measurements were taken with static flow conditions; the zero measurement is unstable and drifts by approximately 0.15 l/s during this period. When the flow rate was increased to 0.81 l/s the zero stability was still problematic. The noise levels at the 0.58 l/s flow rate were much higher than at the other flow rates suggesting that the flow meter was suffering from some form of interference. The problem was related to either the pump or the variable speed driver. By closing the valve upstream of the pump and starting the variable speed driver, the noise was present at zero flow. This suggested that the problem was probably caused by electrical interference from the variable speed driver, by making small

adjustments to the frequency the problem was reduced. After approximately 2500 measurements the flow meter became more stable, however after repeated testing the zero stability could not be maintained for long enough to conduct a complete flow test. An acceptance criterion for stability was based on the flow trace being as good as the flow trace after 2500 measurements in figure 6.1, but for the entire flow test.

Based on this stability work the frequencies chosen for test evaluation were 30 Hz, 60 Hz, 120 Hz and 160 Hz.

6.2.2. Coil drive voltage

The amplifier that supplied the coils was voltage driven, therefore by adjusting the size of the potential the signal size measured at the electrodes was affected.

The power supply was voltage driven but the flux generated by the coils is related to the size of the current flowing through the coils. With a constant voltage drive any changes in temperature can affect the resistance of the coil wires and consequently the amount of current flowing through the coils. If the voltage drive supplied too much power to the coils then the coil wire temperature increased, this increased the resistance of the wire. As the wire resistance increased the current flow reduced and the flux within the measuring section fell, as a consequence the output of the flowmeter went down. This was an inherent problem with the electronics used to operate the flow meter. To limit this temperature effect the voltage supplied to the coils was experimented with to ensure a stable output with time. The frequency,

voltage and current measurements, which produced a relatively stable output, are displayed in table 6.2.

Table 6.2. The voltage and current values used to supply the coils at each frequency

Frequency / Hz	Voltage / V (pk-pk)	Current / A (pk-pk)
30	15	1.5
60	20	1.6
120	19	1.0
160	19	0.8

6.2.3. Environmental conditions

A number of stability problems related to the flow meters environment were discovered. It was found that the high impedance capacitive electrodes were sensitive to vibration and also changes in temperature and humidity.

If a person walked near to the flow meter whilst it was in operation then the vibrations produced could be witnessed when looking at the buffered electrode signals using an oscilloscope. These voltages spikes did not seem to affect the DSP flow measurement.

The laboratory was built on top of a large water sump used to feed the flow rigs at the Stonehouse factory. The sump temperature tended to be greater

than the room temperature. There were a number of vents from the sump into the laboratory, consequently the humidity in the laboratory tended to be greater than the humidity outdoors. Within the laboratory there was a roller door, which occasionally allowed strong draughts to pass into the laboratory when opened. This draught had a strong affect on the zero stability at all frequencies. It was believed that the draught was changing the capacitance between the electrode and ground through changes in temperature and humidity. To minimise the effect of draughts some foam spacers were placed around the ends of the flow meter. The draught excluders greatly improved the stability of the flow meter.

Temperature effects were unfortunately an inherent problem with the design of the flow measuring system (as already mentioned in section 6.2.2). The signal processing had no way of compensating for changes in the flux output. The normal approach with A.C. flow meter designs is to use a search coil within the flow meter as a reference to monitor the flux levels (Schwiderski, 2003). The DSP system had no indication of whether the flux levels had changed as it compared the digitally generated signal with the amplified electrode signal. This was a major flaw in the design of the DSP as it wrongly assumed that the flux was constant. To try and limit the temperature effects a cardboard housing was made to fit around the flow meter to help insulate it from rapid changes in laboratory temperature. Another source of changing temperature related to the process liquid. The process liquid temperature tended to increase throughout a flow run due to the energy put into the liquid by the pump. Fortunately the length of the flow runs was short enough that only a small change in temperature was observed (approximately 1° C / hour).

This small change in temperature did not seem to affect the performance of the flow meter.

6.2.4. Quadrature voltages

When the flow meter was first assembled the DSP measurement was indicating a large flow signal despite the flow being stationary. This was caused by quadrature voltages and was found to be much larger than the flow signal. The quadrature voltage or transformer effect was caused by an asymmetrical loop comprising of the electrodes, their wiring and a loop through the liquid, which passes through the magnetic field (Cushing 1999). The design of the flow meter allowed the magnetic circuit to be moved relative to the flow tube, the electrode wiring could also be moved. By moving the magnetic circuit and the position of the electrode wires the quadrature voltages could be reduced. Despite adjustments the quadrature voltage was still present. Initially the electrode wires were brought out perpendicular to the magnetic field as shown in figure 6.2.

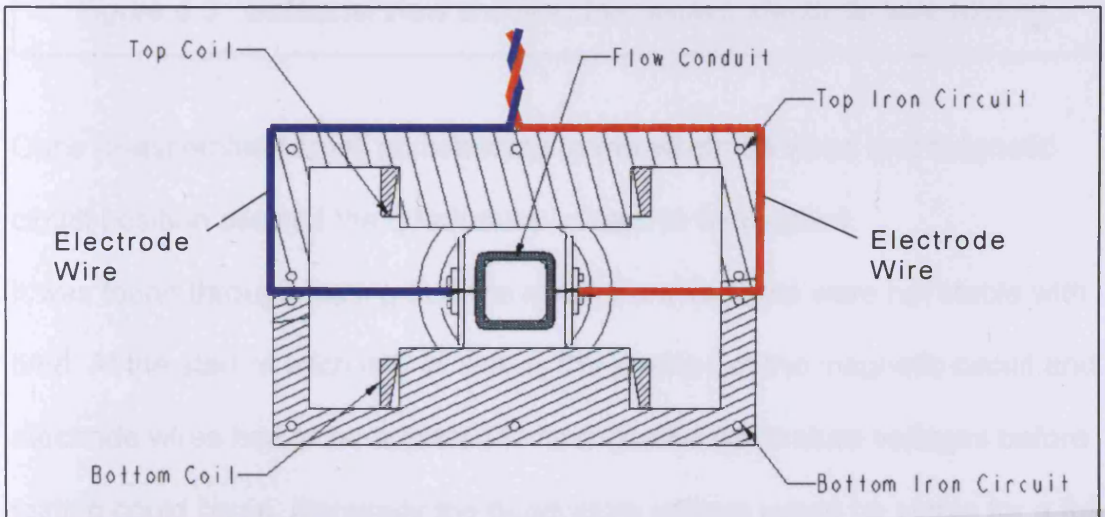

Figure 6.2. Sectional view showing the original electrode wire routing

It was impossible to align the electrode wires so that no quadrature voltage was present. The main problem was keeping the electrode wires straight between leaving the amplifier PCB's and reaching the edge of the iron circuit. The electrode wire routeing was changed. Vertical holes were drilled through the magnetic circuit directly above where the wires were terminated to the amplifier PCB's. The electrode wires were then fed vertically through the holes thus removing part of the unnecessary circuit loop (as shown in figure 6.3).

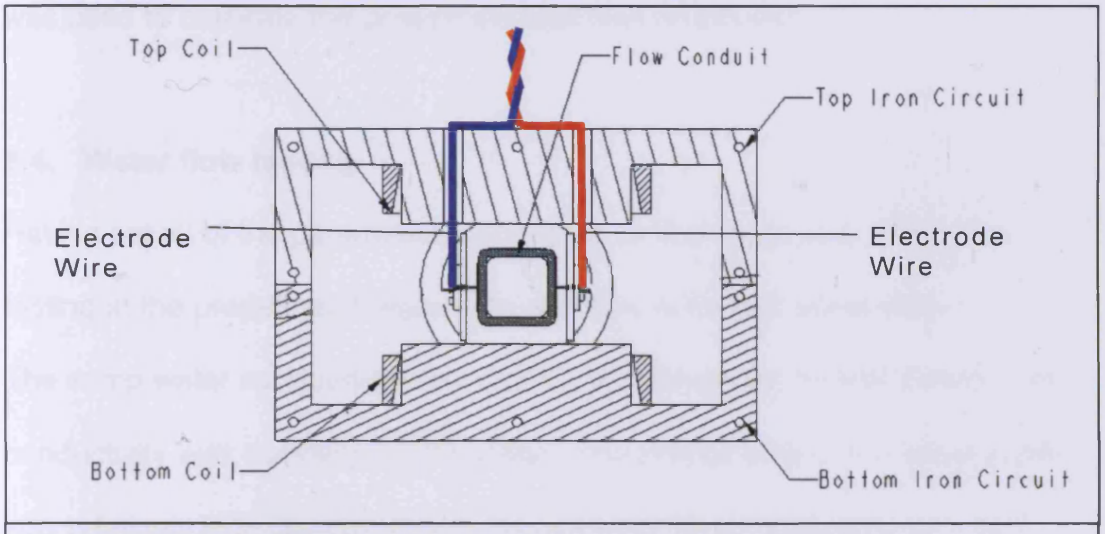

Figure 6.3. Sectional view showing the revised electrode wire routing

Once re-assembled small adjustments to the electrode wires and magnetic circuit position allowed the quadrature voltage to be nullified.

It was found through testing that the quadrature voltages were not stable with time. At the start of each day of testing the position of the magnetic circuit and electrode wires had to be adjusted to tune out the quadrature voltages before testing could begin. Generally the quadrature voltage would be stable for a full day of testing but occasionally the post processed results would show that the

angle between the flow signal and the quadrature voltage had changed. When this occurred minor adjustments were made before the flow test was repeated.

6.3. Data collection

The technique described in chapter 5 for processing the results was used. To monitor the reference flow conditions the MassMeter, which was installed upstream of the flow meter, was used to record the mass flow rate, temperature and viscosity during each flow run. The reference information was used to calibrate the post-processed flow information.

6.4. Water flow testing

Having set all of the parameters so that the performance was stable, the testing at the predefined frequencies and flow rates was conducted.
The sump water conductivity was monitored throughout the test period. The conductivity was constant at 700 μS/cm. The conductivity of the sump water was relatively high compared with the tap water in the laboratory (σ = 400 μS/cm). A possible explanation for the high conductivity of the sump water was due to its age and the addition of chemicals. The water had been dosed with chemicals to stop bug growth and as a consequence the water had not been changed in over four months. Over time the water will have absorbed carbon dioxide and minerals that will have raised its conductivity (Farrington 2005).

6.4.1. 30 Hz flow testing

The flow meter system was set-up with the DSP operating at a frequency of 30 Hz. The quadrature voltage was reduced using the process described in section 6.2.4. The MassMeter and the electromagnetic flow meter system were set recording simultaneously. From conducting test flow runs the length of time required at each flow rate was chosen as at least 600 measurements. The length of the flow run was important for ensuring the student T uncertainty was acceptable and that fair comparisons between measurements could be made. The 30 Hz processed flow data is shown in figure 6.4.

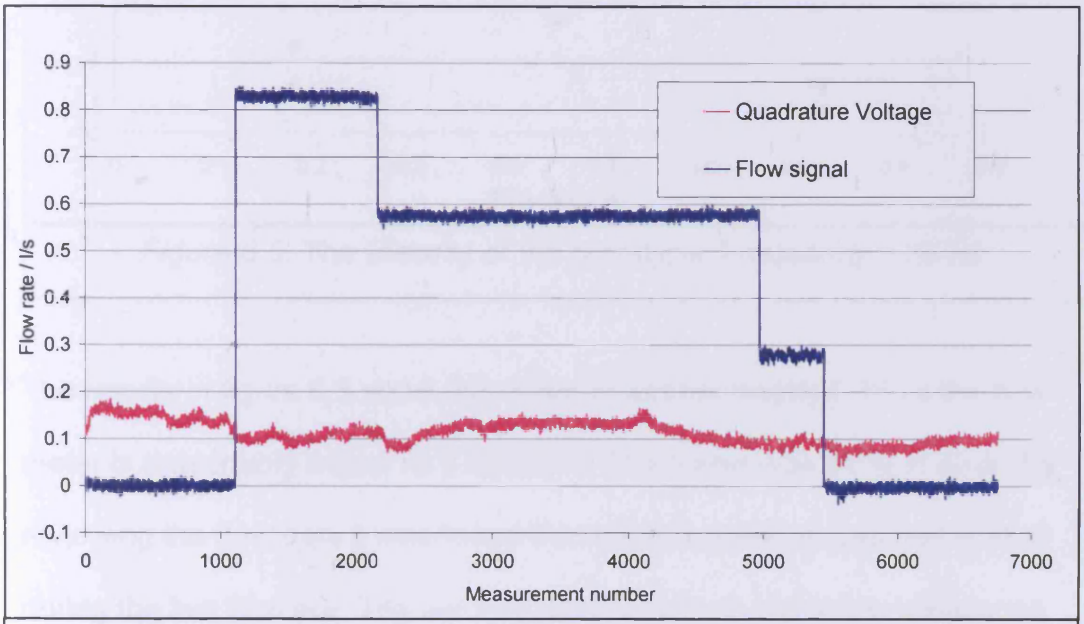

Figure 6.4. Prototype flow testing with water, Frequency = 30 Hz

The results in figure 6.4 show that the technique for rejecting the quadrature voltage has worked very well, the flow meter output is very stable and experiences no noticeable zero drift. When the measurement results were compared with the reference flow data the results were within 3 %. As only a

limited number of flow rates had been tested the linearity with an additional 2 different flow rates was tested. The error compared with flow rate is shown in figure 6.5.

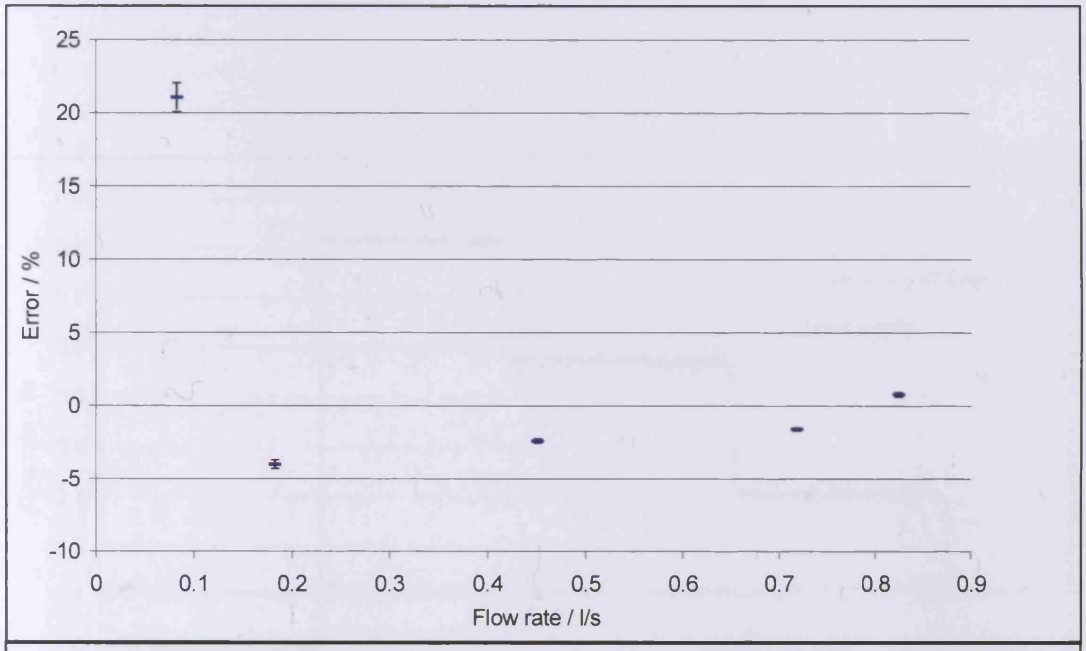

Figure 6.5. The linearity of the prototype, Frequency = 30 Hz

The results in figure 6.5 show that down to approximately 0.18 l/s the flow meter is reasonably linear. At 0.08 l/s the flow meter was 21 % in error. By reviewing the flow data it was found that the flow meter output had shifted during the last flow run. The linearity results show that the flow measuring system was not as accurate or as stable as the reference flow meter or Turner's prototype when tested using a MagMaster transmitter.

The peak-to-peak signal level at a peak-to-peak current of 1.5 A was 107 μV / (m/s).

6.4.2. 60 Hz flow testing

The frequency was changed to 60 Hz and the flow runs repeated, the results are shown in figure 6.6.

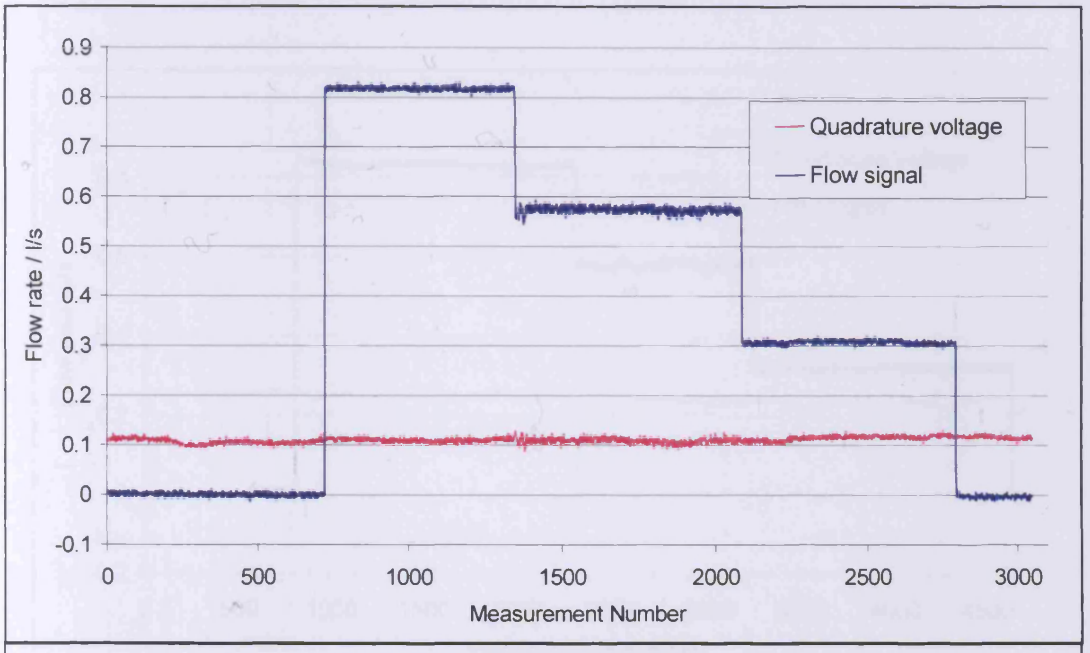

Figure 6.6. Prototype flow testing with water, Frequency = 60 Hz

The results in figure 6.6 show that the flow meter was stable throughout the flow test. The quadrature voltage does not vary by as much as the 30 Hz results. The average standard deviation for each flow rate was 0.009 l/s at 30 Hz whereas at 60 Hz it was 0.004 l/s, which is less than half the standard deviation. These observations suggest that the flow meter operates more effectively at 60 Hz than at 30 Hz.

The peak-to-peak signal level at a peak-to-peak current of 1.6 A was 93 μV / (m/s).

6.4.3. 120 Hz flow testing

The frequency was changed to 120 Hz and the flow runs repeated (figure 6.7).

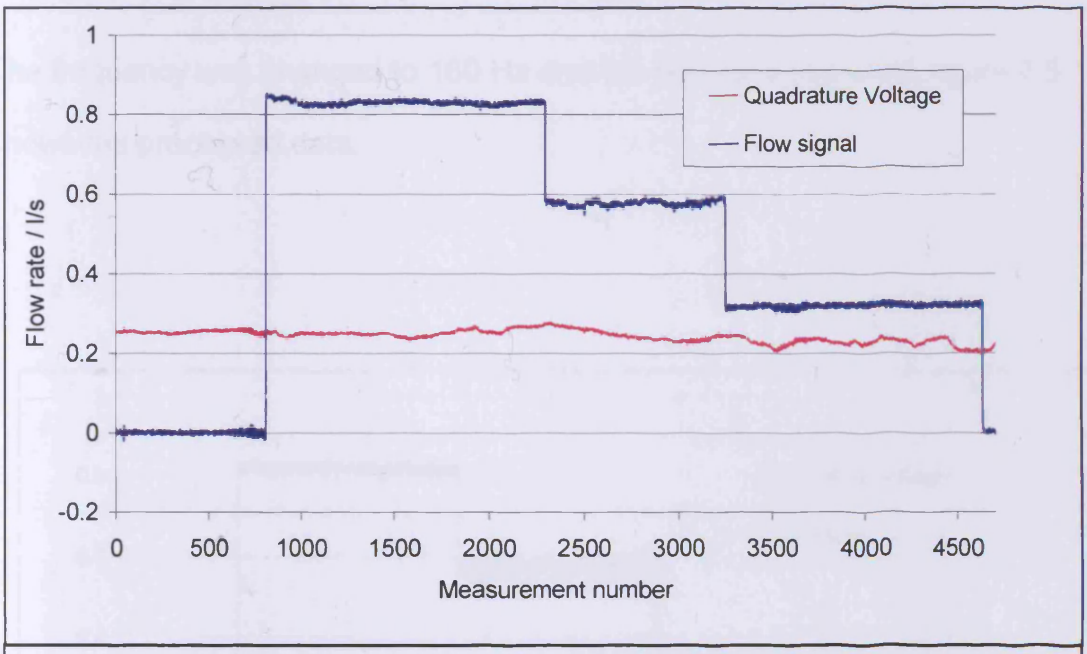

Figure 6.7. Prototype flow testing with water, Frequency = 120 Hz

The results in figure 6.7 show that the flow meter is less stable at 120 Hz than at 60 Hz. The technique of removing the flow signal from the sine transform or quadrature signal has not been totally affective. At approximately the 950th measurement the flow signal is not stable and it is clear that a small amount of the quadrature voltage is present in the flow signal. This suggests that the phase between the quadrature voltage and the flow signal has changed.

When the flow signal became unstable the standard deviation between measurements increased.

The peak-to-peak signal level at a peak-to-peak current of 1.0 A was 54 μV / (m/s).

6.4.4. 160 Hz flow testing

The frequency was changed to 160 Hz and the flow runs repeated, figure 6.8 shows the processed data.

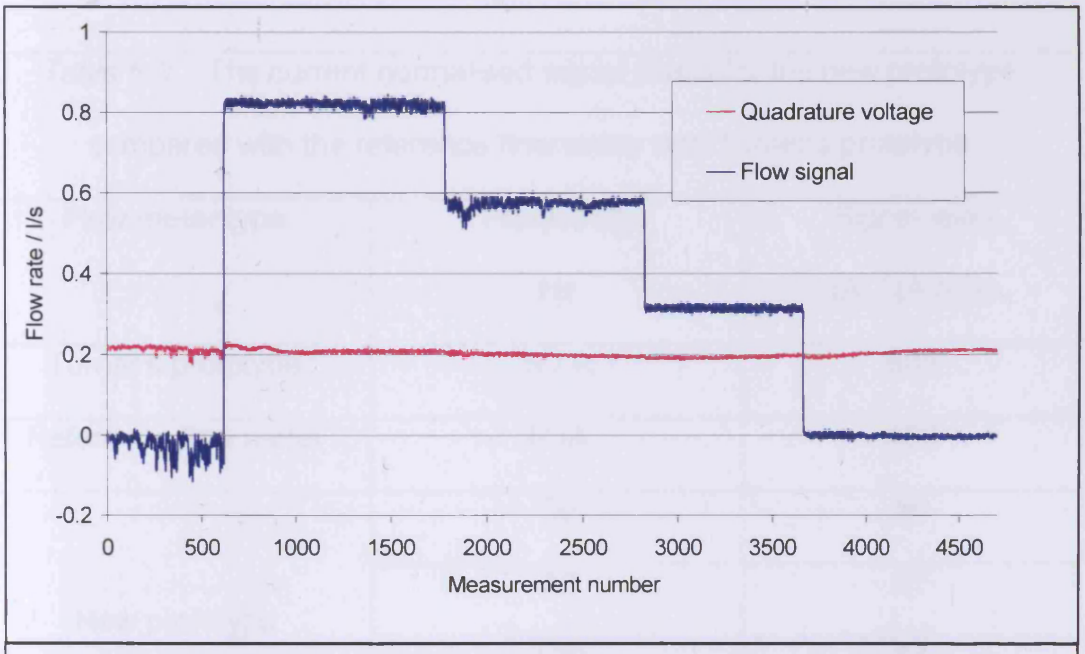

Figure 6.8. Prototype flow testing with water, Frequency = 160 Hz

Figure 6.8 shows that the flow meter was becoming unstable at 160 Hz, more so than when compared with the results in figure 6.7 for testing at 120 Hz. After the first 600 seconds the stability largely returned.

The peak-to-peak signal level at a peak-to-peak current of 0.8 A was 43 μV / (m/s).

6.4.5. Comparing the signal levels with Turner's prototype and the reference flow meter

The peak-to-peak signal levels measured at each frequency were current normalised for comparing the results with Turner's prototype and the reference flow meter. The results are shown in table 6.3 together with the results for Turner's prototype and the reference flow meter.

Table 6.3. The current normalised signal levels for the new prototype compared with the reference flow meter and Turner's prototype

Flow meter type	Frequency Hz	Signal level μV / (A.m/s)
Turner's prototype	N / A	638
Reference flow meter	N /A	400
New prototype	30	69
	60	57
	120	54
	160	53

From table 6.3 it is clear that the amount of signal recovered from the field generating coils is poor compared with the reference flow meter and Turner's prototype. The magnetic circuit in the new prototype does not generate as much flux in the measuring duct when compared with the other flow meters. Despite this lack of signal the measuring system is able to comfortably measure the flow rate of water. The work conducted by Cushing (1958) showed that with an insulating liquid the attenuation of the signal is based upon the permittivity of the liquid being measured. As a consequence the signal attenuation of BP180 dielectric oil would be approximately half the level presented in table 6.3. The consequence of this degradation in signal coupled with the expected increase in noise levels may make it very difficult to measure the flow rate of insulating liquids.

6.5. Demineralised Water flow testing

The water was removed from the flow rig and the sump was scrubbed in preparation for filling with demineralised water. The sump was filled with demineralised water, which had an electrical conductivity of 2 μS/cm. A portable demineralising plant was used to maintain the conductivity.

The flow traces for the 30, 60, 120 and 160 Hz flow tests were very similar to those presented in section 6.4. It was found to be very difficult to compare the performance with the different water conductivities and frequencies. As attempted in Chapter 3 the standard deviation data was used to make

performance comparisons. The standard deviation result for the 60 Hz flow testing with water and demineralised water is shown in figure 6.8.

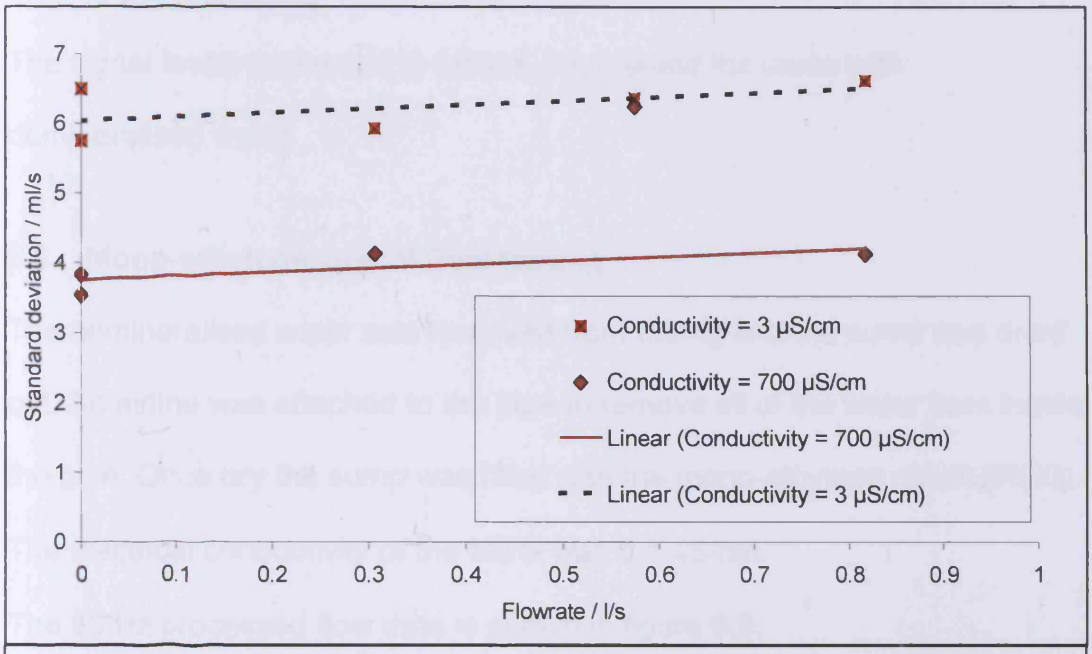

Figure 6.8. A comparison between the standard deviation measurements taken from flow tests conducted using the new prototype operating at a frequency of 60 Hz with water and demineralised water

Care had to be taken when making comparisons, as the flow data could be subject to stability problems. The results in figure 6.8 for the water tests at 700 µS/cm showed an uncharacteristically high standard deviation at a flow rate of 0.58 l/s. When the flow trace was examined it was unusually noisy because of interference from the variable speed driver. This result was considered an outlier and not included when creating the trend line through this set of data. From the trend lines it was clear that at 60 Hz the standard deviation was approximately 2.3 ml/s greater with a conductivity of 3 µS/cm compared with 700 µS/cm. When compared with Turner's prototype the standard deviation with 420 µS/cm water was 0.8 ml/s and with 4 µS/cm it was 1.4 ml/s. With Turner's prototype this was an increase of 75 % whereas with the new prototype it was an increase of 60 %.

The results from testing at 30 Hz, 120 Hz and 160Hz showed a similar increase in standard deviation when the 3 µS/cm results were compared with the 700 µS/cm results.

The signal levels presented in table 6.3 remained the same with demineralised water.

6.6. Mono-ethylene Glycol flow testing

The demineralised water was removed from the rig and the sump was dried out. An airline was attached to the pipe to remove all of the water from inside the pipe. Once dry the sump was filled with the mono-ethylene glycol (MEG). The electrical conductivity of the MEG was 0.1 µS/cm.

The 30 Hz processed flow data is shown in figure 6.9.

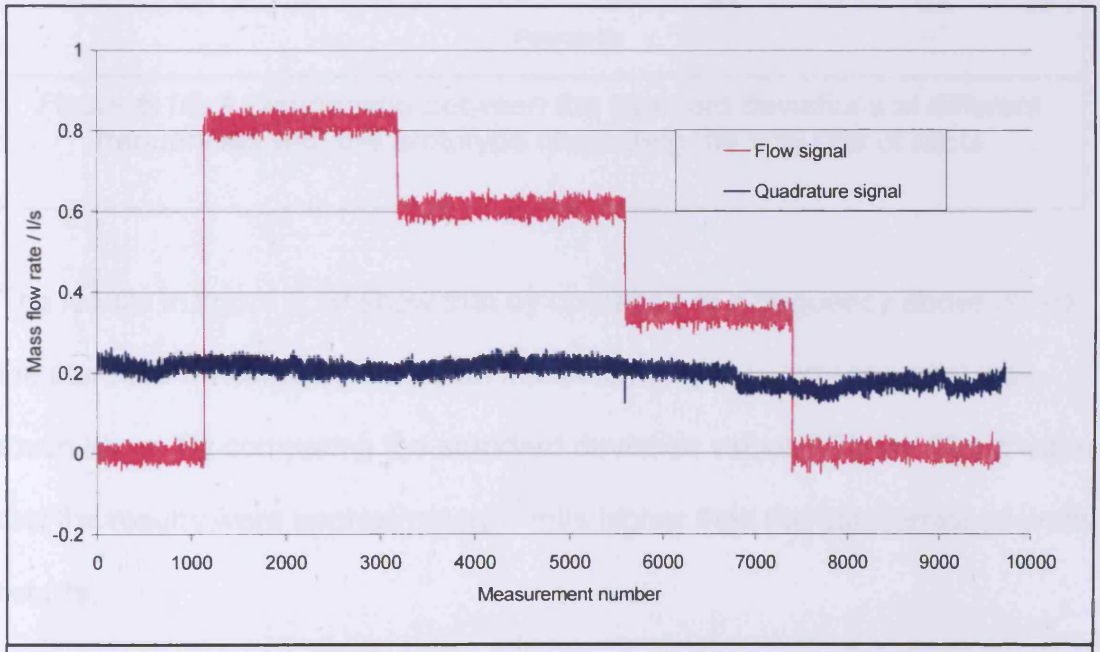

Figure 6.9. Prototype flow testing with MEG, Frequency = 30 Hz

By comparing the flow trace in figure 6.9 with that of figure 6.4 it was apparent that the flow signal with MEG operating at 30 Hz was significantly noisier than

with tap water. The other frequencies were tested and were visually no different to the traces with demineralised water. The standard deviation results for all frequencies operating with MEG are presented in figure 6.10.

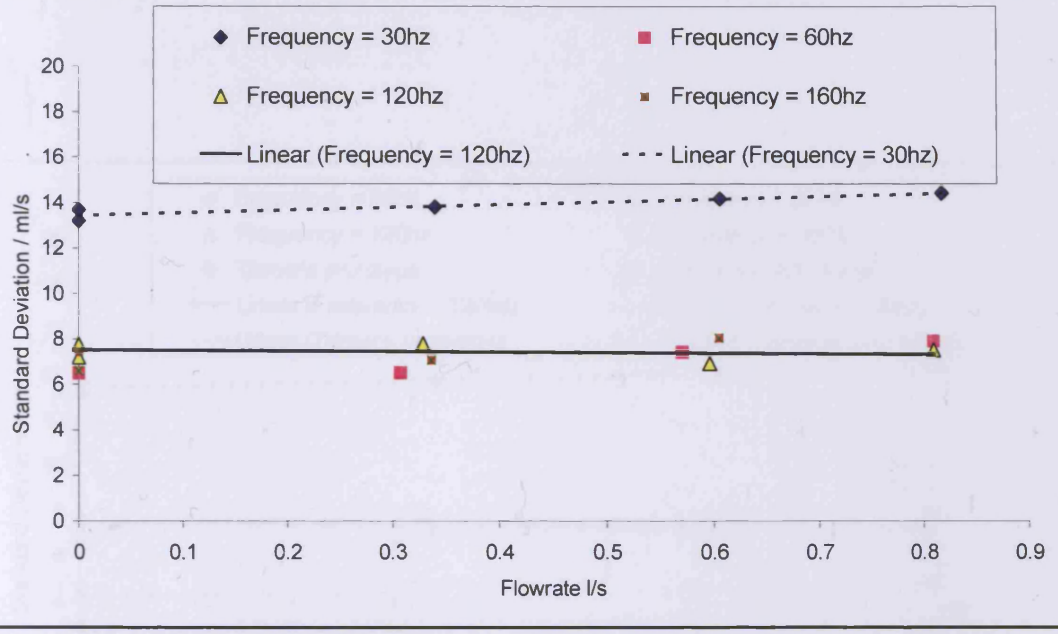

Figure 6.10. A comparison between the standard deviations at different frequencies with the prototype measuring the flow rate of MEG

The results in figure 6.10 show that by operating at a frequency above 30 Hz the standard deviation (which is an indication of measurement noise) was much lower. By comparing the standard deviation values with the 60 Hz water test the results were approximately 1 ml/s higher than the demineralised water results.

6.6.1. MEG testing with Turner's prototype and the reference flow meter

Once MEG testing with the new prototype was completed the flow meter was removed from the rig and Turner's prototype and the reference flow meter were installed. The flow meters were tested over the same flow range as the new prototype. The standard deviation results are shown in figure 6.11.

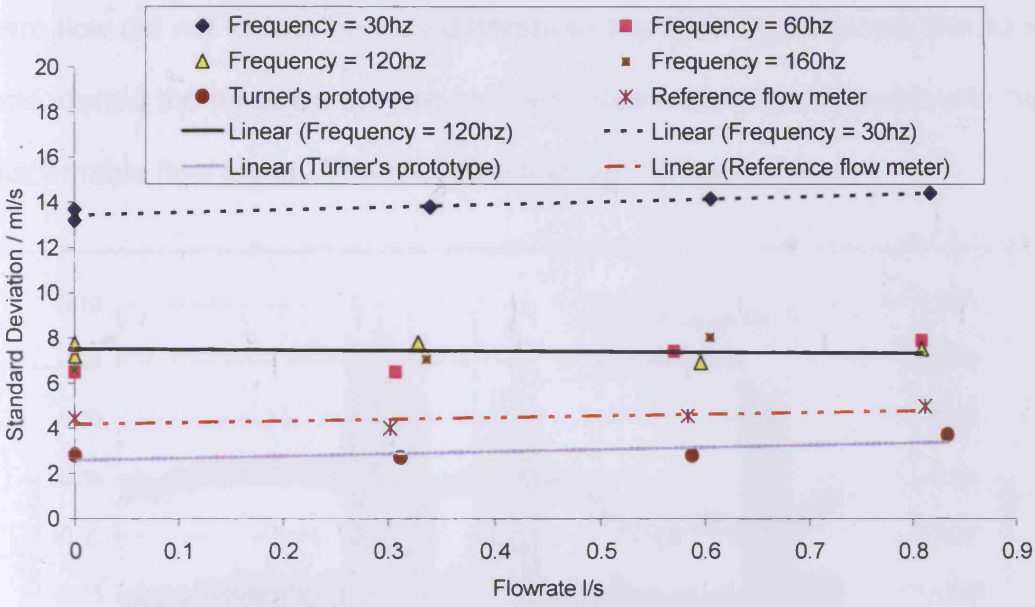

Figure 6.11. A comparison between the standard deviations of all flow meter designs tested measuring the flow rate of MEG

The results in figure 6.11 show that the conventional flow meters have lower standard deviations than the new prototype, even when tested with the MEG.

6.7. BP 180 Dielectric oil flow testing

The Mono-ethylene glycol was removed from the rig and the sump was dried out. An airline was attached to the pipe to remove the remaining MEG from the flow rig pipe work. The sump was filled with the BP180 dielectric oil. The electrical conductivity of the BP180 was measured by Amare (1995) and reported as 5.7e-7 μS/cm.

The DSP frequency was set to 30 Hz and the flow test started. The noise at zero flow did not look to be very different to any other liquid. When the pump was started the noise on the raw sine and cosine data was extreme with no discernable flow signal. The results are shown in figure 6.12.

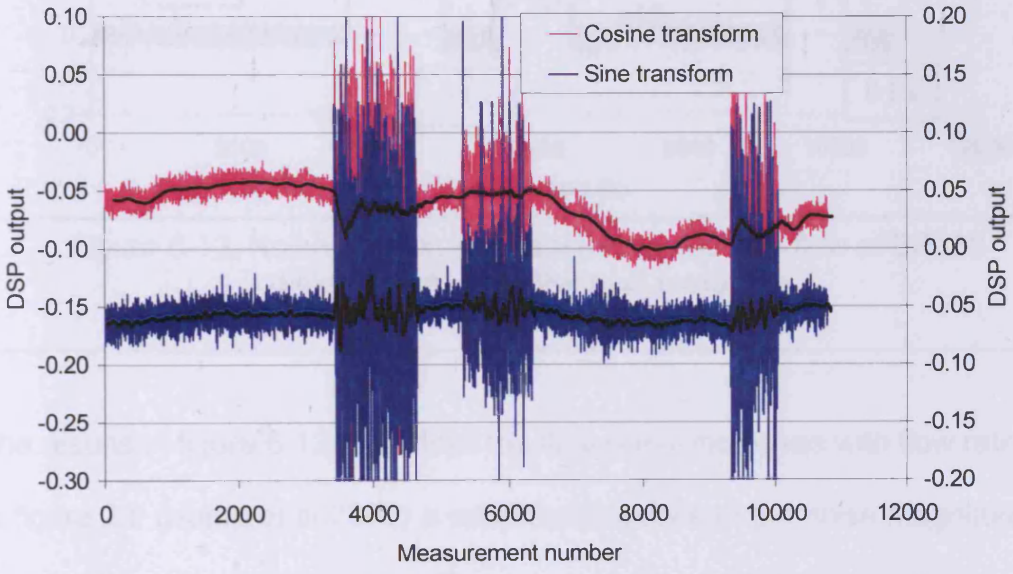

Figure 6.12. Test results for the new prototype operating at a frequency of 30 Hz with BP180 dielectric oil flowing through the rig

Despite attempts at post processing the results, no flow signal was present. However from studying the data the amplitude of the noise looked to be related to the flow rate. By calculating the magnitude of the sine and cosine components a rough measurement of flow rate was achieved, by also

subtracting a proportion of the sine component the measurement stability was greatly improved. The results are shown in figure 6.13.

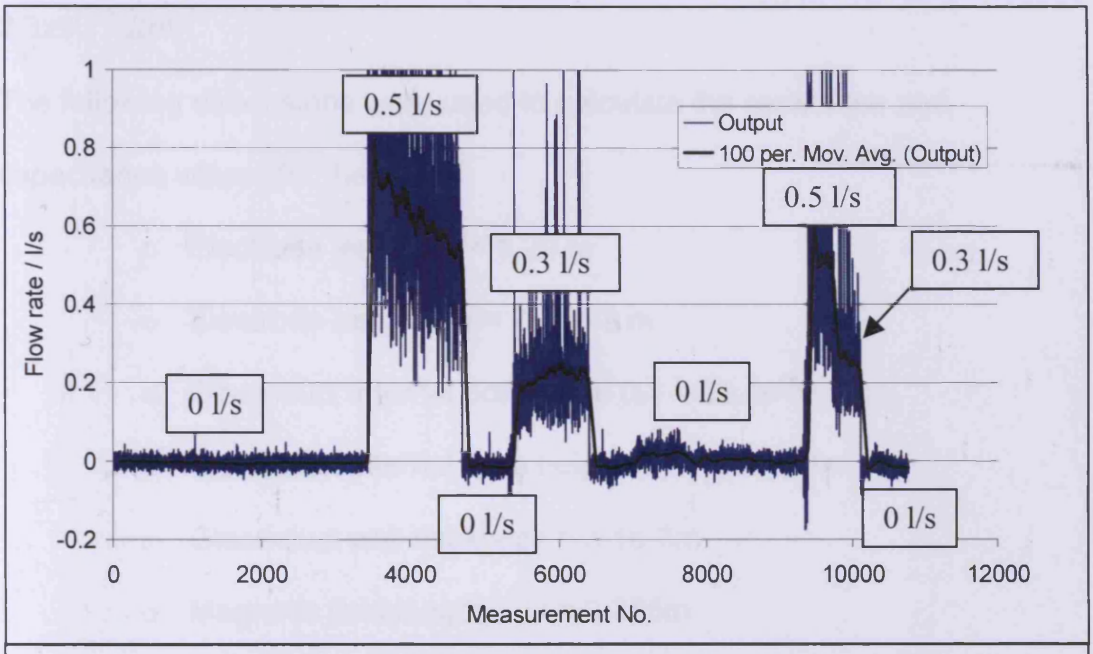

Figure 6.13. Noise magnitude measurement of the flow of BP180 dielectric oil using the new prototype

The results in figure 6.13 show that the flow noise increases with flow rate. In figure 2.5 (Hemp et al 2002) a relationship between the noise magnitude and the flow rate was observed. The results in figure 6.13 confirm that the noise magnitude is related to the flow rate.

The frequencies 60 Hz, 120 Hz and 160 Hz were tested and like the 30 Hz results no flow data was observed. The frequencies 240 Hz, 640 Hz and 1280 Hz were also tested but again no flow signal was present.

To try and understand what may be going wrong an equivalent circuit was developed based on the electrical properties of the Oil, the glass and the physical dimensions of the flow meter. The electrical properties for the borosilicate glass were taken as K = 5 and ρ_R = 1x10^{12} Ωm. The electrical properties of the BP180 Dielectric oil were taken as K = 1.95 and ρ_R = 2.3x10^{10} Ωm.

The following dimensions were used to calculate the resistance and capacitance values for the model:

- Electrode length (l) = 0.29 m
- Electrode height ($2a$)= 25.4e-3 m
- Glass duct internal bore width (w) = 25.4e-3m
- Glass duct internal bore height ($2a$)= 25.4e-3m
- Glass duct wall thickness = 3.1e-3m
- Magnetic field length ($2L$) = 0.386m

The resistance was calculated using equation 6.1.

$$R = \frac{\rho_R l_c}{A} \qquad (6.1)$$

The capacitance was calculated using equation 6.2.

$$C = \frac{A\varepsilon_r}{a} \qquad (6.2)$$

The source impedance within the flow meter was calculated using equation 2.7. Turner's (2003) analysis was restricted to conduction currents only. Assuming that the source impedance of the generator is based upon the resistivity of the liquid, the cross-sectional dimensions of the duct and the length of the magnetic field, the source capacitance should be related to the

same physical dimensions. Using the permittivity of the metered liquid, the source capacitance was calculated using equation 6.3.

$$C = \frac{\varepsilon_r w 2L}{a} \qquad (6.3)$$

An equivalent circuit was created and was considered representative of the flow meter with the oil flowing through it. The circuit diagram is shown in figure 6.14.

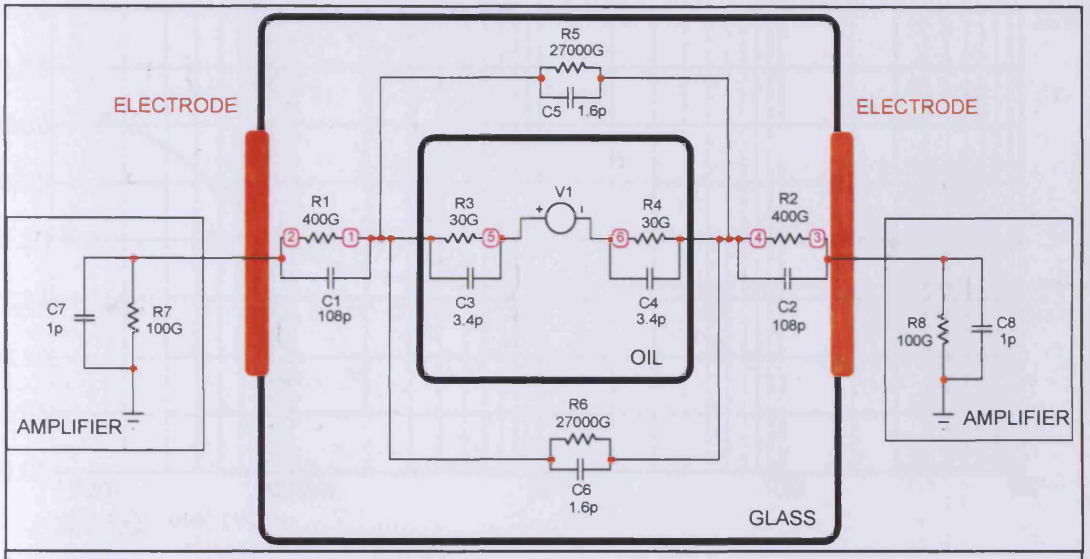

Figure 6.14. A Circuit diagram of the new prototype with BP180 oil in the flow duct

In explanation the voltage generated across the width of the duct is an AC signal (V1) with a source impedance R3 and R4 and a source capacitance C3 and C4. R1 and R2 are the resistances between the electrode surface and the inside of the glass tube; C1 and C2 are the capacitances between the electrode and the inside surface of the glass wall. R5, C5, R6 and C6 represent the resistances and capacitances between the electrodes through the top and bottom wall section of glass. Finally R7, C7 and R8 and C8 are the buffer amplifiers impedances and capacitances to ground.

The circuit was modelled using a circuit analysis program called Micro-Cap 8.0.0.0 Evaluation version. An AC potential of 1 V was applied to the generator (V1). The circuit analysis package was programmed to calculate and plot the potential at nodes 3 and 4 on a graph against frequency. The results are shown in figure 6.15.

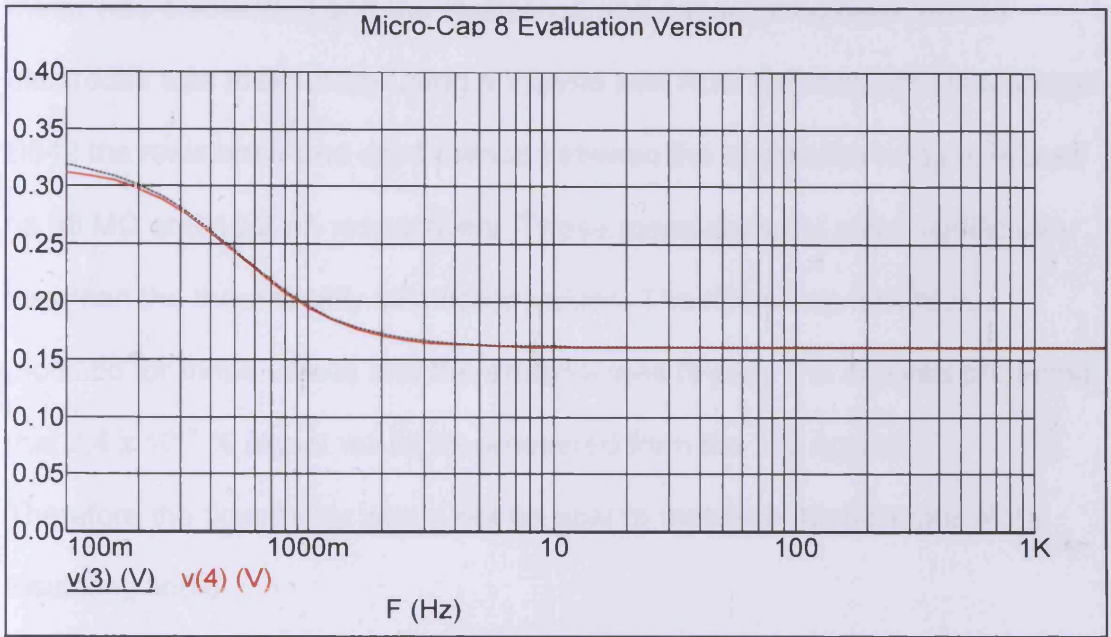

Figure 6.15. A Circuit analysis of the new prototype as postulated in figure 6.14.

The results in figure 6.15 show that with a 1 V signal generated within the flow only 0.156 V will be measured at the electrode. The potential drop across the glass tube is 0.006 V and will not be a problem. The total potential measured across both electrodes is 0.312 V; therefore the signal recovery with oil should be approximately 31 % of the total generated signal. When modelled with water, demineralised water and MEG the signal recovery was 99.1 %. The analysis was also conducted with Aniline which has a conductivity of 0.09 µS/cm and a dielectric constant of 7.2. The signal recovery was also found to

be 99 % at a frequency of 100 Hz indicating that the flow meter should operate satisfactorily with a liquid that is lower than present state of the art (20 μS/cm).

The micro-cap analysis predicted that a flow signal would be seen, even with the 30 Hz flow testing, however no flow signal was present. The experimental results suggested that the model was not representative of the test. The flow meter was dismantled and the resistance and capacitance between the electrodes was measured. Using a Wayne kerr Auto balance universal bridge B642 the resistance and capacitance between the electrodes was measured as 58 MΩ and 10.2 pF respectively. These measurements were significantly less than the theoretically calculated values. The micro-cap model was modified for these values and the analysis was re-run. The analysis predicted that 2.4×10^{-9} % signal would be recovered from the 1 V applied.

Therefore the flow meter would not be able to measure the flow rate of the insulating liquid.

Whilst attempting to improve the mutual electrode resistance the glass tube was cracked at one end rendering the flow tube unusable.

Once the flow tube became damaged it was no longer safe to flow the oil through it, however it was possible to measure the zero flow noise spectrum with the BP180 dielectric oil, the results are shown in figure 6.16.

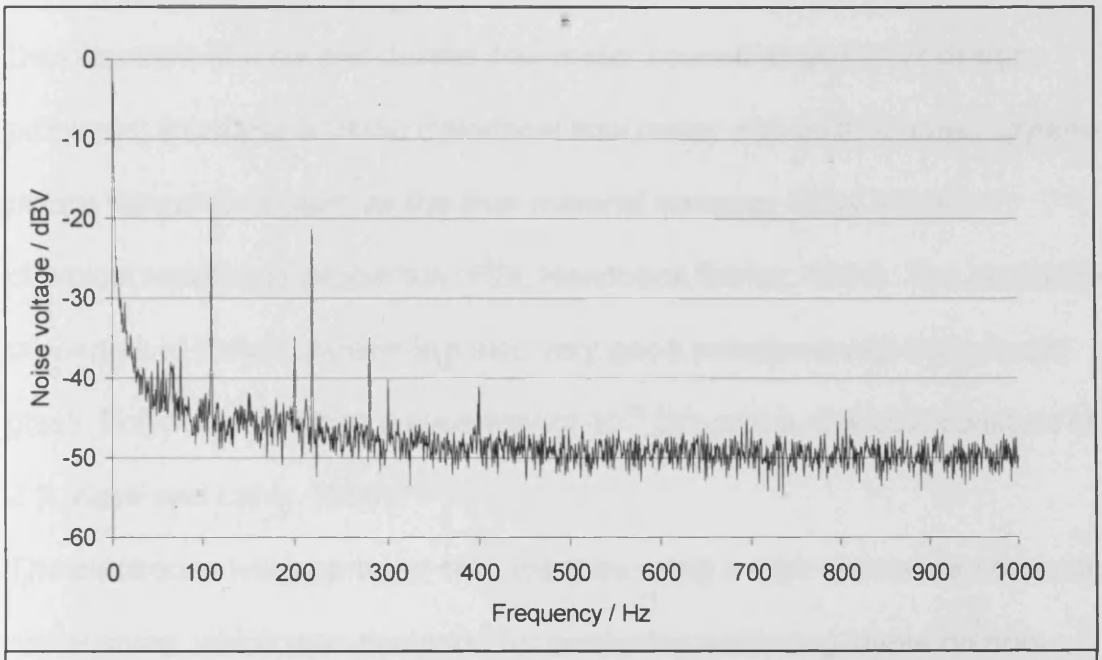

Figure 6.16. Spectrum analysis of the new prototype with BP180 dielectric oil in the flow duct

The results in figure 6.16 show that the noise levels are significantly greater than the zero noise levels with demineralised water.

6.8. A Description of the Development of a Cylindrical Prototype and the Test Work Conducted so Far

6.8.1. Introduction

After the glass flow tube broke a new prototype was developed. A brief description of the developed flow meter will be given along with the test work conducted so far, including the partial success at measuring the flow of BP180 dielectric oil.

6.8.2. Flow Meter Design

Development of a square ducted flow meter caused a number of design problems; therefore a DN50 cylindrical flow meter was built. A polypropylene plastic tube was chosen as the liner material because it has excellent chemical resistance properties (PDL Handbook Series, 1994). The insulating properties of Polypropylene are also very good compared with borosilicate glass. Polypropylene has a resistivity of 10^{14} Ωm and a dielectric constant of 2.2 (Kaye and Laby, 1989).

The electrodes were sprayed onto the tube using a high resistance conductive nickel spray, which was designed for producing screening layers on non-conductive materials. Four sets of electrodes were produced; each electrode subtended a half angle β of 60° and was 50 mm long. Each set of electrodes was separated by a 5 mm gap as shown in figure 6.17.

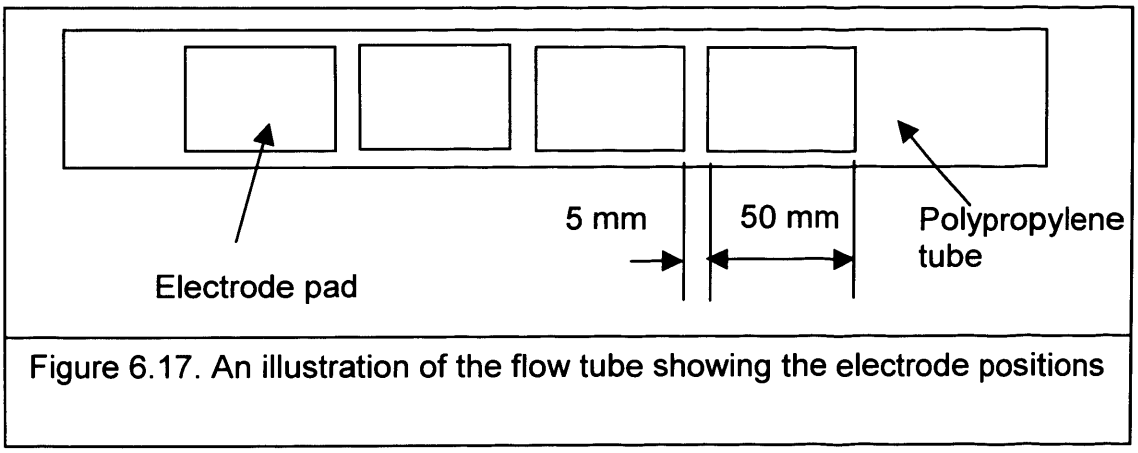

Figure 6.17. An illustration of the flow tube showing the electrode positions

The four sets of electrodes were produced so that if desired they could be connected together to allow the performance with different lengths of electrode to be tested. This design will allow 50 mm, 100 mm, 150 mm and 200 mm long electrodes to be tested. The flow meter was set-up to measure

the voltage generated with 50 mm long electrodes. A 300 mm long, 65 mm diameter plastic tube was fed over the top of the electrode flow tube and mounted coaxially in position using plastic sub flanges positioned at either end of the flow tube. Each side / half of the outer tube was sprayed with the nickel spray with an air gap of approximately 5° left at the top and bottom of the flow meter. Each conductive half of the screen tube was insulated from the other so that they could be connected to the driven screen terminals of the amplifiers. By driving each half of the screen tube, the high impedance electrode signals mounted on the flow tube should be protected from stray capacitance and external interference. Electrode wires were connected to the nickel pads and fed through holes in the driven screen tube. The buffer amplifiers were then attached to the electrode wires and the two driven screens were also electrically connected to the driven screen terminals on the PCB's.

The magnetic circuit consisted of two air cored rectangular saddle coils with the same radius as the driven screen tube. These coils were placed on the top and bottom of the flow tube so that a field would be produced in the electrode region. Also a search coil was positioned inside the field region to allow changes in the flux output to be monitored.

To operate the flow meter the coils were energised with an A.C. voltage powered by a QSC Audio PLX1202 power amplifier.

The electrode and search coil signals were connected to a VKA phase sensitive detector manufactured by KENT Instruments. The flow signals detected by the VKA phase sensitive detector were outputted to a chart

recorder using a 4-20 mA output. A block diagram illustrating how the VKA phase sensitive detector operates is shown in appendix E.

6.8.3. Flow Testing

With a single set of electrodes connected to the voltage sensing amplifiers the flowmeter was installed in the NAMAS flow rig. The performance with water was then analysed. The maximum frequency that could be reliably used was found to be 960 Hz. The coils were energised with a frequency of 311 Hz and the linearity of the flow meter was tested. The results are shown in figure 6.17.

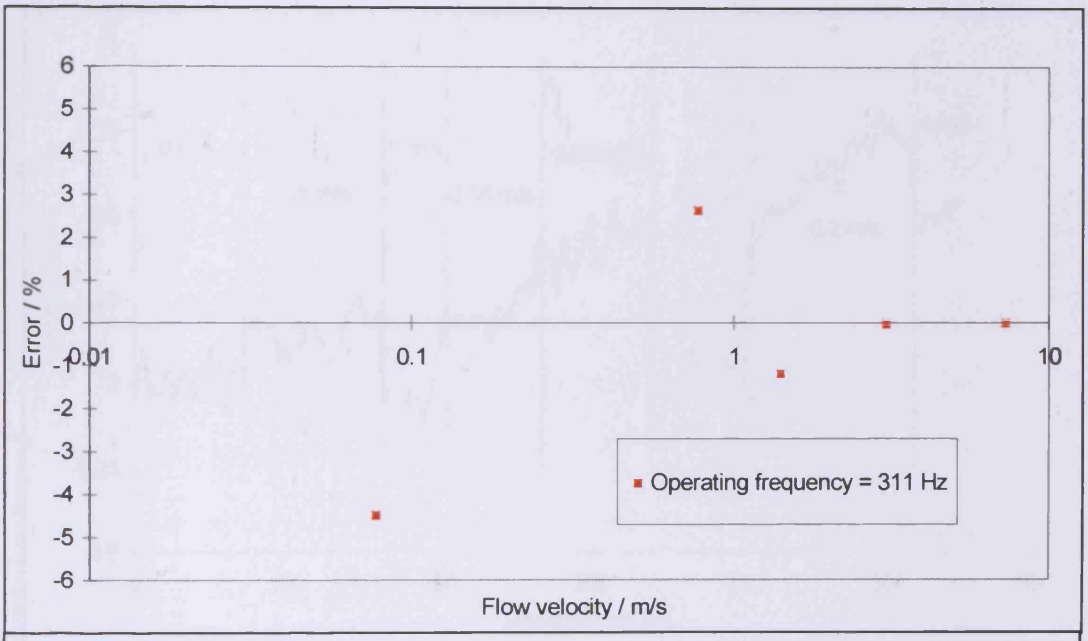

Figure 6.17. Flow testing a DN50 polypropylene flow meter operating with a VKA phase sensitive detector using the NAMAS rig

The results in figure 6.17 show that the flow meter is accurate to within +/- 5 %.

Once the performance had been evaluated with water the flow meter was installed in the oil flow rig. When tested with the BP180 dielectric oil the noise

levels within the pipe caused the differential amplifier within the VKA to saturate, rendering a flow measurement impossible. As the noise frequency had been measured in figure 6.16 it was known that above a frequency of approximately 300 Hz the noise voltages would be considerably less. A low pass RC filter was attached to the VKA inputs to filter out all frequencies below 300 Hz. The frequency was set to 400 Hz and the flow re-started. Figure 6.18 shows a flow trace at 400 Hz with three different velocities.

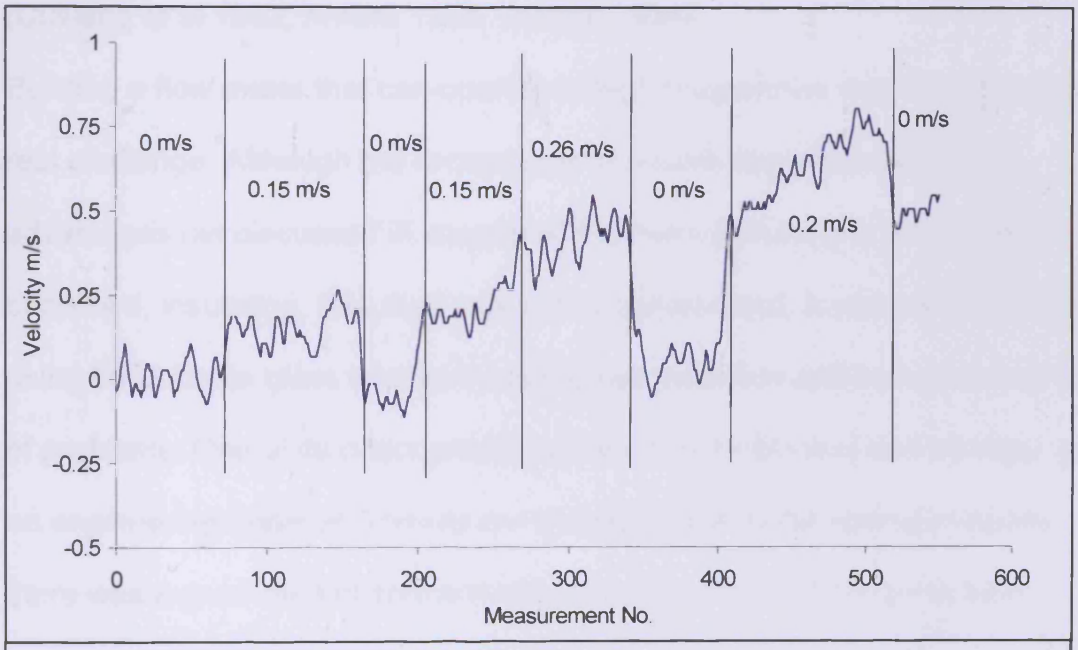

Figure 6.18. A flow trace from the DN50 polypropylene flow meter operated using a VKA phase detector measuring the flow of BP180 dielectric oil

Figure 6.18 shows that the prototype flow meter has detected a small flow signal when tested using the insulating liquid. The flow signal was very small compared with the water test results indicating that a proportion of the flow signal was probably being lost through stray capacitance. After approximately

the 400th measurement, zero stability problems began to affect the measurement. If the flow signal had been of a similar size to the water measurements then the zero shifts would not have been so problematic, as they were not noticed at this frequency when tested with water.

6.9 Discussion

This chapter has shown that it is possible to measure the flow rate of an insulating liquid as claimed by a number of scientists mentioned in this thesis (Cushing et al 1962; Amare 1995, Durcan 1998).

Building a flow meter that can operate at high frequencies was found to be a real challenge. Although the rectangular or square duct flow meter had advantages (as discussed in chapter 4) the manufacture of a long, square sectioned, insulating, flow duct was not straightforward. It became clear that using borosilicate glass was an inappropriate selection and caused a number of problems. One of its major pitfalls related to its brittleness and strength as an engineering material. Throughout the glass flow meter testing program there was a great deal of concern about the sturdiness of the glass tube. Ultimately the glass tube did break during the testing program. The relative permittivity of the glass tube was greater than the dielectric oil, BP180; this caused part of the signal to be shunted through capacitive losses. Using the micro-cap analysis the signal recovery was calculated assuming that the flow conduit was manufactured from PTFE, where K = 2.1 and ρ_R = 10^{16}. The signal recovery was found to be 0.497 V; this is an improvement over the theoretical glass tube flow meter of 59 %. The affect of changing the length of

the magnetic field region was also analysed, by increasing the length of the magnetic field the source impedance reduces and the source capacitance increases. When measuring insulating oils the electrode amplifier is operating close to its input impedance limit therefore increasing the length of the magnetic field will improve its measurement performance.

Based on the micro-cap analysis the glass flow meter should theoretically produce a flow signal. Based on the signal level at 160 Hz (66.25 μV / (m/s)) and the calculated signal attenuation of 0.157 a signal level of 10.34 μV / (m/s) would have been generated. The signal level at 1 m/s would have been equivalent to –100 dBV. The results in figure 6.16 show that even with zero flow the noise levels are 5 ½ decades greater than the 1 m/s signal at 160 Hz. This result proves that the glass flow meter would not have been able to measure the flow of a dielectric liquid when operated at its maximum frequency.

The initial testing with the polypropylene prototype has produced some encouraging results. The flow meter design has a distance of 7.5 mm between the electrode surface and the driven screen surface. If this gap could be reduced so that the driven screen was positioned much closer to the electrode surface the amount of stray capacitance should be reduced and a larger signal will be measured. If tested using current sensing electrodes the signal should not suffer from as much stray capacitance because the electrodes are at a virtual earth.

Chapter 7

Conclusions

7.1. Introduction

This chapter will state the main conclusions of this research project and give recommendations for further work.

7.2. Conclusions

The research work conducted has shown a clear advantage with elongated electrodes over small diameter electrodes when tested with low conductivity liquids.

- Measurements found that the line electrode was quieter with static flow and more so with flowing liquids when compared with the small diameter electrode.
- The noise present at the electrode surface with conductive liquids was attributed to Johnson noise. By combining the electrode resistance equations derived by Turner (2003) with the Johnson noise equations good correlation between the theoretical and experimental zero flow noise spectra was found.
- The circuit analysis work has shown that the source impedance and source capacitance have a direct affect on the signal level that can be recovered, therefore a long magnetic field and electrode will improve signal to noise levels.

- The polypropylene prototype was successful in sensing a flow signal when tested with BP180 dielectric oil. It can be claimed that the performance with liquids that are currently beyond the limit of present day flow meters could now be measured to a satisfactory level using the electromagnetic flow meter.

To operate with insulating liquids the flow duct should be manufactured from a material that has a dielectric constant of at least a similar magnitude to the insulating liquid being measured to ensure unnecessary signal shunting does not occur.

A square or rectangular duct flow meter has been shown as the ideal conduit geometry for low conductivity flow meter designs. This geometry allows a large area electrode to be used whilst improving the performance with different velocity profiles compared with conventional cylindrical geometry flow meters.

The established weight function theory has been evolved to allow the difference in signal output between current sensing and voltage sensing amplifier designs. The analysis process described can be used with any magnetic field or electrode geometry.

7.3. **Recommendations for further work**

To continue this research an experimental analysis of the performance with current sensing and voltage sensing electrodes when operated with an insulating liquid should be made. Through comparing the performance it should be possible to state definitively which amplifier arrangement will operate more effectively with low conductivity liquids.

As the dielectric flow meter has been identified as being permittivity sensitive methods of measuring the relative permittivity should be investigated and furthermore how the most suitable measurement technique might be incorporated into a flow tube.

Electronics that can operate a flow meter at appropriate frequencies for measuring insulating liquids should be developed. This electronics would preferably be able to sense small changes in the flux levels within the measuring section to improve measurement stability.

Further work to improve the accuracy of the weight function prediction would be beneficial, such as the integration of a computational fluid dynamics solution to allow the ANSYS program to automatically calculate the weight function potential.

References

ABB, 1995. *Commander 50 Controller/Alarm unit – User guide.* Issue 1

ABB, 1997. *MassMeter – Coriolis Flow Measurement, Data sheet.* Issue 1

ABB, 2002. *Electromagnetic flow meter, SM4000, Data sheet.* Revision 1.

ABB, 2003. *Electromagnetic flow meter, MagMaster Water Waste Version, Data sheet SS/MAG/ww_8.* Issue B

ABB, 2006. *ACS400 Technical data sheet* [online]. Available from http://www.abb-drives.com/products/acs400/acs400_technical.asp. [accessed on 26th September 2006]

ABEDIAN B., SONIN A.A., 1982. *Theory for electric charging in turbulent pipe flow*, J. Fluid Mech. Vol. 120, pp. 199-217.

AKZO NOBEL, 2004. *Akzo Nobel, Mono Ethylene Glycol, Product information Sheet* [online]. Available from http://www.ethylenamines.com/NR/rdonlyres/C3E3C863-7629-4B05-83A8-d64fa562119b/0/pismeg200410. [Accessed on 20th September 2006].

AL-KHAZRAJI Y.A., BAKER R.C. 1979. *Analysis of the performance of three large-electrode electromagnetic flow meters,* J. Phys. D: Appl. Phys., Vol. 12. pp. 1423 – 1434.

AMARE T., 1995. *Electromagnetic Flowmeter for Dielectric Liquids.* PhD thesis. Cranfield university.

ASQUITH P.M., 1980. *VKA Synchronous Analogue Multiplier.*

ASQUITH P.M., 2003a. *MagMaster Operating Modes.* Internal design document.

ASQUITH P.M., 2003b. *Capacitive electrode Buffer amplifier design.* Internal design package.

ASQUITH P.M., 2006. *Private meeting regarding capacitive electrode amplifier designs.*

BALLENTYNE D.W.G., WALKER L.E.Q. 1958. *A Dictionary of Named Effects and Laws in Chemistry, Physics and Mathematics.* Chapman and Hall Ltd.

BARNES R.G., FORAN D., 2001. *Positive Displacement Flowmeters for Liquid Measurement*, in SPITZER D.W., (EDITOR) *Flow Measurement*, Ch15.

BEVIR M.K., 1969. *Induced Voltage Electromagnetic Flowmeters.* PhD thesis. University of Warwick.

BOAST W.B., 1964. *Vector Fields ////A Vector Foundation of Electric and Magnetic Fields.* A Harper International Student Reprint.

BROWN A.E., LYNNWORTH L., 2001. *Ultrasonic flowmeters*, in SPITZER D.W., (EDITOR) *Flow Measurement*, Ch20.

BS 5958-1:1991. *Code of practice for – Control of undesirable static electricity – Part 1: General Considerations.*

BS 5958-2:1991. *Code of practice for – Control of undesirable static electricity – Part 2: Recommendations for particular industrial situations.*

BS EN ISO 6817:1992. *Measurement of conductive liquid flow in closed conduits – Method using electromagnetic flow meters.*

BS ISO 5168:2005. *Measurement of fluid flow – Procedures for the evaluation of uncertainties.*

Cushing V., 1958. *Induction Flowmeter*, Rev. Sci. Instr. Vol. 29, No. 8. pp. 692-697.

CUSHING V., REILY D.M., SCHEIN T.R., 1962. *Induction Flowmeter for Dielectric Fluids*, Experimental Verification, Final report under contract NASr-53, NASA.

CUSHING V., REILY D.M., EDMUNDS G.W., 1964. *Development of an Electromagnetic Induction Flowmeter for Cryogenic Fluids*, Final report under contract NASw-381for Lewis research centre, NASA.

CUSHING V., 1965. *Electromagnetic Flowmeter*, Rev. Sci. Instr. Vol. 36, No. 8. pp. 1142-1148.

CUSHING V., 1974. *Electromagnetic flowmeter*, Proc. of flow symposium, 1971, Pitts, USA, Vol. 1, Part 2. pp. 723-733.

CUSHING V., 1999. *Comprehensive flowmeter for all materials*, Final report under grant DE-FG05-92ER81353, USDOE oak ridge field office.

CUSHING V., 2002. *Electromagnetic Flowmeter for Insulating Liquids*, IEEE Instrumentation and Measurement Technology Conference, pp. 103-109.

DURCAN L.P., 1998. *Development of baseline stability in an electromagnetic flowmeter for dielectric liquids.* PhD thesis. Cranfield university.

FARRINGTON J., 2005. *Private meeting regarding the sump water conductivity and factors that could affect it.*

FARNELL IN ONE. 2004. *FARNELL in one, Electronics components catalogue*, Book 2.

FURNESS R.A., 1989. *Fluid Flow Measurement.* Longman.

FRANKLIN B., 2001. *Fluid Dynamics Effects in Pipes and their Influences on Flowmeter Performance*. PhD thesis. University of Wales.

HEMP J., SANDERSON M.L., KOPTIOUG A.V., LIANG B., SWEETLAND D.J., AL RABEH R.H., 2002. *Problems in the theory and design of electromagnetic flowmeters for dielectric liquids. Part 1: Experimental assessment of static charge noise levels and signal to noise ratios*, Flow Meas. Instr. 13. pp. 143-153.

HEMP J., YOUNGS I., 2003. *Problems in the theory and design of electromagnetic flowmeters for dielectric liquids. Part 3a. Modelling of zero drift due to flux linkage between coil and electrode cables*, Flow Meas. Instr. 14 pp. 65-78.

HIRST MAGNETIC INSTRUMENTS LTD., 2006. *Hirst Magnetic Instruments Ltd., Gaussmeters, Hall Effect Principle* [online]. Available from: http://www.hirst-magnetics.com/instruments/gauss_p4.shtml [Accessed 18th September 2006].

HUSSAIN Y.A., BAKER R.C., 1985. *Optimised noncontact electromagnetic flowmeter.* J. Phys E: Sci. Instrum., Vol. 18.

HUSSAIN Z.D., 2001. *Differential Pressure Flowmeters*, in SPITZER D.W., (EDITOR) *Flow Measurement*, Ch8.

ISO 9368-1:1990. *Measurement of Liquid flow in closed conduit using weight and volumetric methods – Part 1: Weighing methods – Section 1.2 Procedures for checking static weighing systems.*

KAYE G.W.C., LABY T.H., 1989. *Tables of Physical and Chemical Constants and some Mathematical Functions. Published by* Longman Scientific and Technical. 15th Edition.

KEECH R.P., 2004, Private meeting about AC signal demodulation.

KHANNA R., 2006. *Power Designer, Expert tips, tricks and techniques for powerful designs, Analysing Power Modules* [online], Available from: http://www.national.com/appinfo/power/files/PowerDesigner_107.pdf. [Accessed 13th February 2006]

LANSDOWNE W.B., 2006, Private meeting with Lansdowne, a Profusionist, about triple heart by-pass operations.

LOWARA, 2006, *SV Vertical multistage centrifugal pumps.* [online]. Available from: http://www.lowara.com/product.php/4568. [Accessed 25th September 2006]

McHALE E.J., HUSSAIN Y.A., SANDERSON M.L., HEMP J., 1985. *Capacitively-coupled Magnetic Flowmeter*, US Patent 4,513,624

MILLER D.S., 1990. *Internal Flow Systems.* BHRA (Information services). 2nd Edition.

MILLER R.W., 1983. *Flow Measurement Engineering Handbook.* McGraw-Hill Book Company.

MILLS R.C., DONEY B., 2001. *Magnetic Flowmeters*, in SPITZER D.W., (EDITOR) *Flow Measurement*, Ch11.

NATIONAL INSTRUMENTS CORP., 1996. *PC-LPM-16/PnP User Manual, Multifiunction I/O Board for the PC.*

PDL Handbook Series, 1994. *Chemical Resistance, Volume II – Thermoplsatic Elastomers, Thermosets and Rubbers. 2nd Edition.*

PLANT M., 1991. *Basic Electronics,* Published by Hodder & Stoughton. 2nd Edition

QSC Audio Products inc., 2006. *CX 2-Channel Series Amplifiers* [online]. Available from: http://www.qscaudio.com/products/amps/cx/cx2/cx2.htm [Accessed 28th September].

ROSALES C., SANDERSON M.L., HEMP J., 2002a. *Problems in the theory and design of electromagnetic flowmeters for dielectric liquids. Part 2a: Theory of noise generation by turbulence modulation of the diffuse ionic charge layer near the pipe wall*, Flow Meas. Instr. 13 pp. 155-163.

ROSALES C., SANDERSON M.L., HEMP J., 2002b. *Problems in the theory and design of electromagnetic flowmeters for dielectric liquids. Part 2b: Theory of noise generation by charged particles*, Flow Meas. Instr. 13 pp. 165-171.

ROSALES C., SANDERSON M.L., 2003. *Streaming current noise generation in electromagnetic flowmeters measuring conducting fluids*, Flow Meas. Instr. 14 pp. 97-108.

RUMMEL T., KETELSEN B. 1966. *Inhomogeneous Magnetic-Field Enables Inductive Flow-Measurement of all Flow-Profiles, Which Appear in Practice,* Regelungstechnik, book 6.

SCHWIDERSKI H.W., 2003. *Private meeting regarding ABB's A.C. transmitter.*

SHERCLIFF J.A., 1962. *The theory of electromagnetic flow-measurement*, Cambridge university press.

SIERRA-ESPINOSA F.Z., 1997. *The Turbulence Structure of the Flow in a 90 Degree Pipe Junction: A Comparison of Numerical Predictions to Experimental Laser Doppler and Particle Image Velocimetry Results.* PhD thesis. University of Wales.

SMITH L., RUESCH J.R., 2001. *Mass Flowmeters*, in SPITZER D.W., (EDITOR) *Flow Measurement*, Ch12.

STOLL R.L., 1974. *The Analysis of Eddy Currents,* Clarendon Press, Oxford.

TURNER R.B., 1985. *Comparison of A.C. Magnetic Flow meters and Pulsed D.C. Meters.* ABB Internally circulated report.

TURNER R.B., 2002a. *A Mag flowmeter for low conductivity applications,* Presentation to ABB senior management in Stonehouse, UK. Presented by Lincoln D.M., June 2002.

TURNER R.B., 2002b. *Magnetic Flow Meters are M.H.D. Generators*, ABB Internally circulated technical report.

TURNER R.B., 2005. *Electromagnetic flow meter*, European Patent No. EP1521062.

VICKERS A., 2004. Meng Dissertation UEE087TM. University of the West of England.

WADA, ICHIRO. 1992. *Electromagnetic Flowmeter.* US Patent No. 5,125,276

WILSON H.A., 1905. *On the electric effect of Rotating a Dielectric in a Magnetic Field*, Philosophical transactions of the royal society A. vol. 204, pp. 121-137.

WILSON.M.P., 2001. *Historical Persepctive*, in SPITZER D.W., (EDITOR) *Flow Measurement*, Ch2.

YOUNG H.D., FREEDMAN R.A., 1996. *University Physics*, 9th ed., Addison-Wesley Publishing Company, Inc.

APPENDIX A

An Example of a batch file used to create an ANSYS weight function model

```
!ANSYS text file
!Created by Michael Armitage

!Title: Weight function analysis
!Model: !Cylindrical DN50 flow meter, Current sensing electrodes
!
!
FINISH
/CLEAR
KEYW,PR_SET,1
KEYW,PR_STRUC,0
KEYW,PR_THERM,0
KEYW,PR_ELMAG,1
KEYW,PR_FLUID,0
KEYW,PR_MULTI,0
KEYW,PR_CFD,0
KEYW,LSDYNA,0
/PMETH,OFF
!*
/PREP7
!*
ET,1,36              !current source element, used to build coil

et,2,5          !magnetic brick
KEYOPT,2,1,1        !voltage degree of freedom

et,3,200        !mesh dummy element, used to set up initial 2D mesh before
extrusion
                !contributes nothing to the solution
keyopt,3,1,6  !4 node quads
keyopt,3,2,0  !do shape testing

!set material properties

!free space (2)
mp,murx,2,1          !permeability
mp,rsvx,2,20e12              !resistivity

!water (4)
mp,murx,4,1
mp,rsvx,4,20
```

```
!iron circuit (3)
!TB,BH  ,3
dof,volt
!paste your BH data here. tbpt,,H,B noting the extra comma.

!data from 5.5 material library silicon steel

!TBPT,,  59.5238095   , 0.200000000
!TBPT,,  119.047619   , 0.400000000
!TBPT,,  158.730159   , 0.550000000
!TBPT,,  396.825397   ,  1.15000000
!TBPT,,  555.555556   ,  1.30000000
!TBPT,,  793.650794   ,  1.40000000
!TBPT,,  1587.30159   ,  1.55000000
!TBPT,,  3968.25397   ,  1.63500000
!TBPT,,  7936.50794   ,  1.65500000
!TBPT,,  15873.0159   ,  1.67500000
!TBPT,,  31746.0317   ,  1.70138960
!TBPT,,  63492.0635   ,  1.75000000
!TBPT,,  95238.0952   ,  1.79000000
!TBPT,,  190476.190   ,  1.90980000
!TBPT,,  285714.286   ,  2.02960000
!TBPT,,  380952.381   ,  2.14950000

mp,murx,3,1000          !permeability if you want to do a linear solution, just
unrem this line
mp,rsvx,3,20e12



!some dimensions

!electrode
!work in radians
elang=30            !angle subtended by electrode in degrees
elangr=elang*3.14159/180 !convert to radians

!iron circuit
icir=.100/2             !iron circuit inside radius
icor=.103/2             !iron circuit outside radius
iclen=.3                !iron circuit length

!coil
cmr=.045                !coil mean radius
cow=.018                !coil bundle width .0225
cot=.010                !coil bundle thickness
coang=115/360*2*3.14159     !angle subtended by coil 115
len=.058                !length of coil
```

```
wir=.05/2                   !flow inside radius
slice=.008                  !thickness of slice

cdc=0.18                    !coil drive current
turns=340                   !number of turns
current=cdc*turns           !amp turns for coil elements

!*************************************************

!conduit


!real constants for the coils
r,1,2,current,cow,cot               !straight bits
r,3,3,current,cot,cow               !pipe curve

!the basic form of the coil
!nodes to define coil corners
alpha=3.14159/2-coang/2
n,1,0,0,-len
n,2,cmr*cos(alpha),cmr*sin(alpha),-len
n,3,0,cmr,-len
n,4,cmr*cos(alpha),cmr*sin(alpha),+len
n,5,0,cmr,len
n,6,-cmr*cos(alpha),cmr*sin(alpha),+len
n,7,0,0,+len
n,8,-cmr*cos(alpha),cmr*sin(alpha),-len


!make some elements between nodes
!"real,1" are straight bits, "real,3" are curved
/eshape,1
type,1
mat,1
real,1
e,2,4,1
e,6,8,1

real,3
e,3,2,1
e,8,3,1
e,4,5,7
e,5,6,7

!reflect nodes for other coil
nsym,y,10,all

!merge common nodes
```

```
nummrg,all

!elements between nodes
type,1
mat,1
real,1
e,12,14,1
e,16,18,1

real,3
e,13,12,1
e,18,13,1
e,14,15,7
e,15,16,7

!put the conduit and all components in
!conduit

!draw end view and mesh
cyl4,0,0,0,0,icor,90
cyl4,0,0,0,0,icir,90

cyl4,0,0,0,0,wir,90
cyl4,0,0,icor,elang,wir,90 !segment subtended by electrode


aovlap,all          !overlap areas

type,3              !element type 3, mesh dummy element

esize,0.0007        !element nominal dimension
amesh,7                   !mesh flow area
esize               !reset elemnt size
smrtsize,2          !intelligent meshing size control for rest of meter (1 = fine,
10 = coarse
!esize,0.002
amesh,all           !mesh all unmeshed

!extrude gubbins
esize,,1            !number of elements through thickness of extrustion
type,1              !
vext,all,,,,,slice


!change material attributes for iron circuit

vsel,s,,,1
vsel,a,,,2
eslv,r
```

```
emodif,all,mat,3
allsel

!change material attributes for gap
vsel,s,,,4
vsel,a,,,5
eslv,r
emodif,all,mat,2
allsel

!change material attributes for water
vsel,s,,,3
eslv,r
emodif,all,mat,4
allsel

/solu

!flux perpendicular symmetry condition
nsel,s,loc,y            !all nodes at y = 0
d,all,mag
allsel

!electrode
da,18,volt,1            !set voltage at electrode


!ground plane
ASEL,S,LOC,X,0              !everything at x = 0
da,all,volt,0           !set voltage at ground plane
allsel

magsolv,3,,,,,1             !solve it

FINISH
/POST1
! The element table list
ESEL,S,MAT,,4               !select water elements
ETABLE, ,B,X                !flux density
!*
ETABLE, ,B,Y
!*
ETABLE, ,EF,X       !electric field
!*
ETABLE, ,EF,Y
!*
ETABLE, ,CENT,X  !element centre position
!*
ETABLE, ,CENT,Y
```

```
!Vector calculations
SMULT,by.efx,BY,EFX,1,1,
SMULT,bx.efy,BX,EFY,1,1,
SADD,whw,BY.EFX,BX.EFY,1,-1, ,
ETABLE, ,VOLU,
SMULT,whw.vol,WHW,VOLU,1,1,
PLETAB,WHW,AVG                !plot picture of weight function
ssum                          !calculate and sum element table items
```

APPENDIX B

Manufacturing drawing for the Borosilicate glass flow conduit

ABB Ltd.

BS 308 DO NOT SCALE

© 2005

A3

USED ON

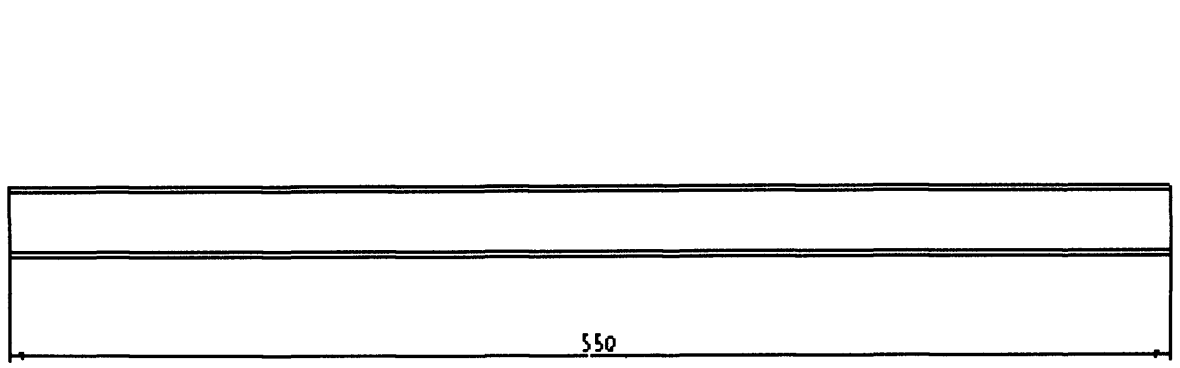

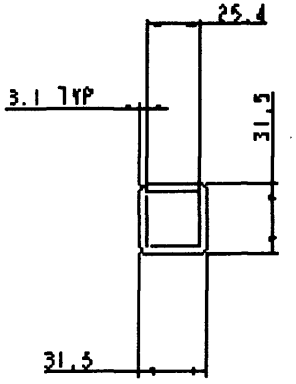

DRA FILE: GLASS_TUBE_DIMS

A	DHL	19-Sep-03	383	ORIGINAL ISSUE

DRAWN: D.M.LINCOLN

DATE: 19/09/03

CHECKED

APPROVED

TOLERANCE (U.O.S.)
WHOLE NO. ± 0.5
1 DEC PL ± 0.1
ANGLES ± 0.5°

SCALE: 0.500

DIMENSIONS IN mm

MATERIAL: BOROSILICATE GLASS

TITLE: GLASS FLOWTUBE DIMENSIONS

FINISH: NATURAL

DRAWING NO. SK 6410

SH 1 OF 1

APPENDIX C

Circuit diagram for the DSP CODEC

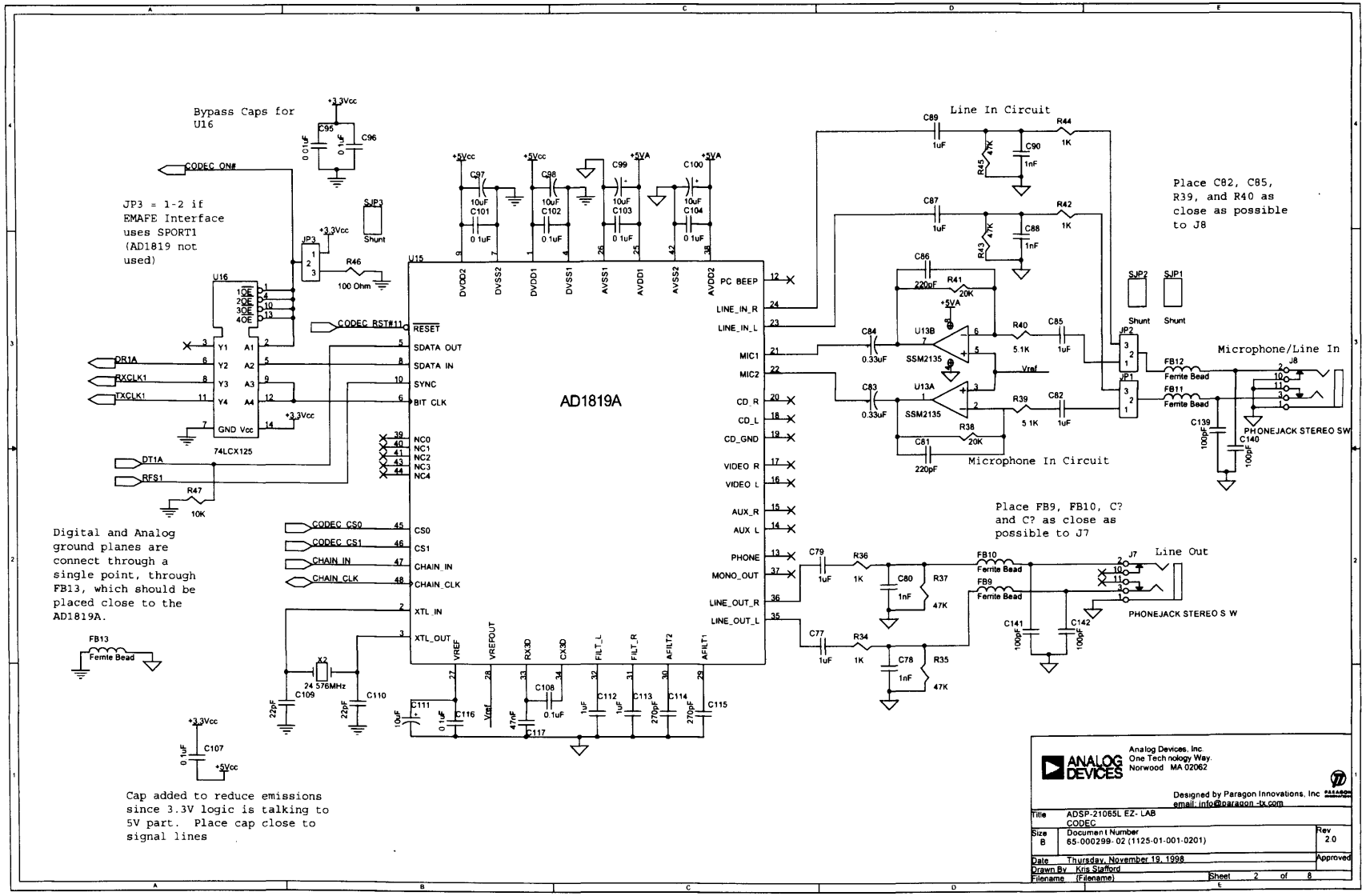
Bypass Caps for U16
JP3 = 1-2 if EMAFE Interface uses SPORT1 (AD1819 not used)
Digital and Analog ground planes are connect through a single point, through FB13, which should be placed close to the AD1819A.
Cap added to reduce emissions since 3.3V logic is talking to 5V part. Place cap close to signal lines
Line In Circuit
Microphone In Circuit
Place C82, C85, R39, and R40 as close as possible to J8
Place FB9, FB10, C? and C? as close as possible to J7
Microphone/Line In
Line Out
PHONEJACK STEREO SW
AD1819A
74LCX125
Analog Devices, Inc
One Technology Way
Norwood MA 02062
Designed by Paragon Innovations, Inc
email: info@paragon-tx.com
Title ADSP-21065L EZ-LAB CODEC
Size B
Document Number 65-000299-02 (1125-01-001-0201)
Rev 2.0
Date Thursday, November 19, 1998
Approved
Drawn By Kris Stafford
Filename (Filename)
Sheet 2 of 8

APPENDIX D

Designing and Building a Suitable Flow Rig

Designing and Building a Suitable Flow Rig

D1.1. Introduction

The aim of this project was to test a number of flow meters using different conductivity liquids. For this aim to be realised it was first necessary to build a test rig.

D1.2. Basic requirements and component sourcing

Building a test rig for use with insulating liquids was more complicated than producing a rig for use with water. One of the major problems with insulating liquids is associated with static electricity and the possibility of creating an ignition hazard. Due to the risks of ignition hazard the rig was designed and built following the recommendations of BS 5958, parts 1 and 2 (1991); which is the code of practice for the control of undesirable static electricity. With the range of chemicals that may be used in the rig a basic specification for the flow rig was developed and is given in table D.1.

Table D.1. Basic Requirement Specification

Temperature Range	• Up to 40°C
Pipe work requirements	• To suit DN25 and DN50 pipe work • A minimum of five diameters of straight pipe work upstream and downstream of the sensor • PN10 pressure rating
Flow rate control requirements	• Variable pump speed • Down stream valve to control line pressure and flow rate • By-pass valve to reduce line pressure

Table D.1 (Continued). Basic Requirement Specification	
Reference flow measurement	• A flowmeter capable of measuring conductive and insulating liquids
Health and Safety requirements	• A Closed loop flow rig to ensure the chemicals being flowed cannot produce harmful aerosols that can be breathed in or act as an ignition hazard. • Spillage containment • Over temperature cut-off • Pipe work electrically earthed
Power supply	• 3-phase mains
Chemical compatibility	• All components must be compatible with the following liquids: o Mineral Oil o Glycols o Alcohols o Demineralised water o Water

Based on the requirement specification a flow diagram of the layout was produced and is shown in figure D.1:

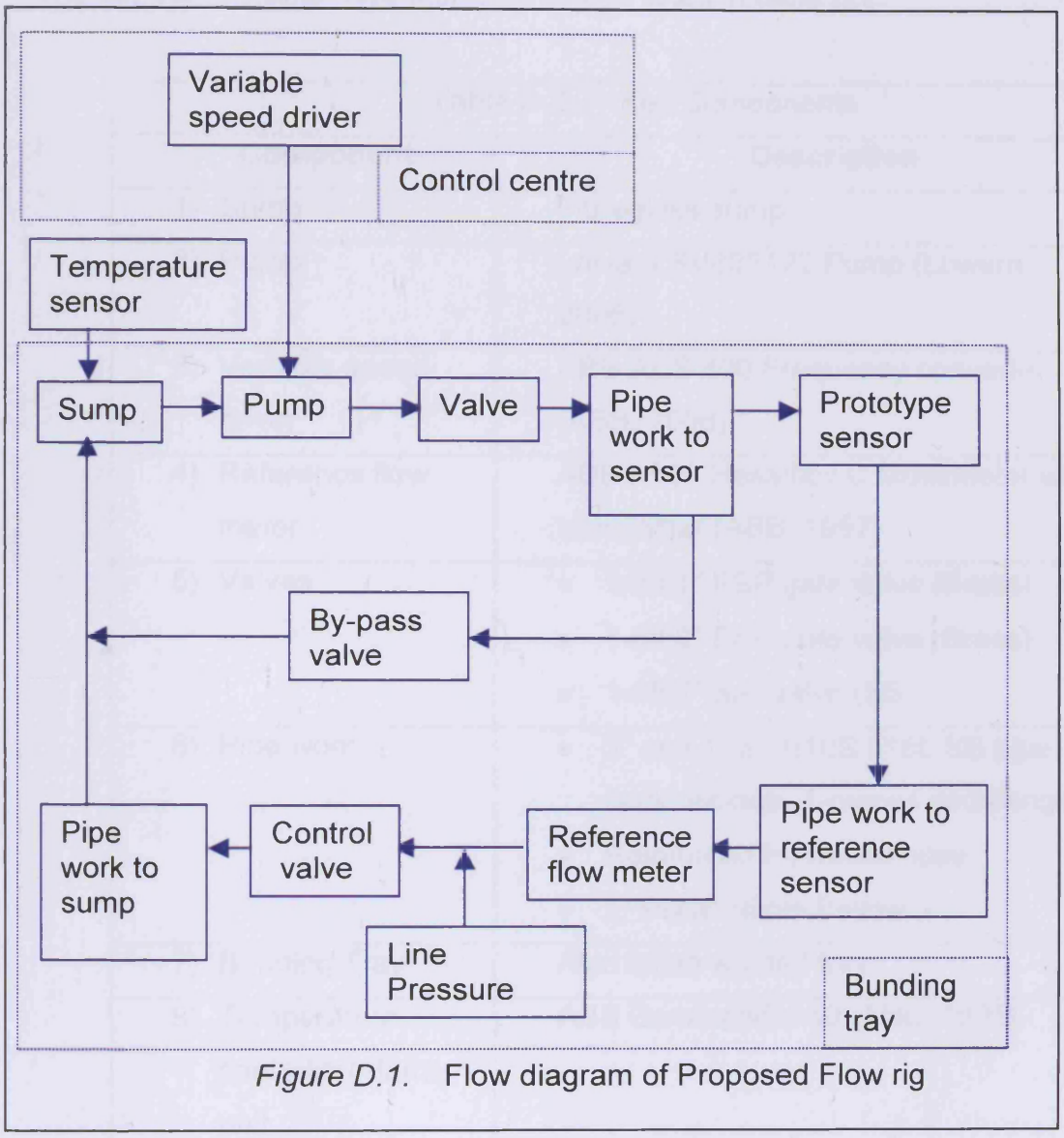

Figure D.1. Flow diagram of Proposed Flow rig

The key components were then sourced as listed in table D.2:

Table D.2. Key Components

Component	Description
1) Sump	Fibreglass sump
2) Pump	Lowara SV805T22 Pump (Lowara, 2006)
3) Variable speed driver	ABB ACS 400 Frequency converter (ABB, 2006)
4) Reference flow meter	ABB K500 Hastelloy C MassMeter with transmitter (ABB, 1997)
5) Valves	• 1-off 1" BSP gate valve (Brass) • 1-off 2" BSP gate valve (Brass) • 1-off 2" Ball valve (SS)
6) Pipe work	• 2" and 1" SCH10S 316L SS pipe work, elbows, T-pieces and flanges. • Reinforced Hydraulic hose • 2" PN16 Nitrile Bellow
7) Bunding Tray	Aluminium welded tray
8) Temperature controller/Alarm unit	ABB Commander 50 (ABB, 1995)

D1.3. Producing a 3D model of the rig assembly

As each suitable component was identified a three dimensional model of the part was made, the design then evolved from the block diagram into a 3D model of the rig as detailed in figure D.2.

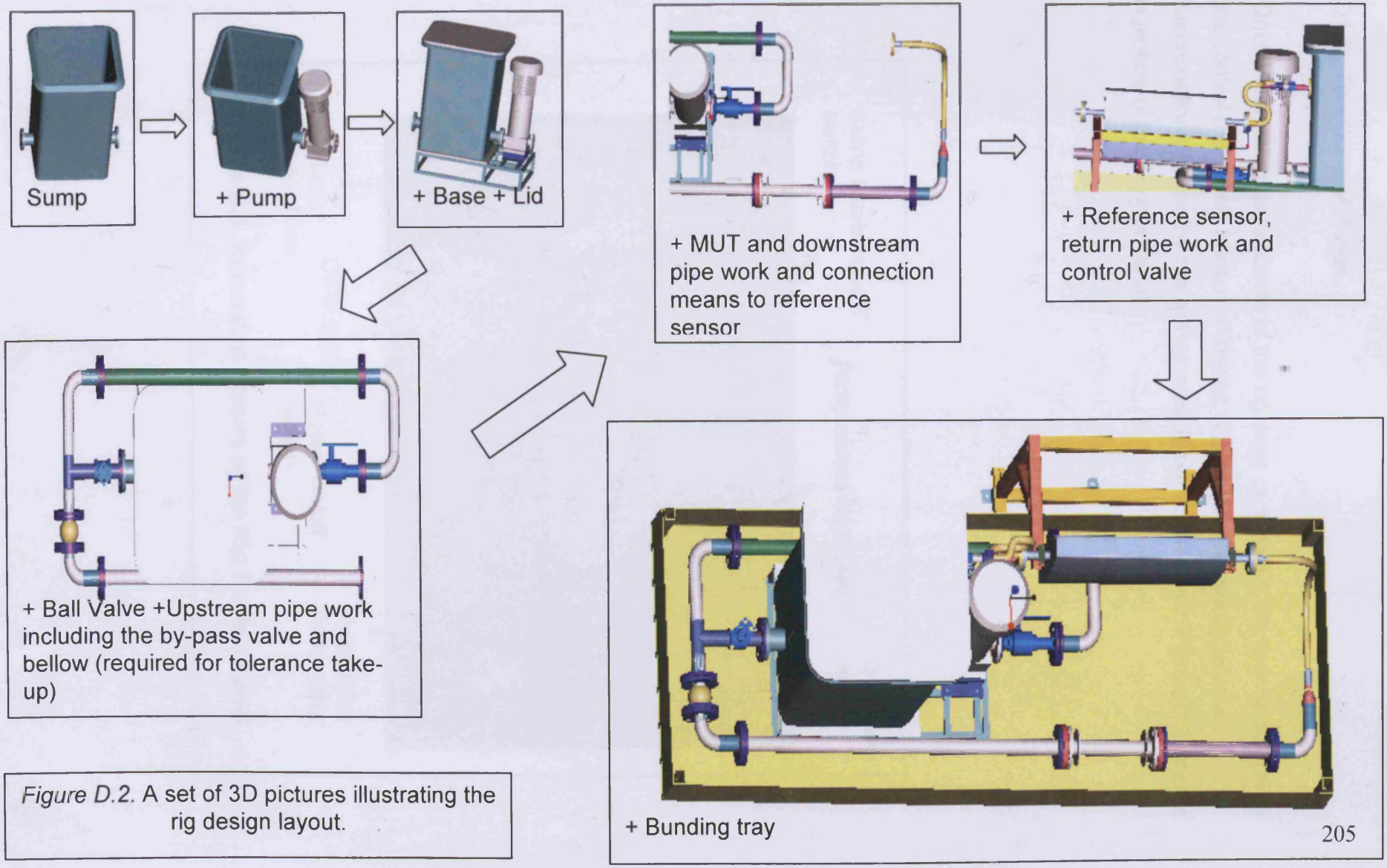

Figure D.2. A set of 3D pictures illustrating the rig design layout.

D1.4. The Control Panel

Once the mechanical aspects of the rig were completed, the task of designing the control panel was started. Working with an on-site electrician the functionality required by the author was designed and built. Figure D.3. shows a picture of the control panel.

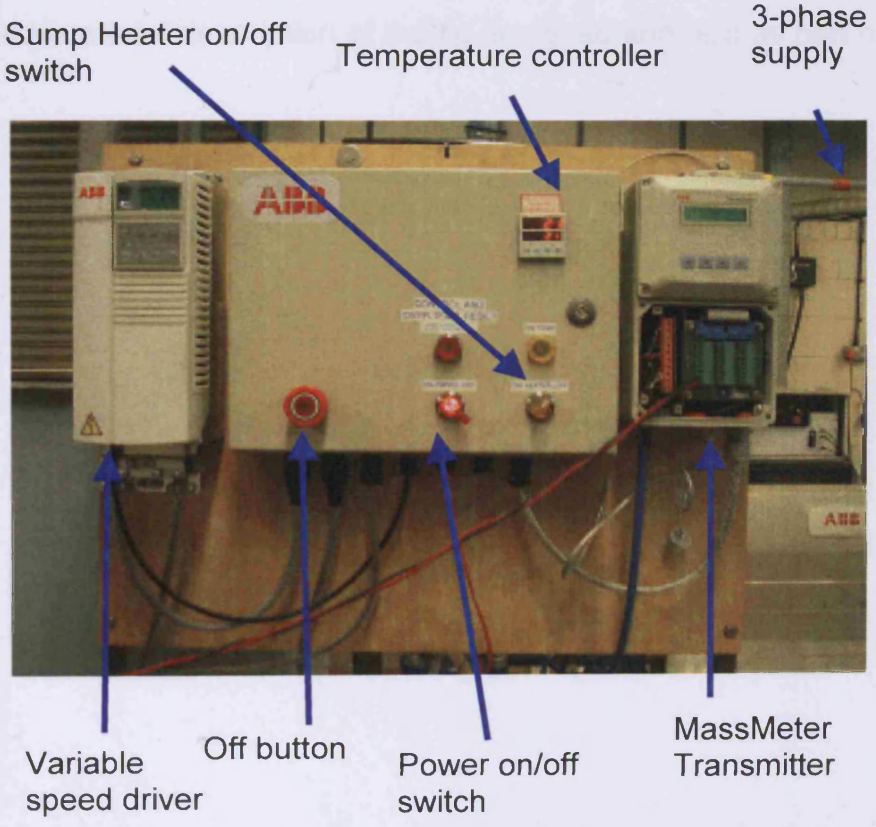

Figure D.3. Annotated Picture of the Rig Control Panel

D1.5. Commissioning the rig

Before using the rig it was checked over by the Health and Safety officer. One issue arose from this inspection, each flange needed a guard to ensure that any leaks would be directed into the sump rather than spray up and possibly harm workers in the vicinity.

Once the guards were produced a standard flow meter was fitted into the rig to check the performance using water. The output of the pump produced line pressures of up to 6 bar and flow rates of 6 l/s with 50mm diameter pipe work.

D1.6. Discussion

This concludes a brief description of the rig designed and built as part of this project.

APPENDIX E

A Block diagram of the VKA phase sensitive detector used to test the DN50 Polypropylene Prototype

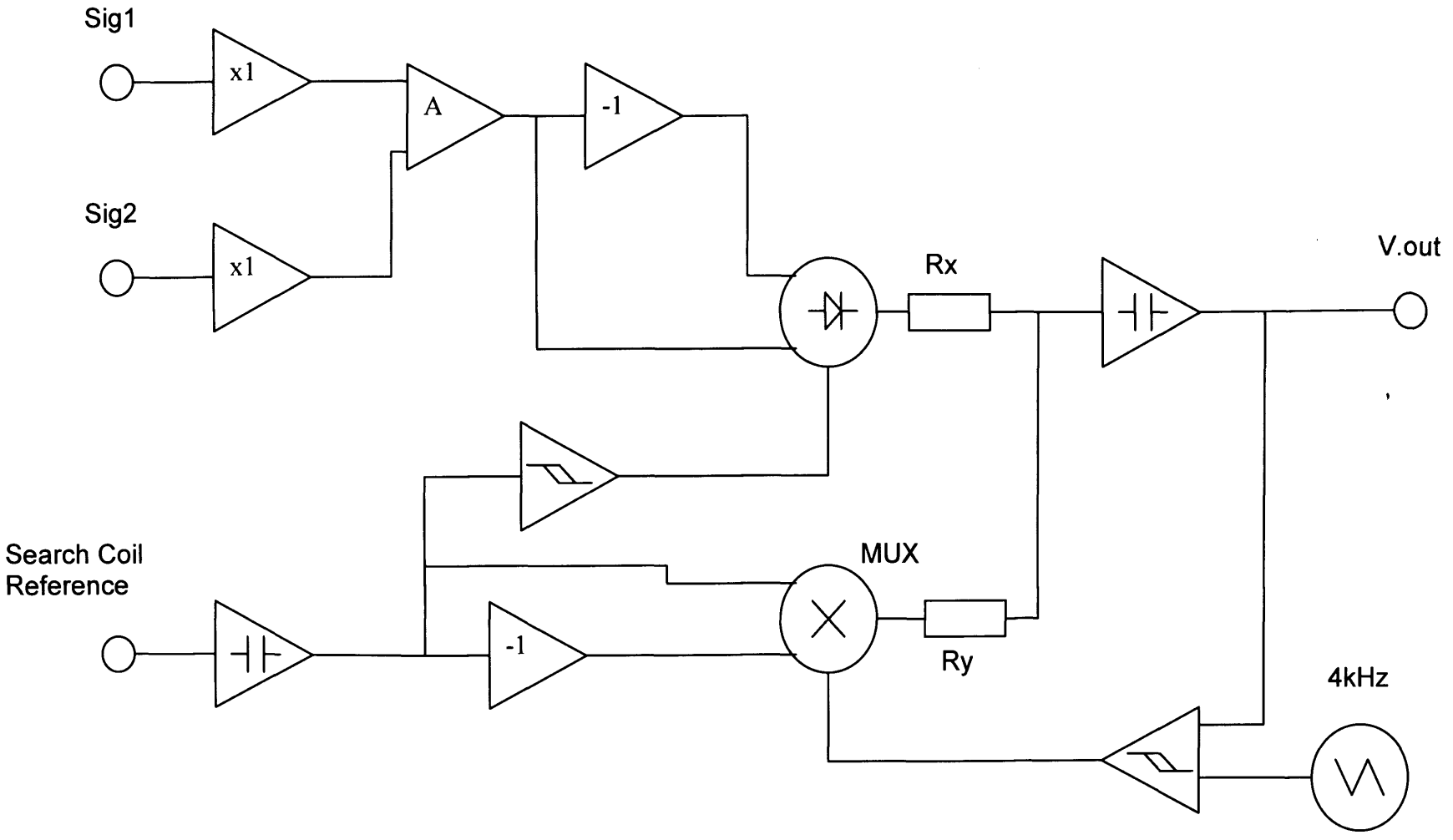

Block Diagram – Synchronous Analogue Multiplier (Asquith, 1980)